
UNIVERSITY OF BIRMINGHAM

# Melting Point Depression in Biodegradable Polyesters

by

Shona Murphy

A thesis submitted to

The University of Birmingham

for the degree of

MASTER OF RESEARCH

School of Engineering

Metallurgy and Materials

The University of Birmingham

## Synopsis

Investigation into the crystallisation kinetics and melting point depression of poly(L-lactide-co-*meso*-lactide) with approximately 3.3% D-lactide content (PLA 3051D) was undertaken. The rate of crystallisation was too slow for a crystallisation exotherm to be detected by the DSC, therefore hot-stage microscopy was used as an alternative method to characterise the crystallisation behaviour. Light intensity with time during isothermal crystallisation of a thin polymer film (<15μm) was measured. The results were normalised in order to calculate crystallisation half-life ($t_{0.5}$). From half-life calculations, the optimal crystallisation temperature was found to be 118°C. By replacing the light dependant resistor with a digital camera, the diameter growths of individual spherulites could be measured minute-by-minute. Using the results obtained through hot-stage microscopy, re-processing of PLA could be carried out to restore the original crystallinity at $T_{max}$ 118°C. Plots showing % crystallinity with storage time at 118°C indicated a storage time of 2 hours was required to restore the crystallinity to 40%. Studies using the high pressure DSC found that with increasing $CO_2$ pressure up to 60 bar, the melting point decreased from 152 to 142°C .

An alternative biodegradable polymer, polycaprolactone CAPA 6800 was investigated with high pressure DSC as a comparison polymer to polylactic acid. Similarly to PLA, the melting point of PCL showed a significant reduction (55 to 40°C) when soaked with increasing pressures of $CO_2$.

**Acknowledgments**

I would like to express my sincere gratitude to all who aided me during the time of my MRes. In particular, I would like to thank Dr Mike Jenkins and Dr Gary Leeke for their guidance and support. I would also like to give my appreciation to Frank Biddlestone who has provided me with invaluable technical assistance. Finally, I would like to thank my family, friends and colleagues for their continuous support and encouragement over the past year.

## Contents

**1.0 Introduction ..... 1**

**2.0 Literature Review ..... 2**

2.1 Polymer Morphology ..... 2

2.2 Polylactic acid (PLA) ..... 4

2.2.1 PLA meso- copolymers ..... 7

2.2.2 PLA synthesis ..... 8

2.3 Polycaprolactone (PCL) ..... 11

2.4 Polymer Degradation ..... 13

2.5 Supercritical Processing ..... 16

**3.0 Projects Aims ..... 20**

**4.0 Experimental ..... 21**

4.1 Materials ..... 21

4.1.1 Polylactic Acid (PLA 3051D) ..... 21

4.1.2 Polycaprolactone (PCL CAPA 6800) ..... 22

4.2 Experimental Methods and Techniques ..... 24

4.2.1 Sample Preparation ..... 24

4.2.2 Differential Scanning Calorimetry (DSC) ..... 25

4.2.3 High Pressure DSC ..... 30

4.2.4 Hot-stage Microscopy ..... 32

**5.0 Results and Discussion ..... 34**

5.1 Initial Characterisation of PLA3051D ..... 34

5.1.1 Characterisation Using Differential Scanning Calorimetry (DSC) ..... 34

5.1.2 Characterisation Using Hot-Stage Microscopy ..... 35

5.1.3 Re-crystallisation of PLA3051D ..... 42

5.2 Melting Point Depression in PLA 3051D by $CO_2$ ..... 45

5.2.1 Establishing The Optimal Experimental Conditions ..... 45

5.2.2 Measurement of Melting Point Depression in PLA.....49
5.3 PCL CAPA6800 ..... 51
5.3.1 Initial Characterisation of PCL.....51
5.3.2 Characterisation of The Melting Point Depression Using High-Pressure DSC. 51

**6.0 Conclusions and Future Work ..... 54**

**7.0 References ..... 56**

**Appendix 1.....**

Hot-Stage Microscopy Images.....

**Appendix 2.....**

DSC melting traces of re-conditioned samples.....

**Appendix 3.....**

Jenkins, M.J.; and Murphy, S.H. A Comparison of the use of FTIR spectroscopy with DSC in the characterisation of melting and crystallisation in polycaprolactone. *Thermochimica Acta* (submitted)

## 1.0 Introduction

Currently within the EU, approximately 55 million tonnes of polymers are produced which contributes 24% of the global total (230 million tonnes in 2009). Polyethylene (PE-LD, PE-HD, PE-LLD) and polypropylene (PP) account for around 50% of polymer demand with polyvinyl chloride (PVC) being the third largest polymer at 11%. These polymers would typically be used in applications such as packaging, which is the largest end use market segment with a 40.1% share. This is followed by building and construction (20.4%) and Automotive (7.0%) [1]. However, these polymers are difficult to recycle cost-effectively, therefore, the majority are sent to landfill. Those that are not recycled pose a harmful threat to the environment [2], influencing major food outlets and retailers to pursue biodegradable polymer packaging from renewable sources which have a much lower environmental impact [3]. These products can be composted or if left as litter, will degrade.

Commercially available biodegradable polymers from renewable sources are typically either polyesters or polysaccharides [4]. Aliphatic polyesters are the more commonly known and studied biodegradable polymers which include Polylactic Acid (PLA), Polycaprolactone (PCL), Polyhydroxyalkanoates (PHAs) and Polyglycolic Acid (PGA). Of the polymers derived from renewable sources, only PLA is produced in sufficient quantities to be a commercially viable solution. PLA is currently extruded where the products are thermoformed into cups, containers or trays to replace polystyrene and PET. However, PLA possesses an inherent thermal degradation during extrusion as it quickly loses its thermal stability when heated above its melting point, this significantly reduces its processing window compared to other polymers. Consequently, manufacturing products from PLA becomes difficult, therefore screw extruders have been modified in order to reduce PLA's thermal degradation during

extrusion. A solution to the limitations of extruding PLA would be to use a supercritical fluid as a solvent. Supercritical carbon dioxide ($scCO_2$) is the preferred choice for these applications, due to its properties of being non-toxic, non-flammable, chemically inert, environmentally safe and inexpensive. Its solubility in many polymers is substantial, being influenced by temperature, pressure and, sometimes, weak interactions with the constituent groups in the polymer. Dissolved $CO_2$ causes a reduction in the viscosity by plasticisation, allowing processing at lower temperatures [5]. For these reasons, melting point depression in biodegradable polyesters using $CO_2$ will be investigated.

## 2.0 Literature Review

### *2.1 Polymer Morphology*

Polymers, also known as macromolecules, consist of significant numbers of ordered monomer repeat units that are covalently bound. These polymers exist as either amorphous or semi-crystalline. Polymers that contain ordered crystalline regions and unordered amorphous regions are known as being semi-crystalline. The individual chain folded lamella crystals are separated by amorphous regions as shown in fig. 2.1 [6]. Those that do not contain any crystallinity are known as amorphous [7]. The degree of crystallinity ranges for every polymer and may be influenced through thermal processing. Chain configuration has high implications to the polymer's properties and applications. Polymers can undergo thermal transitions upon heating and cooling. These transitions are called glass transition ($T_g$), crystallisation ($T_c$) and melting ($T_m$) and are changes in the degree of molecular motion within the polymer [8]. There are two mechanisms for crystallisation in polymers; nucleation and growth.

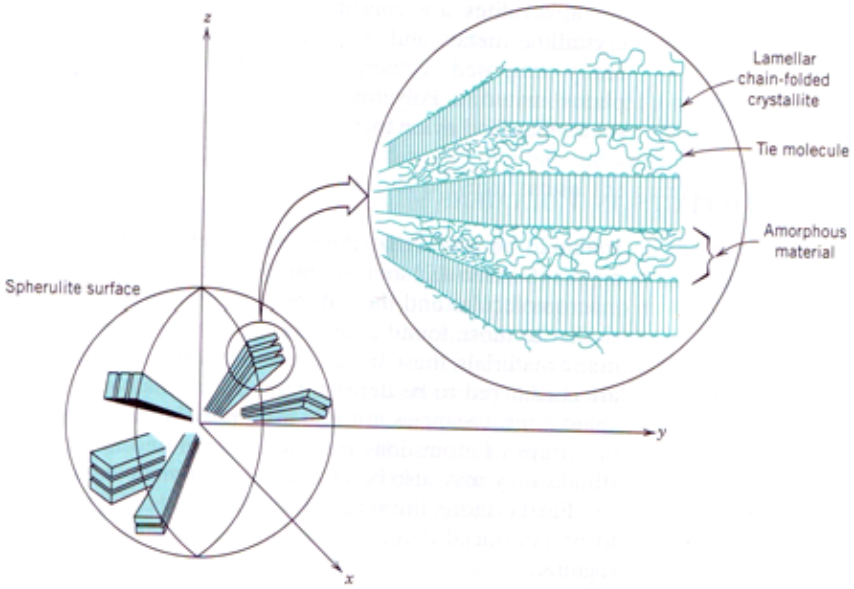


Fig. 2.1. Example of the structure of a sphreulite containing amorphous and crystalline regions [6].

Nucleation can be divided into homogeneous nucleation (attachment of a polymer chain to a nucleating agent e.g. dust or dirt) and heterogeneous nucleation (aggregation, high entanglement of the polymer chains) [9]. The growth mechanism of crystallisation involves the diffusion of crystallising chains across the melt-crystal interface [10]. Polymers that are crystallised from the melt form spherulites which consist of an aggregate of ribbon-like chain-folded lamellae that radiate from the centre outward. Fig. 2.2 shows an optical micrograph of spherulites in polycaprolactone obtained at room temperature [11].

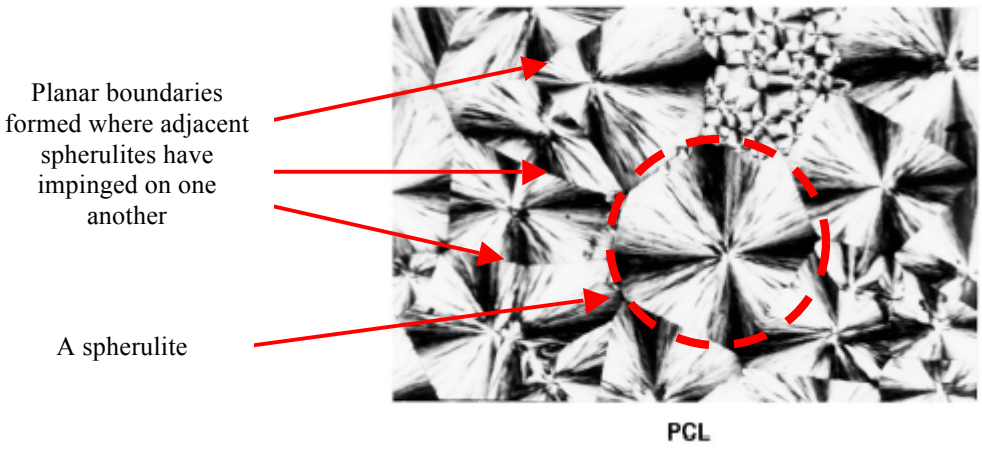


Fig. 2.2 - Optical micrograph of PCL obtained at room temperature [10]

As crystallisation of the spherulitic structure proceeds to completion, planar boundaries are formed between adjacent spherulites therefore losing their perfectly spherical shape. Melting is characterised by amorphous regions increasing in macromolecular mobility and the ordered lamella crystals melting to become an unordered amorphous state.

With the change of molecular motion in a polymer, thermal properties such as specific heat change can also be seen. This enables techniques such as differential scanning calorimetry (DSC) to characterise polymers with addition to hot stage microscopy, which enables the study of their crystallisation kinetics, both of which are important components to this study.

## *2.2 Polylactic acid (PLA)*

Biodegradable polymers are of great interest due to their bio-medical and environmentally friendly packaging applications. Among biopolymers, lactic acid based polymers (PLAs) are extensively used in various medical applications; including drug delivery and scaffolds in tissue engineering. PLA is a versatile polymer; its production is derived from 100% renewable resources such as corn and sugarcane, which is biocompatible, biodegradable and compostable [12], [13]. Therefore it gained attention as an alternative to synthetic polymers. It also has high transparency, molecular weight and mechanical strength, including excellent shaping and moulding properties. Primarily, the use of PLA was limited to biomedical

applications such as sutures [14] and drug delivery systems [15] due to the availability and cost of manufacture. However recently, companies such as NatureWorks LLC have developed the large-scale, economic production of PLA and with its excellent shaping and moulding properties it becomes a good candidate for packaging materials due to its close similarity with poly(ethylene terephthalate) (PET).

Polylactic acid (PLA) is a linear, aliphatic polyester, consisting of lactic acid (2-hydroxy propionic acid, a non-toxic naturally occurring metabolite) building blocks. This building block can exist in optically active D-or L-enantiomers, as shown in fig 2.4. It is well established that depending upon the content of enantiomers, the ratio between $_{L}$-lactide/$_{D}$-lactide within the polymer, variable material properties can be achieved, from semi-crystalline to amorphous [16]. PLA polymers with $_{L}$-content greater than approximately 90% tend to be crystalline while those with lower optical purity are amorphous [17]. PLA quickly loses its thermal stability when heated above its melting point, which significantly reduces its processing window compared to other polymers. By introducing $_{D}$-lactide into a predominantly $_{L}$-lactide polymer, the processing window can be increased by nearly 30°C due to its lower melting temperature [13].

The crystallisation of PLA in its many compositions of enantiomers has previously been studied by many authors. Crystallinity plays an important role in the physical and mechanical properties of PLA, thus determining its potential applications. The crystallinity of PLA is influenced by its composition [18]. Crystallisation rates of varying molecular weights of PLLA films were found (using DSC and optical microscopy (with a depolarised-light intensity method)) to increase with decreasing molecular weight [19]. Similarly an

investigation into the cold crystallisation of poly(L-lactide) (PLLA) of two different molecular weights during heating at 2°C/min was later undertaken by different authors. They found with wide angle X-ray scattering (WAXS) molecular weight does not affect either the crystal form or the final degree of crystallinity, however the crystallisation rate of PLLA decreased with increased molecular weight. These results were consistent with differential scanning calorimetry (DSC), which showed a broad exothermic crystallisation peak for the higher molecular weight PLLA [20].

Crystallisation studies into the addition of poly(D-lactide) (PDLA) into PLLA found a reduction in the overall extent of PLLA crystallisation. Racemic blends of low molecular weight PDLA and high molecular weight PLLA homopolymers were prepared through solution blending, leading to the formation of a 1:1 stereocomplex. In comparison with pure PLLA, the stereocomplex had a higher melting temperature and also crystallised at higher temperatures from the melt. The addition of 0.25-15 wt% PDLA into PLLA showed that PDLA crystallites acted as heterogeneous nucleation sites for subsequent PLLA crystallisation, with an increase in the number of nucleation sites of nearly 5 orders of magnitude at 15 wt% PDLA. This increase was significantly larger compared with the addition of talc, a known nucleating agent for PLA. However, the addition of PDLA led to a reduced spherulite size and a reduction in the overall extent of PLLA crystallisation, which was attributed to the hindered mobility of the PLLA chains due to tethering by the stereocomplex [21]. These results were confirmed in another study where the addition of small amounts (1.5, 3 & 6%) of D-lactide in random copolymers containing predominantly L-lactide was investigated. Similarly, the crystallinity, spherulite growth rate and lamella thickness decreased substantially with increasing D-content in the copolymer [22].

### *2.2.1 PLA meso- copolymers*

Whilst the crystallisation behaviour of homo- and copolymers of poly(L-lactide) and poly(D-lactide) has been vastly studied, there is a significant lack of literature on *meso*- copolymers. However, the crystallisation kinetics of poly(L-lactide-co-*meso*-lactide) has been studied over a range of 0-9% *meso*-lactide by DSC. Crystallisation half-life increased by approximately 40% for every 1 wt% *meso*-lactide content, driven mainly by a reduction in melting point [23]. This study was later extended by different authors who investigated the addition of 0-12% *meso*-lactide into the crystallisation and microstructure of poly(L-lactide-*co-meso*-lactide). They found that bulk crystallinity, melting temperature and spherulite growth rate decreased dramatically with increasing *meso*-lactide content. The conclusions were that the *meso*- defects are rejected from the crystalline regions, therefore the concentration of interfibrillar regions increased with higher comonomer content [24]. Other studies observed that a reduction in lamellar thickness and crystallinity occurred with increasing *meso*- content [25] and [26]. More recently the solid-state structure and melting behaviour of random copolymers of L-lactide with 0, 2, 4 and 10 mol % *meso*-lactide has been studied. The crystalline morphology of all copolymers changed from spherulitic to hexagonal lamellae stacking with increases in crystallisation temperature [27].

The literature review on crystallisation in PLA has shown that copolymers poly(L-lactide) and poly(D-lactide) have been studied in much depth, however there is a significant lack of literature on *meso*- copolymers. Copolymerisation of poly(L-lactide) with comonomer units such as *meso*-lactide allows for the production of a wide range of physical properties and biodegradation rates. Therefore, poly(L-lactide-co-*meso*-lactide) with approximately 3.3% D-lactide content has been chosen for this study in order to further current literature.

### *2.2.2 PLA synthesis*

Conventional synthetic polymers rely on reserves of oil and gas which take millions of years to regenerate and are a declining resource. The monomer used to manufacture polylactic acid is obtained from annually renewable crops so can be produced by carbohydrate fermentation or chemical synthesis. Currently, the majority of lactic acid production is based on the fermentation route. The starch produced during photosynthesis of plant cells is extracted from plant matter and converted to a fermentable sugar (e.g. glucose) by enzymatic hydrolysis. The carbon, hydrogen and oxygen in these natural sugars are then converted to lactic acid through fermentation (see fig. 2.3) [28].

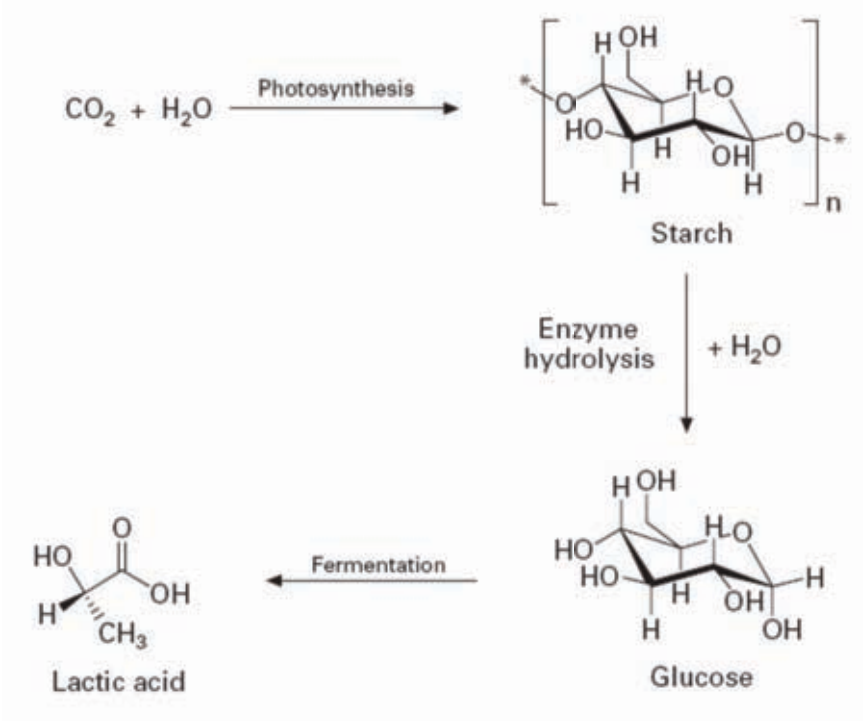


Fig. 2.3. Production of lactic acid from renewable resources [12].

The fermentation of sugar produces chiral lactic acid; chiral molecules exist as 'mirror images' or stereoisomers. Lactic acid can exist as the L- or D-stereoisomer (fig. 2.4).

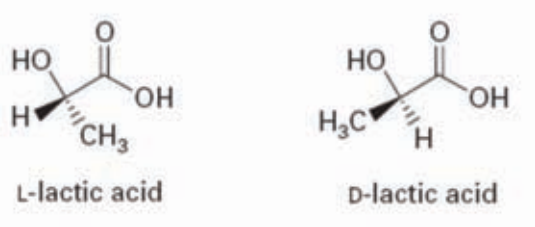


Fig. 2.4 The stereoisomers of lactic acid [12].

PLA can be polymerised using several techniques, including direct condensation polymerisation, azeotropic dehydration condensation and polymerisation through lactide formation (see fig. 2.5).

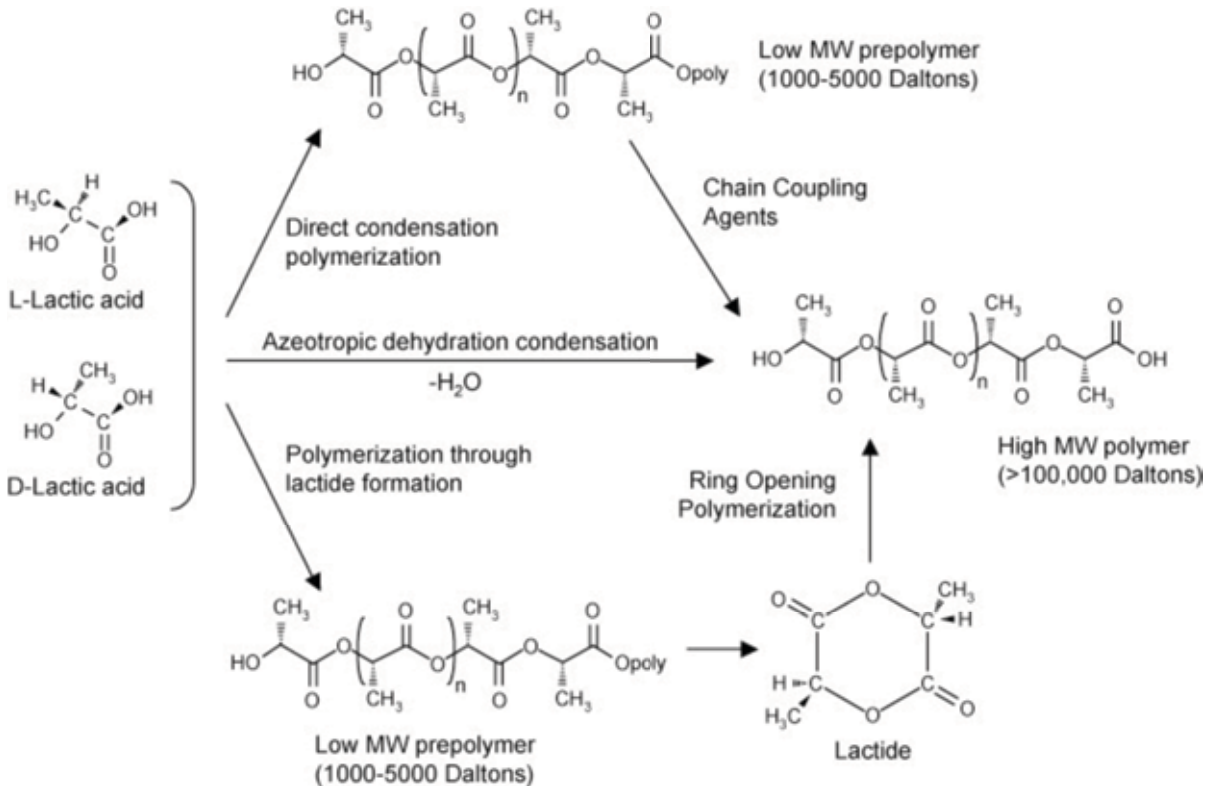


Fig. 2.5. Synthesis of PLA from D- and L- lactic acids [17].

Direct condensation polymerisation of lactic acid involves the removal of water by condensation and the use of a solvent under high vacuum and temperature. However, there

is increased racemisation with this method and only low to intermediate molecular weights can be produced (mainly due to the difficulties of removing water and impurities) [12]. Commercially available high molecular weight PLA is produced using ring opening polymerisation. This process is based on removing water under milder conditions to produce a cyclic lactide intermediate, without the need for solvent.

Production of the cyclic lactide dimer results in three potential forms; L-lactide, D-lactide and L,D- or D,L-lactide, called *meso*-lactide (figure 4).


Fig. 2.6. Dimeric lactide isomers [12].

Controlling the purity of the lactide using vacuum distillation it is possible to produce a wide range of molecular weights. This is achieved by varying the amount and the sequence of D-lactide units in the polymer backbone. Polymers with a high L-lactide content can be used to produce crystalline polymers, whilst the higher D-lactide polymers (>15%) are more amorphous. These changes impact melt behaviour, thermal properties, barrier properties and ductility [29].

### *2.3 Polycaprolactone (PCL)*

Polycaprolactone (PCL) is a semi-crystalline linear aliphatic polyester [30] and its physical properties determine its applications. The chemical structure of polycaprolactone is shown in fig. 2.7. PCL is a polymer derived from the chemical synthesis of crude oil, although not produced from renewable raw materials, it is fully biodegradable. Fig. 2.8 shows the production of ε-caprolactone from cyclohexanone at Solvay. This is a method that occurs before polymerisation and results in the production of the PCL monomer. Two main pathways to produce polycaprolactone have been described in the literature; the polycondensation of a hydroxycarboxylic acid: 6-hydroxyhexanoic acid and the ring-opening polymerisation (ROP) of a lactone: e-caprolactone (e-CL). Ring-opening polymerisation (ROP) is a preferred route of preparation of PCL because it gives a polymer with a higher molecular weight and a lower polydispersity. The main mechanisms for the ROP of lactones depend on the catalyst: anionic, cationic, monomer-activated and coordination–insertion ROP. During ROP of ε-CL using an initiator and a catalyst, both intermolecular transesterification and intramolecular transesterification can occur as side reactions. These reactions occur particularly at high temperature and generally encountered during the later stages of polymerisation. As a result the broadening of the polydispersity and loss of control of the polymerisation occurs [31].

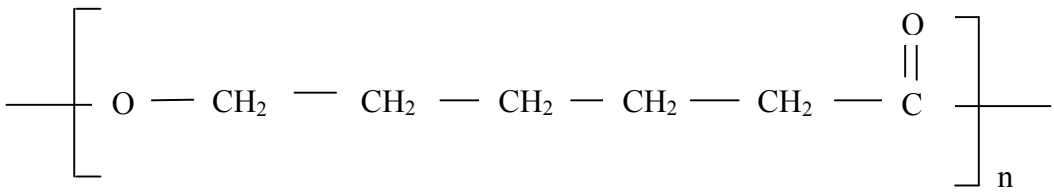


Fig. 2.7. The chemical structure of Polycaprolactone.

As a well characterised polymer it is receiving much attention having many very useful applications, being both biocompatible and biodegradable. It was initially investigated for use as a biodegradable packaging material after the realisation of its degradability by microorganisms. PCL is also degraded by hydrolysis in physiological conditions and is now one of several degradable polymers approved for use in the human body as drug delivery devices, adhesion barriers, sutures and staples and is being extensively investigated as a biomaterial for tissue repair and regeneration [32]. PCL is useful for applications involving controlled release devices for bioactive molecules such as growth factors and hormones and extended-residence supports for cell growth and tissue development [33].


Fig. 2.8. The production of PCL monomer; ε-caprolactone from cyclohexanone at Solvay [31].

## *2.4 Polymer Degradation*

Polylactic acid can be hydrolysed quite easily to produce lactic acid, lactide and oligomers, which are afterward decomposed into water and carbon dioxide by microorganisms [34]. Polycaprolactone is also biodegradable by hydrolysis and enzymatic degradation. Figure 2.9 illustrates the different biodegradation methods for PLA. Bioegradation of PLA and PCL is a desirable mechanism in specific situations and one which justifies their selection for certain applications. It is influenced by the solid-state morphology, degree of crystallinity and the primary chemical structure of the material. Degradation involves chain scission of the main chain where the ester bonds are located, resulting in the formation of oligomers.

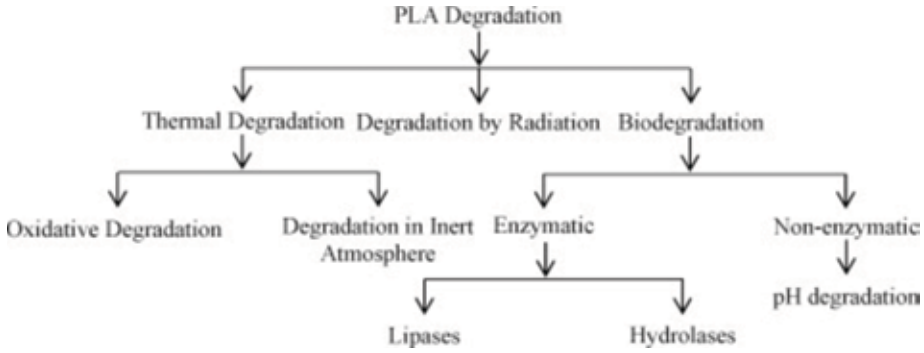


Fig. 2.9. Different biodegradation methods for PLA [35].

Biodegradation of PLA occurs in three steps; depolymerisation, the production of lactic acid and the consuming of lactic acid by enzymes producing $CO_2$ and $H_2O$. Enzymes such as lipases and PHA depolymerases cleave the ester bond of aliphatic polyesters, including PLA and PCL. The hydrophobic domains of enzymes adhere to solid substrates. The rate of enzymatic degradation decreases with increases in crystallinity, as enzymes selectively degrade the amorphous regions first. Non-enzymatic biodegradation includes chemical methods such as pH degradation where a change of pH in the atmosphere results in random

cleavage of the polymer chain backbone. This leads to a decrease in the mechanical properties such as tensile strength [35].

Degradation by hydrolysis is the principal mode of degradation for lactic acid based homopolymer and copolymer and can be seen in fig. 2.10. This occurs in three steps. The first involves the diffusion of water, initially into the more amorphous zones of the polymer, which is followed by random hydrolysis. The second involves fragmentation of the polymer into OLLA and finally, more extensive hydrolysis occurs accompanied by phagocytosis, diffusion and metabolism. The rate of hydrolytic degradation is primarily dependent on temperature and humidity [35].

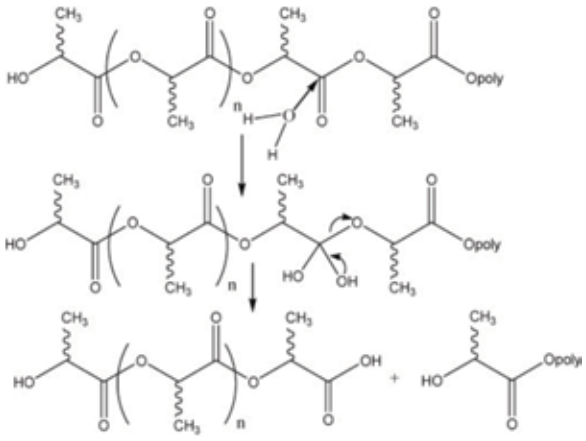

Fig. 2.10. Hydrolysis of PLA [35].

The hydrolytic degradation of PLA has been found to vary with crystallinity. Lower degradation occurs with higher crystallinity (L-lactide content), whereas copolymer polylactides degrade much faster, the rate increasing with increasing comonomer concentration [36]. Highly crystalline PLA can take years to hydrolyse fully due to the impermeability of the crystalline region, whereas amorphous PLA is degraded in weeks [13]. This has functional significance in biomedical applications such as bone tissue scaffolds where the rate of degradation must match the rate of bone healing for the scaffold to be

successful. "PLA copolymers are found to have less resistance to hydrolysis than a PLLA/PDLA polyblend having the same percentage of L-and D-lactide because a polyblend can form more stereocomplexes, which is the most stable structure PLA can form." [37 pp.168] As well as crystallinity, degradation is also dependent on a number of other factors including; molecular weight, purity, temperature, pH and water permeability [38]. PCL biodegrades within several months to several years and similar to PLA it is dependent upon the molecular weight, the degree of crystallinity of the polymer and the conditions of degradation. Many microbes in nature are able to completely biodegrade PCL. The mechanism is the same to that of PLA, the amorphous phase is degraded first, resulting in an increase in the degree of crystallinity while the molecular weight remains constant. Cleavage of ester bonds subsequently result in a loss of mass. Degradation by end chain scission occurs at higher temperatures while it degrades by random chain scission at lower temperatures. PCL degradation is autocatalysed by the carboxylic acids liberated during hydrolysis[2] but it can also be catalysed by enzymes, resulting in faster decomposition. PCL can undergo enzymatic degradation in the environment, however it cannot be degraded enzymatically in the body [31].

Degradation by radiation involves the significant reduction in molecular weight by chain-scission of the polymer with increasing doses of radiation. As with the other mechanisms of degradation, the amorphous regions of the polymer are mainly affected and consequently, the degree of crystallinity of the material plays an important role. This leads to a reduction in the mechanical properties of the material such as; tensile strength and substantial embrittlement [35].

One of the drawbacks of processing PLA in the molten state is its tendency to undergo thermal degradation, relating to processing temperature and residence time in the extruder.

Thermal degradation can be attributed to many mechanisms including thermohydrolysis by trace amounts of water and zipper-like depolymerisation. Intermolecular transesterification to monomer and oligomeric esters and intramolecular transesterification results in the formation of monomer and oligomer lactides of low molecular weight, consequently influencing the mechanical properties of the end product [17]. It is therefore important that the processing temperatures of PLA are reduced in order to minimise any thermal degradation of the polymer. One solution to this would be to process using supercritical fluids.

### *2.5 Supercritical Processing*

Interest in polymer processing with supercritical fluids acting as solvents or plasticizers has rapidly grown in recent years. Supercritical fluids make excellent solvents due to their special combination of gas-like viscosity and diffusivity and liquid-like density. Unlike liquid solvents, compressed gases can easily be removed by depressurising the system once the desired morphology change has occurred [39]. The use of supercritical fluids is particularly important when the viscosity of the bulk polymer is relatively high, as in the case of high molecular weight polymers. Relatively high viscosities require correspondingly high temperatures to facilitate processing, although this can lead to thermal degradation and deterioration in physical properties of the material being processed. In cases such as these, supercritical fluids can facilitate processing by acting as a solvent, reducing the intermolecular interactions and increasing the chain separation and enhancing the mobility of the polymer, in effect acting as a molecular lubricant [40]. Lewis-acid base type interactions occur between $CO_2$ and the carbonyl groups in the polymer. These consequently reduce chain-chain interactions and increase the mobility of the polymer

segments [41]. In semi-crystalline polymers it is assumed that the gas molecules preferentially penetrate the amorphous regions of the polymer [42]. The plasticisation of the amorphous phase increases the mobility of the polymer chains by reduction of the chain-chain interactions acting as a spacer between polymer chains. The plasticised chain segments may now adopt a crystalline form because of the increased mobility by $CO_2$ [43]. Therefore, scCO2 is able to induce crystallisation and cause it to occur prematurely [44,45,46]. The effects of dissolved carbon dioxide on the glass transition temperature was investigated using ultrasonic measurements of PLA and has been found to decrease nonlinearly as the $CO_2$ concentration increases [44]. Depression in the melting and glass transition temperature as a function of $CO_2$ pressure has been found in sPS and PET using high pressure DSC. Results were obtained over pressures 0-90 atm. The melting points were found to rapidly decrease initially and then level off at higher pressures [39]. Similarly, the glass transition temperature of PLA has been found to decrease as pressure (up to 650 MPa) was applied. Measurements were obtained post-processing using DSC [34].

Figure 2.11 shows the phase diagram for supercritical carbon dioxide ($scCO_2$). $CO_2$ becomes a supercritical fluid above its critical point of 301.1 K and 73.8 bar [47]. Many studies have looked into the use of supercritical $CO_2$ when processing biodegradable polyesters, especially the use of supercritical $CO_2$ in producing foamed products for packaging and tissue scaffolds biomedical applications [48,49,50]. With regards to polymeric foams, supercritical carbon dioxide behaves as a blowing agent. Foams are produced through the gas foaming technique, where the polymer is saturated with a gas or supercritical fluid such as $CO_2$ or $N_2$. This is performed in a system of constant pressure or temperature and then quenched by reducing pressure resulting in nucleation and growth of pores inside the polymer matrix. The pores continue to grow until the polymer vitrifies or an increase in

viscosity arises leading to the removal of the retractive force that is resitricting cell growth. This technique is particularly attractive as it allows the production of microcellular polymers enabling the bulk density of the material to be reduced without compromising its mechanical properties [51].

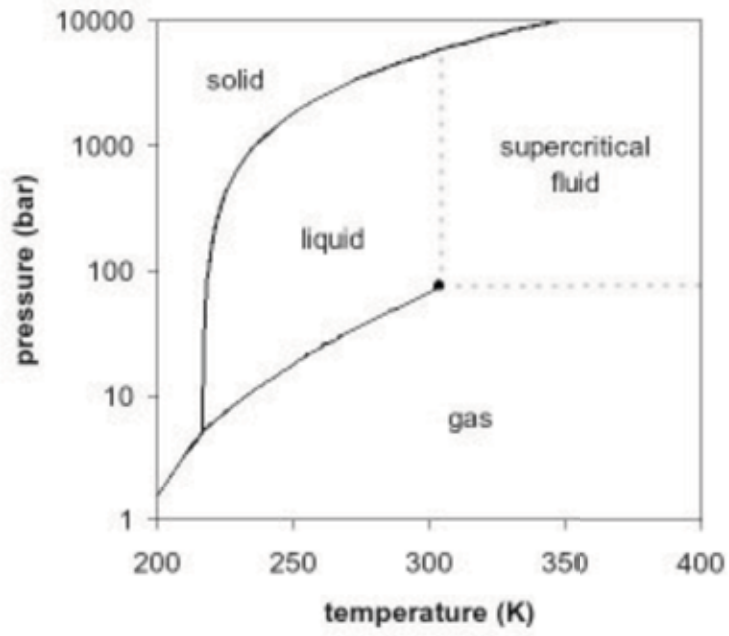


Fig. 2.11. Phase diagram of supercritical $CO_2$ [47]

Porosity of the foam is controlled by variation of pressure, temperature and depressurization rate [5]. Polycaprolactone foams have been produced by a batch foaming technique using $CO_2$-ethanol supercritical mixtures as blowing agents. However, non-uniform foams were produced when processed with pure $CO_2$. The regularity in the porosity became more uniform when ethanol was added to the supercritical mixture [51].

It has also been shown that in $scCO_2$ swollen polymers impregnation of solutes is accelerated. The plasticising and swelling effect of $scCO_2$ lowers the viscosity of biodegradable polymers

allowing bioactive guests to be mixed into the polymer [52]. This can be undertaken at temperatures close to ambient conditions leaving near homogeneous distribution [53].

The literature review of supercritical processing shows a wide range of studies and potential uses and applications for the system, however, melting point depression of semi-crystalline biodegradable polyesters by $CO_2$ is less well documented.

## 3.0 Projects Aims

There is a vast amount of literature published on the addition of D-lactide into predominantly L-lactide polymers [22,54,55,56,21,57]; however the addition of *meso*-lactide is significantly less researched. There is also a significant lack of research into the use of hot stage microscopy to determine the crystallisation kinetics of poly(L-lactide-co-*meso*-lactide). Rather than exploring the foaming process of PLA, the aim of the project is to quantify the melting point depression of PLA, which is an important step in the understanding of how to process PLA with carbon dioxide. Secondary to this, the crystallisation behaviour of poly(L-lactide-co-*meso*-lactide) will be studied using techniques such as differential scanning calorimetry (DSC), high pressure DSC and hot stage microscopy in order to gain a better understanding of the relationship between crystallisation temperature, melting temperature and overall degree of crystallinity, as well as crystallisation and growth rates in this seldom characterised material.

## 4.0 Experimental

### *4.1 Materials*

*4.1.1 Polylactic Acid (PLA 3051D)*

PLA 3051D was supplied in pellet form by NatureWorks LLC (Minnetonka, MN, USA) . Its molecular weight is 180,000 [58]. This grade of PLA is a random co-polymer; poly(L-lactide-co-meso-lactide) with approximately 3.3% D-lactide content and a residual monomer content of less than 0.3 wt.%. The glass to liquid transition temperature is in the region of 60°C and the melting region is typically 160°C. Other typical physical and mechanical properties are shown in table 1. The repeat unit [35] together with the chemical structures for the D, L and Meso stereoisomers [59] are shown in fig 4.1.

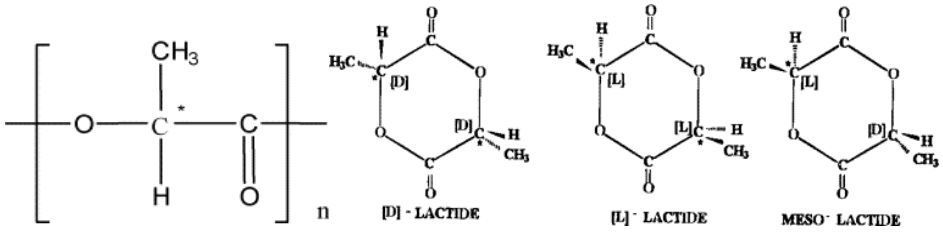


Fig. 4.1. PLA repeat unit [35] and D, L and Meso stereoisomer chemical structures [59].

| **Physical Properties (PLA 3051D)** | |
|---|---|
| Specific Gravity | 1.25 |
| Melt Index, g/10 min (210°C/2.16K) | 10-25 |
| Relative Viscosity | 3.0-3.5 |
| Crystalline Melt Temperature (°C) | 150-165 |
| Glass Transition Temperature (°C) | 55-65 |
| Clarity | Transparent |
| **Mechanical Properties (PLA 3051D)** | |
| Tensile Yield Strength, psi (MPa) | 7,000 (48) |
| Tensile Elongation at Break % | 2.5 |
| Notched Izod Impact, ft-lb/in (J/m) | 0.3 (0.16) |
| Flexural Strength, psi (MPa) | 12,000 (83) |
| Flexural Modulus, psi (MPa) | 555,000 (3828) |

Table 1. Typical properties of PLA, grade 3051D [60]

### *4.1.2 Polycaprolactone (PCL CAPA 6800)*

PCL (CAPA 6800) was supplied in pellet form by Perstorp Caprolactones (UK). PCL, another commercially important polymer, was selected as a comparison polymer to PLA. The molecular weight of CAPA 6800 is 80,000, a high molecular weight caprolactone and a degree of crystallinity of 33.1 ±1% (manufacturers data). Other typical properties provided by the supplier can be seen in Table 2. The melting region for the CAPA 6800 grade is typically 60°C with a glass transition temperature of - 60 °C. Crystallisation of PCL occurs

between the $T_g$ and $T_m$, around 30°C [61]. The repeat unit for CAPA 6800 is shown in fig. 4.2 [62].

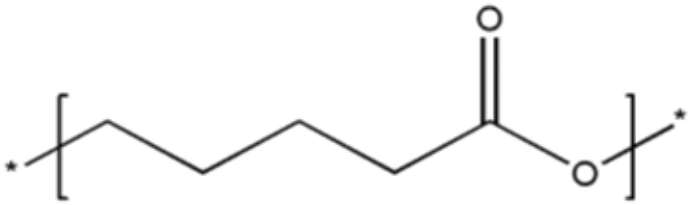

Fig. 4.2. The repeat unit for polycaprolactone (CAPA 6800) [62].

| **Typical Properties (CAPA 6800)** | |
|---|---|
| Physical Form | Approx 3mm pellets |
| Mean Molecular Weight | 80,000 |
| Melting Point | 58°C – 60°C |
| Water Content | <1.0% |
| Colour of 30% m/m Solution (Hazen) | <75 |
| Elongation at Break | 800% |
| Melt Flow Index | 3 g/10 min. with 2.16 kg,1" PVC die at 160°C |

Table 2. The typical properties of polycaprolactone CAPA 6800 [63].

## *4.2 Experimental Methods and Techniques*

### *4.2.1 Sample Preparation*

A sample preparation stage was required because the 'as received' pellets were too large for use in the characterisation techniques adopted for this study. Thermal analysis requires a uniform disc of mass in the region of 5 to 10 mgs. A thin disc allows good thermal contact with the thermal analyser cell and a relatively small mass reduces the effects of thermal lag within the sample. A typical polymer pellet is elliptical in longitudinal cross-section and exhibits a mass in excess of 20 mgs. Therefore attempts were made to cut pellets in half to reduce the mass and create a hemi-spherical sample with a circular transverse cross-section, but this was difficult to execute and led to significant variation in sample mass and cross-section. This process was used only to determine the 'as received' properties of the material but subsequently deemed inappropriate and was discontinued. Instead, a re-processing stage was introduced, enabling the production of a standard plaque suitable for further characterisation techniques.

The PLA pellets were initially dried to remove moisture. PLA is a hygroscopic thermoplastic, it readily absorbs moisture from the atmosphere. The presence of even small amounts of moisture will hydrolyse PLA in the melt phase, reducing the molecular weight, resulting in the decrease of the mechanical properties and the end-product quality. Therefore, the removal of moisture was achieved by storing the pellets at a temperature of 100 °C in a vacuum oven for a period of 4 hours. Since the melting temperature for PCL occurs in the region of 60°C, pellets of PCL were instead dried in a vacuum desiccator for a period of 24 hours prior to the moulding process.

The moulding temperature was selected in accordance with the relevant transition temperatures of the materials, i.e. either the glass transition temperature or the melting point. In the case of PLA, the moulding temperature was set at 200°C and in the case of PCL, the moulding temperature was set at 150°C. Temperatures in excess of the melting points were required in order to ensure the molten polymer was able to flow during the compression stage. In addition, order and preferential orientation of the polymer chains has been found to persist above the observed melting point. Incomplete destruction of the residual order would result in an increase in the rate of re-crystallisation on cooling, which in turn would lead to measured physical properties that would not be representative.

Plaques with a thickness of 0.5mm were produced by compression moulding using a spacer made from PTFE. The use of PTFE (due to it possessing a low coefficient of friction) enabled the easy removal of the plaque from the mould, as PCL especially, is often used as an adhesive in its applications. After 10 minutes under the specific temperatures and a pressure of 10 bar the plaques were removed from the press and allowed to cool to room temperature. For thermal analysis, circular samples with a diameter of 4mm were cut from the plaque using a hole-punch. The typical sample mass was 10mg.

### *4.2.2 Differential Scanning Calorimetry (DSC)*

The glass transition, melting and re-crystallisation behaviour of the materials were measured using a Perkin Elmer differential scanning calorimeter (DSC 7) interfaced to a personal computer (as seen in figures 4.3 and 4.4). The thermal response of the instrument was calibrated from the enthalpy of fusion with a known mass of indium (99.999% pure). The temperature of the calorimeter was calibrated using the melting point of tin. These materials

were selected for calibration as they covered the melting range of PLA and PCL. Corrections were made for thermal lag by extrapolation to zero heating rate. Plots of actual versus experimental melting points were linear and used to calibrate the calorimeter temperature.

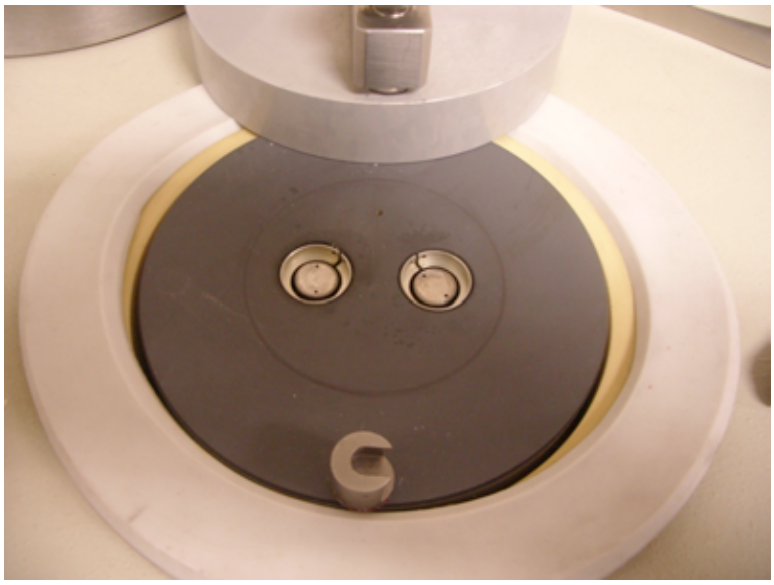

Fig. 4.3. Perkin Elmer differential scanning calorimeter (DSC 7).

Fig. 4.4. DSC sample and reference pans.

Disc shaped samples were contained in aluminium pans and an empty pan was used as a reference. Samples were initially heated at 10 °C/min from 25 °C to a temperature in the melt (selected in accordance with the material under investigation). The samples were then cooled back to 25°C at 10 °C/min to enable the creation of a known thermal history within the sample (and remove any remaining artifacts of the production process).

The glass transition temperature was measured according to the method proposed by Richardson [64]. This method is most appropriate for the 'as received' PLA as the $T_g$ for these samples often appear with a peak superimposed on the glass transition region. In this case, simply taking the mid-point of the transition can lead to erroneous values for the $T_g$. The Richardson method for determining the thermodynamic $T_g$ is shown graphically in fig. 4.5.

The melting point was measured from the DSC trace recorded at 10°C/min. All experiments measuring the melting point were performed with a fixed heating rate of 10°C/min. Samples were of near identical size and shape and therefore of similar mass.

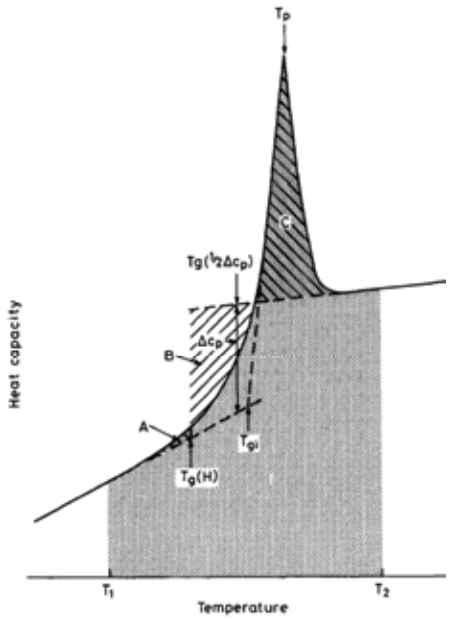


Fig. 4.5. The Richardson method for determining the $T_g$ [64].

The degree of crystallinity was determined as follows; a linear baseline was drawn from the first onset of melting to the last trace of crystallinity and the enthalpy of fusion was then calculated from the area under the endotherm (as seen in fig. 4.6). All experiments measuring the degree of crystallinity were performed with a heating rate of 50°C/min. This heating rate was selected because a faster heating rate was required to accurately measure the degree of crystallinity without influencing the results, it also helps to minimise any re-organisation of the polymer upon heating. Using a slower 10°C/min would enable crystallinity to develop during the experiment in the region between the glass transition and the melting point. However it was important to use 10°C/min when measuring the melting point as lower heating rates reduce the thermal lag in the system, providing a more accurate measure of the thermal transitions within the polymer.

The weight fraction degree of crystallinity (Xc) was defined as,

$$Xc = \frac{\Delta H_f(T_m)}{\Delta H_f^0(T_m^0)} \qquad \text{[eqn]}$$

where $\Delta H_f(T_m)$ is the enthalpy of fusion measured at the melting point and $\Delta H_f^0(T_m^0)$ is the enthalpy of fusion of the completely crystalline polymer. A literature value of 139.3 J $g^{-1}$ for $\Delta H_f^0(T_m^0)$ was used for PCL [65] and 93 J $g^{-1}$ for PLA [66].

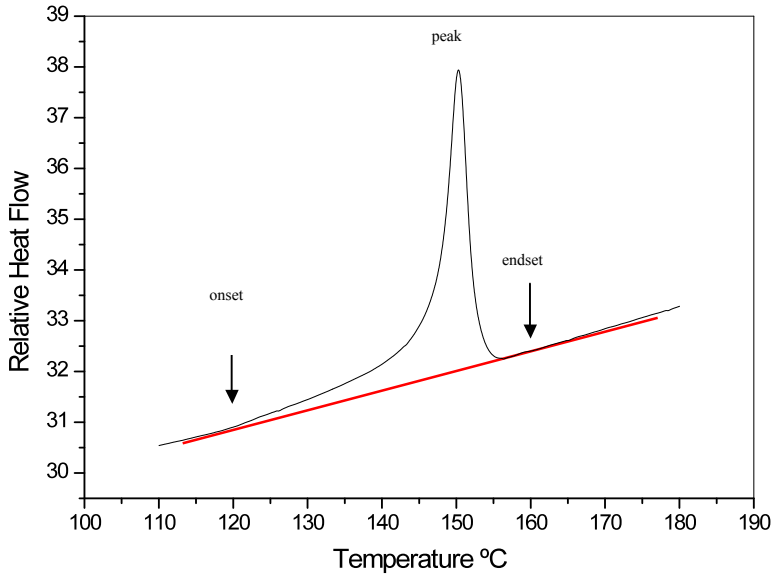


Fig. 4.6. A typical melting trace showing the measures of melting adopted in this study.

The re-crystallisation of the polymers were characterised simply by cooling from the melt at 10°C/min. In this case, re-crystallisation should appear as an exothermic peak between the melting point and the $T_g$. A typical example is shown in fig. 4.7.

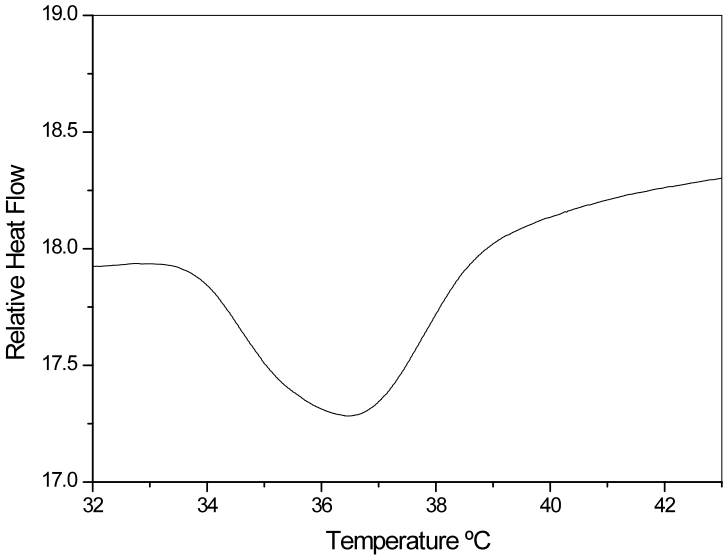


Fig.4.7. A typical re-crsytallisation from the melt in PCL.

### *4.2.3 High Pressure DSC*

The effect of $CO_2$ pressure on the thermal transitions in the above polymers was explored using a high pressure DSC. Enthalpy of fusion and temperature calibration of the DSC was carried out using a combination of tin, indium and zinc. The pressure gauge (seen in fig. 4.9) on the DSC was calibrated using a dead weight gauge. Samples were prepared via the same method as the conventional DSC (0.5mm discs cut from a hot pressed plaque). Each sample was weighed and placed into an aluminium 40µl pan and sealed with a lid. Reference pans were left empty. The lids of both pans were then pierced 10 times with a needle to allow $CO_2$ to diffuse in (shown in fig. 4.10). This method was applied to both reference and sample because conditions within the reference pan needed to be identical to that of the sample, only differing by the absence of a sample in order to allow power compensation measurements to take place.

The inlet of compressed $CO_2$ to the DSC was controlled via a number valves between the $CO_2$ cylinder and the DSC, with pressure regulated by an inlet valve on the DSC (as can be seen in fig. 4.8). A heating rate of 10°C/min and a $CO_2$ soak time of 60 minutes proved to be the best measurement parameters to reduce noise in the DSC trace. $CO_2$ was introduced to the polymer at a temperature of 25°C and after soaking, was heated to 180°C.

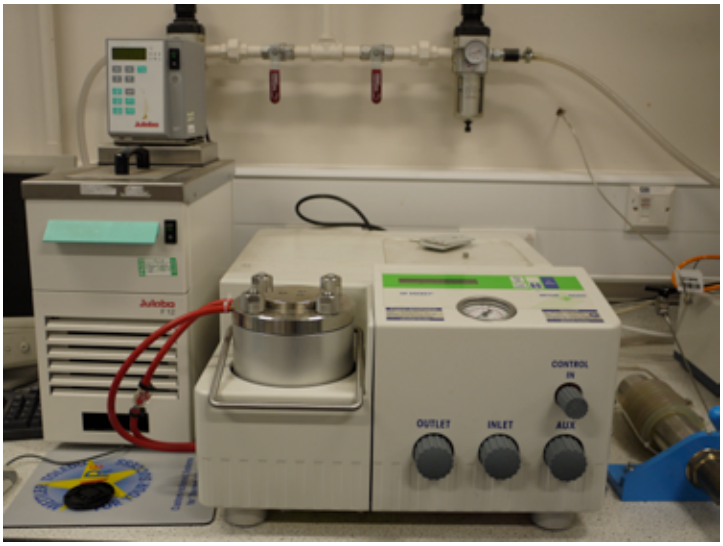


Fig. 4.8. High Pressure DSC and coolant system.


Fig. 4.9. High Pressure DSC.

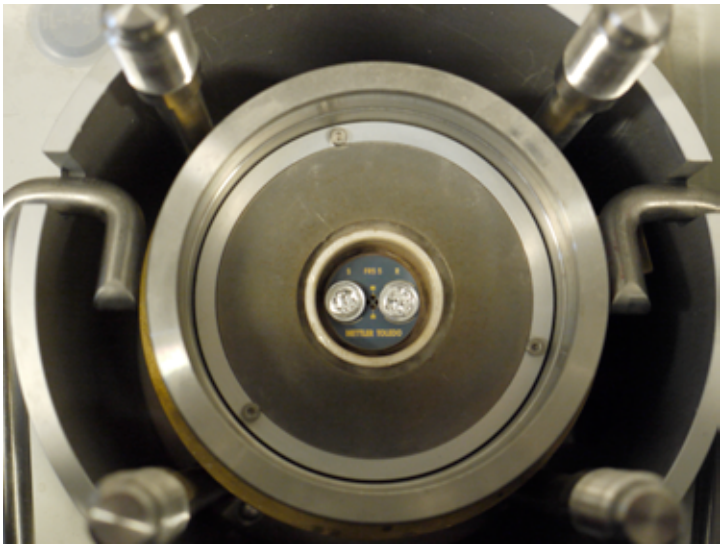

Fig. 4.10. High Pressure DSC sample and reference pans.

### *4.2.4 Hot-stage Microscopy*

Crystallisation behaviour was investigated using a Leitz polarised light microscope fitted with a Linkam TR600 hot-stage as seen in figures 4.11 and 4.12. The hot stage consisted of a furnace which was flushed with nitrogen to create an inert atmosphere around the sample. The temperature was controlled to 0.1°C using the Linkam LK600 controller. The temperature was calibrated using the melting point of sodium nitrate. A white light source was used to illuminate the sample and the transmitted light intensity was measured with a photomultiplier. The resulting variation in voltage was measured as a function of either time or temperature using a National Instruments data acquisition system interfaced to a personal computer.

The polarising filters in the microscope were crossed to exclude the light from the detector, so that the formation of birefringent regions in a crystallising polymer sample depolarised the light, thereby resulting in an increase in the transmitted light detected. The light intensity with time plots therefore reflect the development of crystallinity within the sample. This assumption has been shown to be correct by Pratt and Hobbs [67].

Sections, 15 μm thick, were cut from 3mm moulded plaques of the blends using a Leitz sledge microtome and placed between two glass coverslips. The sample was melted at 180°C for one minute and then cooled to the isothermal crystallisation temperature. The resulting light intensity with time plots were then used to measure the crystallisation kinetics. Photographic images were also recorded using a digital camera which was attached to the microscope.

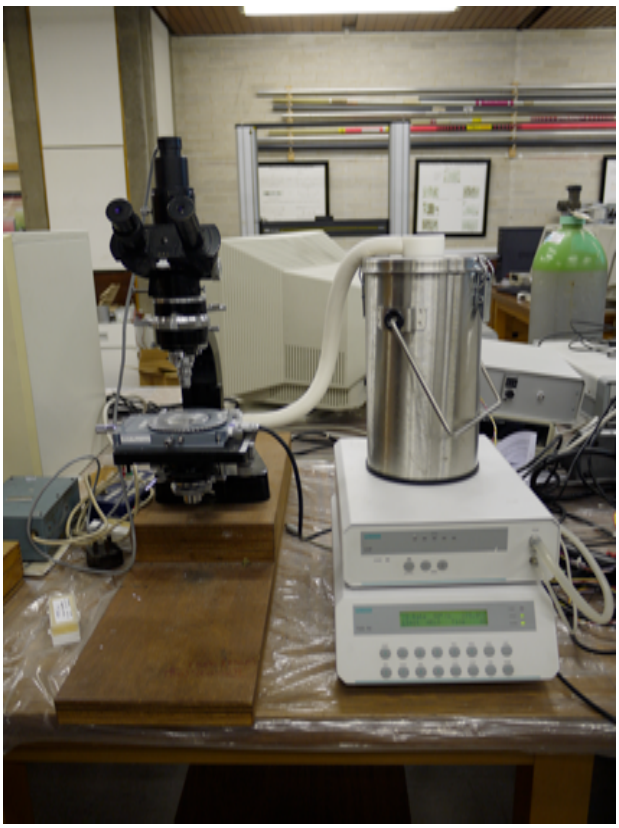

Fig. 4.11. Linkam TR600 hot-stage microscopy with controller.

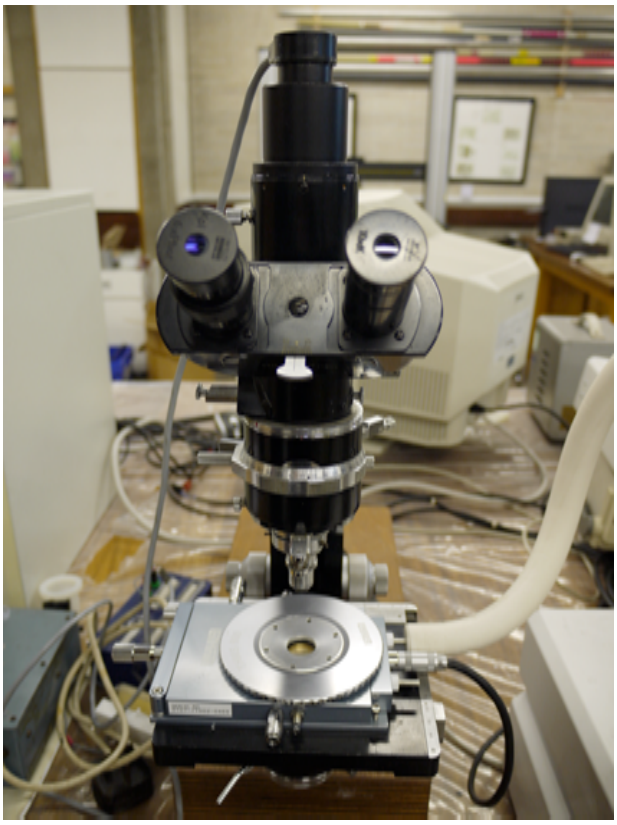

Fig. 4.12. Microscope with hot-stage attachment.

## 5.0 Results and Discussion

### *5.1 Initial Characterisation of PLA3051D*

*5.1.1 Characterisation Using Differential Scanning Calorimetry (DSC)*

The thermal response of an 'as received' PLA3051D pellet is shown in fig. 5.1. Two prominent transitions are apparent. The first was a glass transition typically appearing at 62°C, followed by a broad melting region between the temperatures of 120 to 180 °C. The presence of an endothermic peak on the $T_g$ probably originates from the release of stored strain in the sample from the disc cutting stage of processing. The use of the Richardson method (as mentioned previously) in the calculation of the thermodynamic $T_g$ was able to account for the presence of such a peak. Peak melting was found to occur at 152°C and the degree of crystallinity was found to be 39% ±1. The presence of the shoulder on the melting peak could be attributed to melting of thinner lamellae within the sample or is heating rate dependent. At lower temperatures it is thought that the thin lamella crystallites melt first. At higher temperatures the thicker lamellae subsequently melt [7]. Clearly, the initial morphology of PLA3051D was semi-crystalline. However, on cooling, no crystallisation exotherm was observed. Therefore, it can be concluded that within the timescale of cooling imposed by the DSC experiment (10°C per min), crystallisation was not able to occur. This observation has serious implications for the re-processing of pellets into standard plaques, since cooling from the melt appears to result in an amorphous morphology.

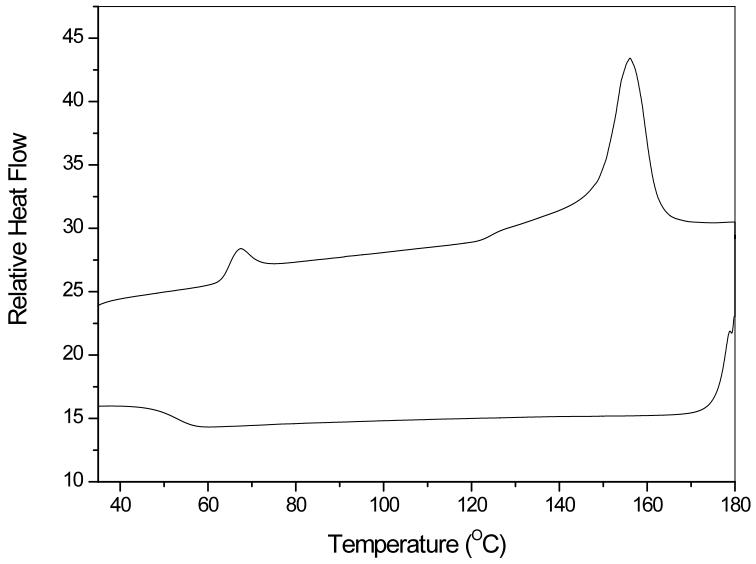


Fig. 5.1. The thermal response of the 'as received' PLA3051D.

### *5.1.2 Characterisation Using Hot-Stage Microscopy*

The timescale required for crystallisation was established in order to restore the initial morphology of the material. Hot-stage microscopy which was used to carry out isothermal crystallisation studies on PLA3051D. Under crossed polarising filters, the formation of polymer crystallites depolarise the light. Therefore, measurement of transmitted light intensity is a direct measure of the crystallinity in the sample under investigation [67]. Fig. 5.2 shows the variation of normalised light intensity with time for a series of crystallisation temperatures. The data confirms that PLA3051D possesses the ability to crystallise, if given sufficient time.

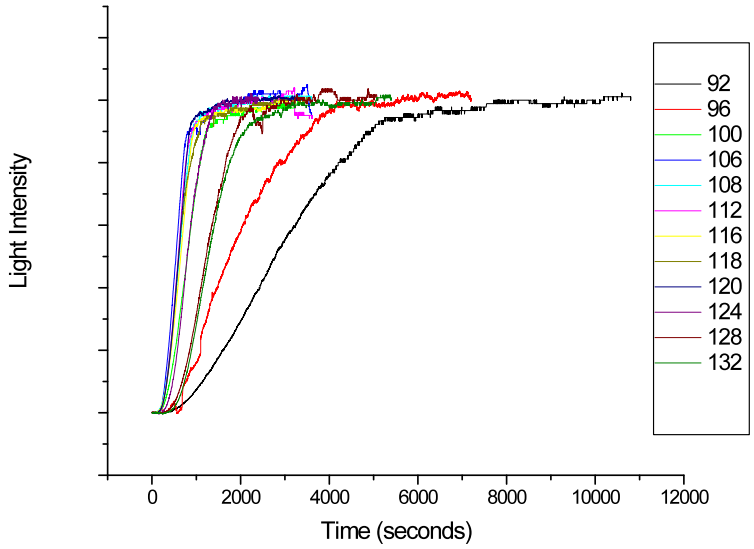


Fig. 5.2. The variation of light intensity with time for a series of crystallisation temperatures.

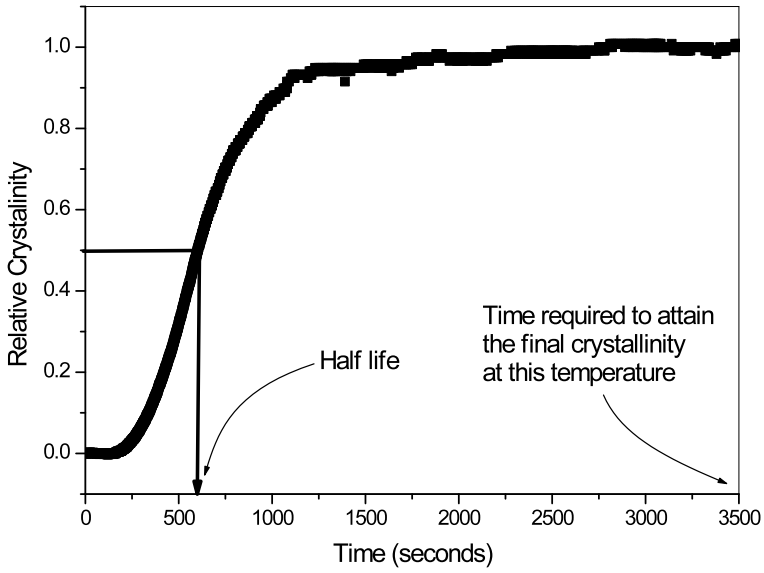


Fig. 5.3. Example of a crystallisation curve produced by hot-stage microscopy and how to determine its half-life.

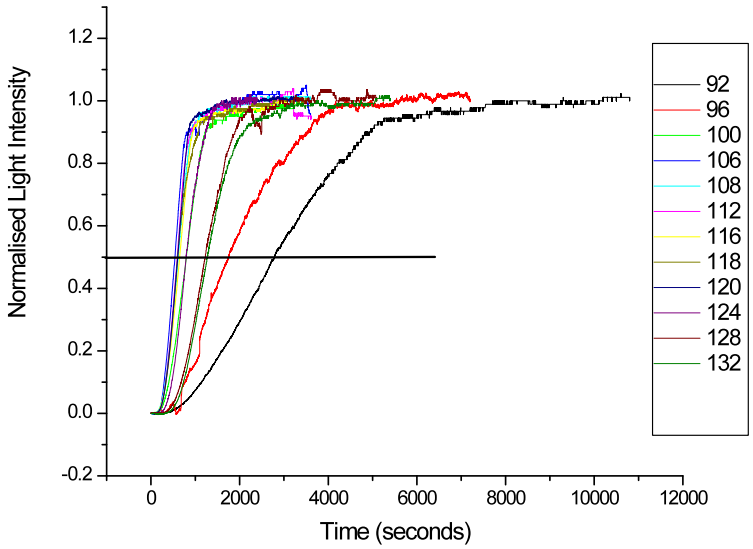


Fig. 5.4. Half-life of PLA3051D over varying temperatures.

The crystallisation rate in polymers is often expressed in terms of a half-life [68]. The crystallisation half-life of a polymer generally exhibits variation with temperature. The hot-stage data for PLA3051D showed no exception. Fig. 5.5 shows the variation of half-life with crystallisation temperature for PLA3051D. The trend can be explained by two competing crystallisation processes; nucleation and growth [69]. At temperatures approaching the $T_g$ (glass transition), the nucleation event is highly efficient but the subsequent growth of the crystallites is limited by relatively high viscosity in the melt. At temperatures approaching the $T_m$ (melting point), the nucleation event is limited, but due to relatively low viscosities, growth proceeds unhindered. These opposing temperature dependencies result in an optimum temperature, generally midway between $T_g$ and $T_m$. This is clearly apparent in fig. 5.5 with the shortest half-life occurring around 118°C. Figures 5.6 to 5.12 show photographic images of spherulites growing under isothermal conditions at 118°C over 60 minutes. Although the experiment ended with a spherulite diameter of 102.40μm, this

would continue to grow until impingement with other spherulites occurred. More spherulite images can be found in appendix 1.

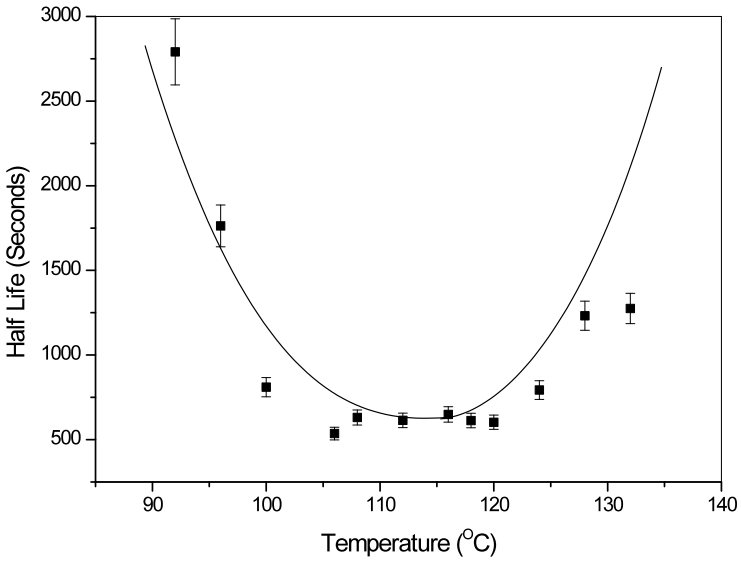


Fig. 5.5. The variation in half-life with crystallisation temperature for PLA3051D.

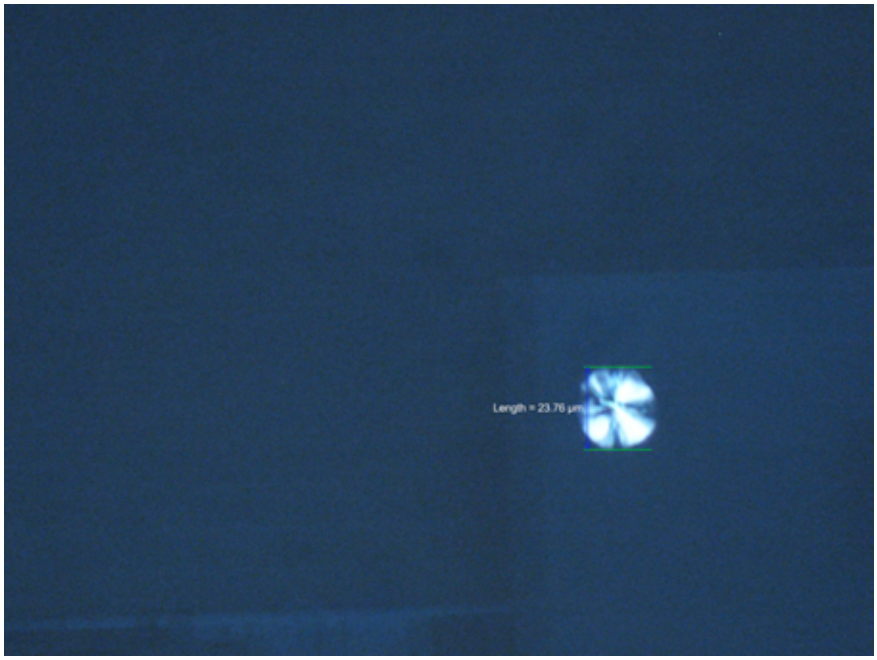

Fig. 5.6. Spherulite at 14 minutes of 118°C. Diameter is 23.76 μm.

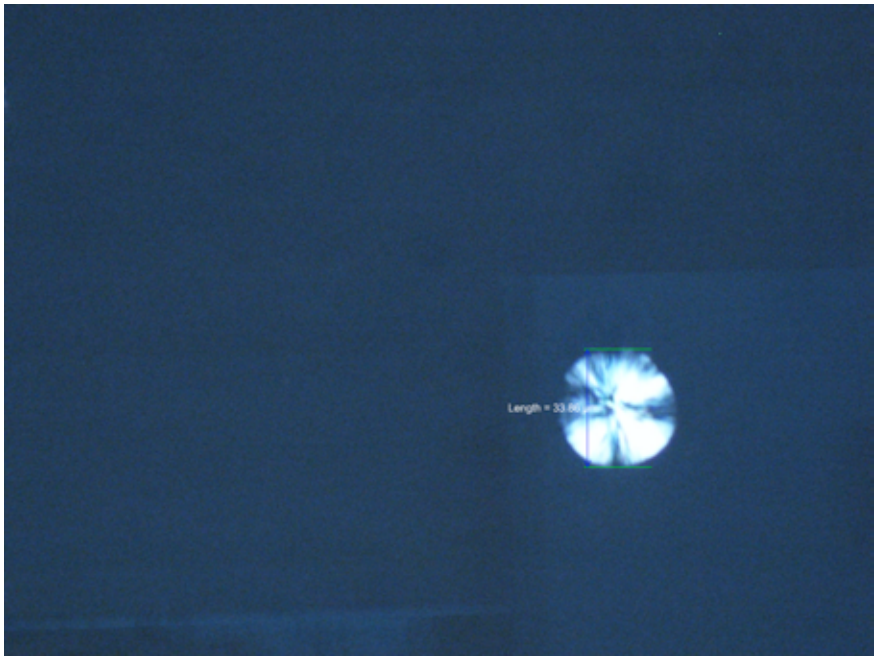

Fig. 5.7. Spherulite at 20 minutes of 118°C. Diameter is 33.86 μm.

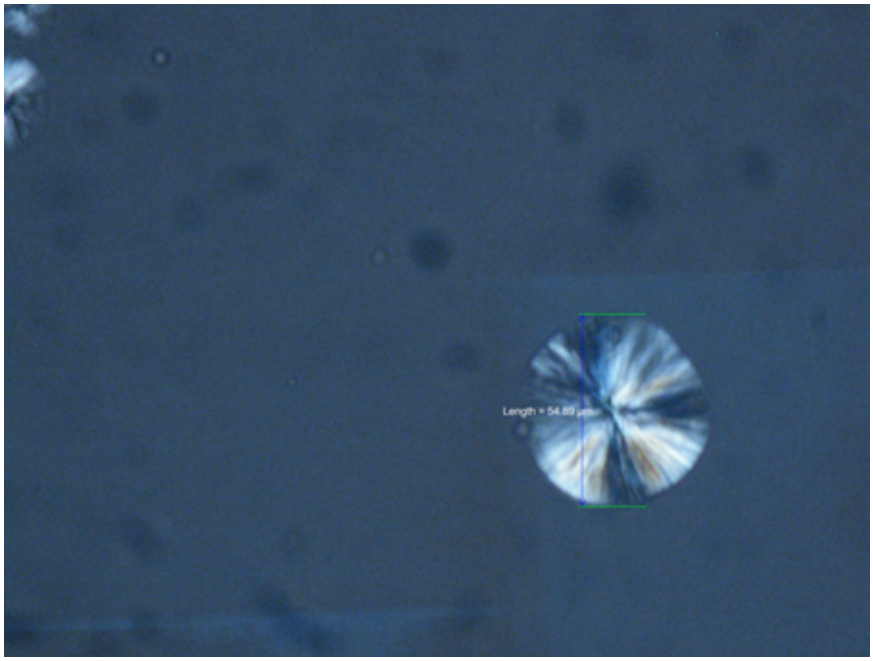

Fig. 5.8. Spherulite at 30 minutes of 118°C. Diameter is 54.89 μm.

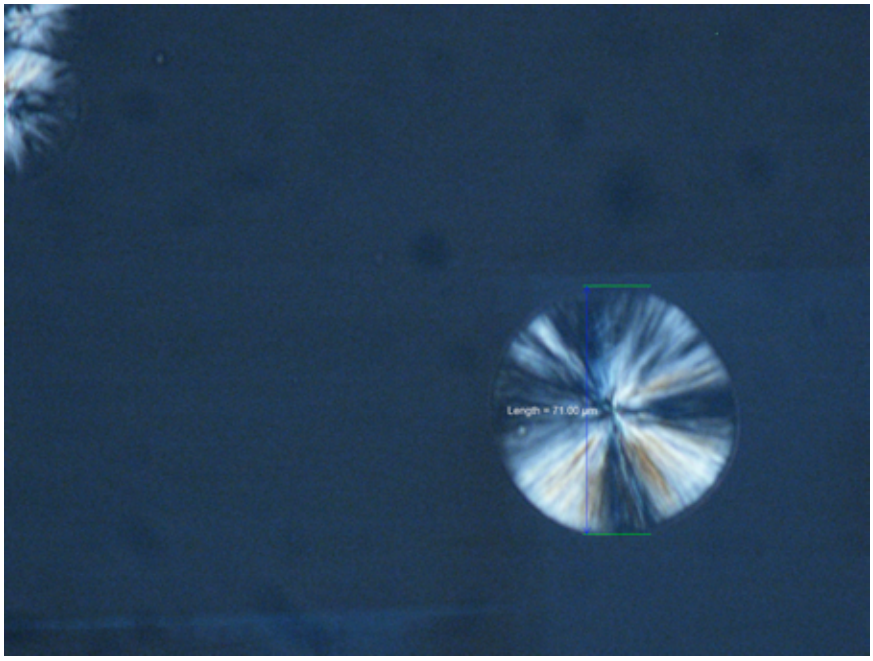


Fig. 5.9. Spherulite at 39 minutes of 118°C. Diameter is 71.00 µm.

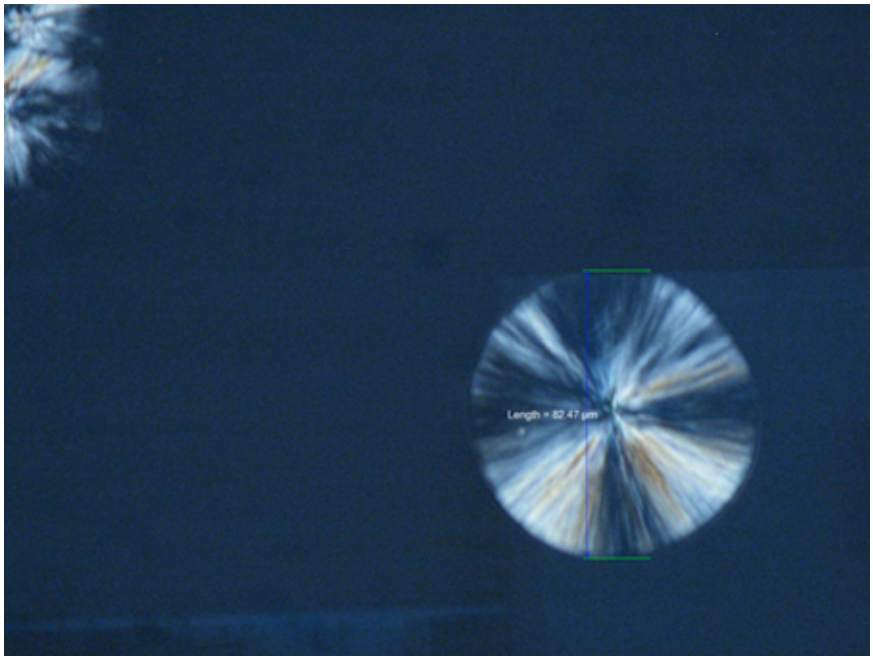


Fig. 5.10. Spherulite at 45 minutes of 118°C. Diameter is 82.47 µm.

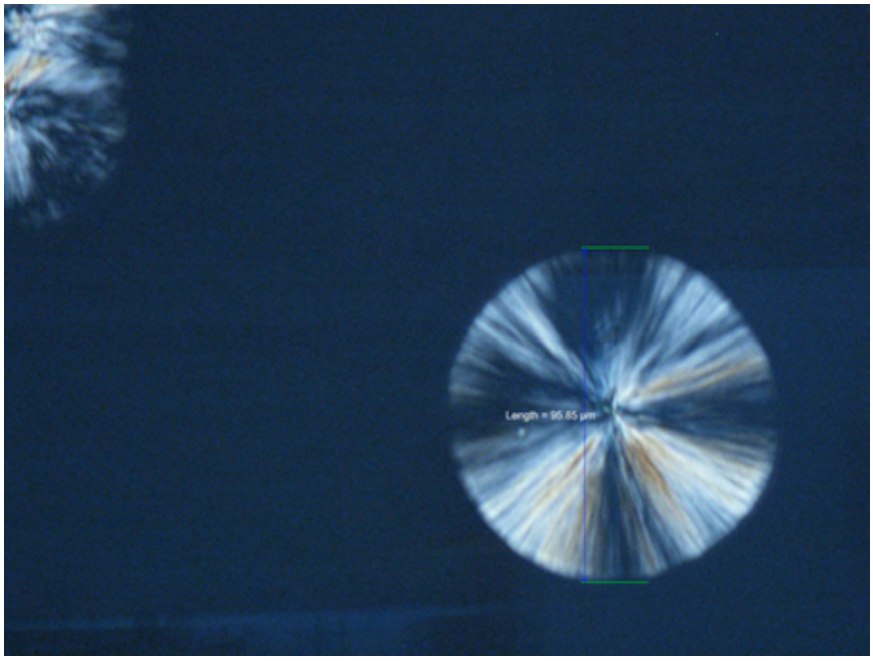


Fig. 5.11. Spherulite at 52 minutes of 118°C. Diameter is 95.85 µm.

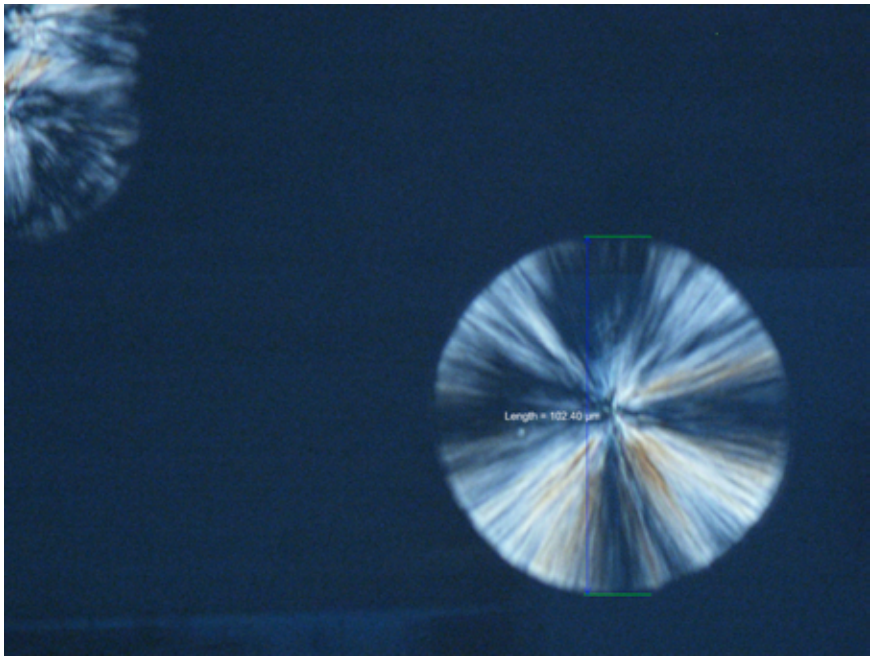


Fig. 5.12. Spherulite at 56 minutes of 118°C. Diameter is 102.40 µm.

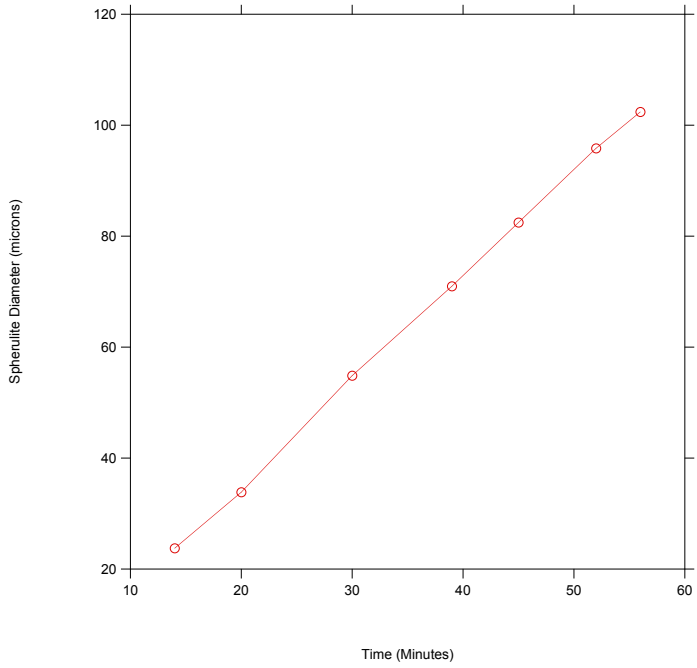


Fig. 5.13. Growth of a single spherulite over 60 minutes held at a temperature of 118°C. Growth would continue until impingement.

### *5.1.3 Re-crystallisation of PLA3051D*

The data presented in fig. 5.5 provided a means of selecting a suitable temperature for the re-crystallisation of PLA3051D, thereby restoring the 'as received' morphology. Given that the crystallisation process in this grade of PLA is relatively slow, a $T_{max}$ crystallisation temperature of 118°C was selected. Sample conditioning was carried out by annealing a series of amorphous samples of PLA3051D in an oven set at 118°C. Samples were removed at various time points up to a maximum of 16 hours. A melting trace of each of the samples was measured and recorded by DSC (shown in fig. 5.14, individual graphs can be viewed in appendix 2) and from this the change in enthalpy could be established by measuring the area under the melting peak (plotted in fig 5.15). The resulting crystallinity in each sample could

then be plotted. Fig. 5.16 illustrates the development of crystallinity in PLA3051D with time at a crystallisation temperature of 118°C. It was clear that a time of 2 hours was required to restore the original degree of crystallinity in this grade of PLA. Fig. 5.17 shows a comparison of the melting regions for both the 'as received' pellet and a sample conditioned for 2 hours at 118°C. The peak melting temperatures were almost identical at 152°C ± 0.5, but the degree of crystallinity in the re-conditioned sample was marginally greater at 40%. The difference in peak shape can be attributed to sample geometry in that the reconditioned disc maintains good thermal contact with the DSC pan to cell throughout the heating run, but the hemispherical sample of 'as received' PLA3051D flows on melting and thermal contact will therefore be non-uniform over the temperature range where melting occurs.

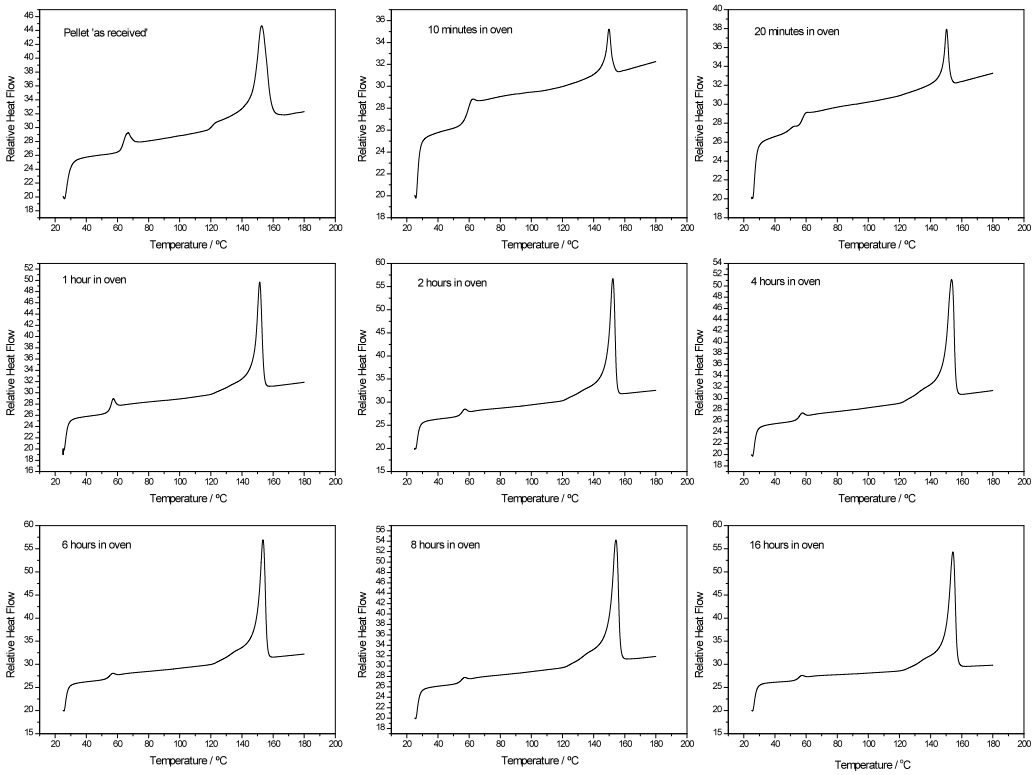


Fig. 5.14. Melting traces of samples held at varying times in an oven at 118°C.

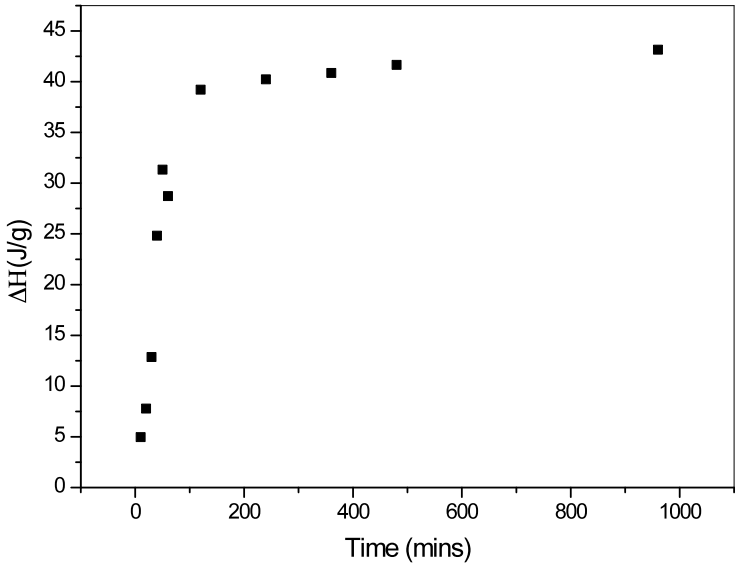


Fig. 5.15. The variation of ΔH plotted against conditioning time.

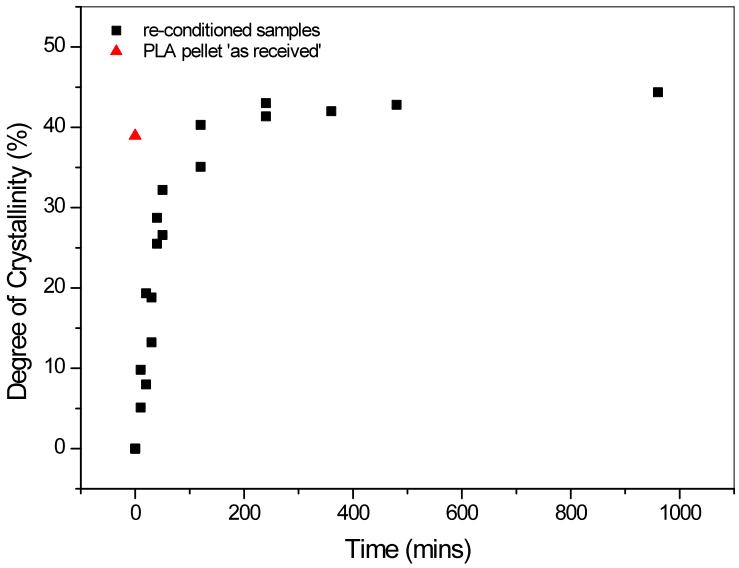


Fig. 5.16. The development of crystallinity with time at 118°C in PLA3051D.

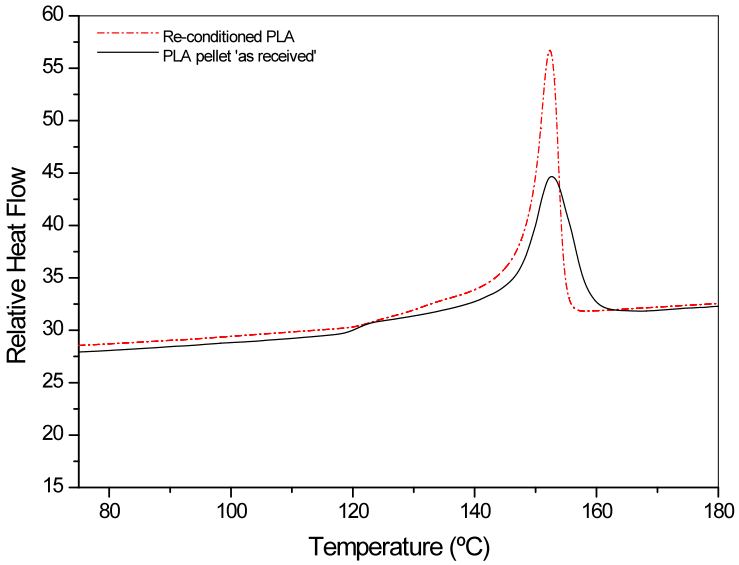


Fig. 5.17. A comparison of the melting regions for both the 'as received' pellet and a sample conditioned for 2 hours at 118°C. The peak $T_m$ of both samples is 152°C.

## *5.2 Melting Point Depression in PLA 3051D by $CO_2$*

### *5.2.1 Establishing The Optimal Experimental Conditions*

Initial melting point depression experiments found that the introduction of $CO_2$ into the system of the high pressure DSC also introduced noise into the results. This is due to convection currents in the high pressure DSC leading to changes in $CO_2$ density. The changes in the density are significant in the vicinity of the critical point of $CO_2$ and leads to inhomogeneous heat distribution in the system. To reduce noise in the DSC traces, certain methods could be applied, for example; running a blank correction method, where the noise recorded with just $CO_2$ and no sample is then subtracted from a result with a sample. An average could be taken of 3 or more results or a smoothing method could be applied within the software. Another alternative would be to take an inert material which has a matching heat capacity and identical weight to the sample of PLA and insert it into the reference pan

(which is normally left empty). Doing this helps to balance the signal and reduce the noise in the system. However, although these noise reduction methods were applied, noise was still significantly apparent in the results. Therefore, alternative variables were investigated with the endeavour to control residual noise.

Many trials were run with attempts to reduce the noise by altering the heating rates of the experiments and the diffusion times of $CO_2$ into the sample. Heating rates of 5, 10 and 20°C per minute were investigated along with diffusion times of 30, 60 and 120 minutes at a set pressure of 50 bar. It should be noted that the melting point depression studies were carried out using a different DSC instrument (manufactured by Mettler). The high pressure DSC presents the heat-flow data in a different way to the Perkin-Elmer system in that endothermic events appear as troughs in the heat-flow versus time curves rather than as peaks in the case of the Perkin-Elmer system. It was noticed that with increasing pressure, noise correspondingly increased. Therefore, 50 bar was chosen because there would be significant noise in the results at this pressure to provide a suitable comparison between variables. A slower heating rate is more desirable because it reduces the potential for thermal lag in the system and provides a more accurate measure of the thermal transitions (glass transition and melting point). A soak period where $CO_2$ has sufficient time to diffuse into the sample and settle to the same temperature is ideal. Figures 5.18 to 5.20 show these results. Fig. 5.18 compares the 30 minute soak time against the heating rates 5, 10 and 20 °C/min. Increasing the heating rate reduced the noise and increased the $T_m$ peak height. Soaking for 60 minutes (Fig. 5.19) produced traces with less noise in comparison to the 30 minute soak, with the same trend of increasing peak height with faster heating rates. Fig. 5.20 shows the results of soaking for 120 minutes. The plot showed that noise was greatest under this condition and also increased with faster heating rates. 20°C/min exhibited profound noise to the extent

that the melting peak could not be detected so this trace was not included in fig. 5.20. Therefore, it was decided that a heating rate of 10°C per minute and a diffusion time of 60 minutes provided the best compromise between noise and accuracy of results and this method was selected for all future experiments.

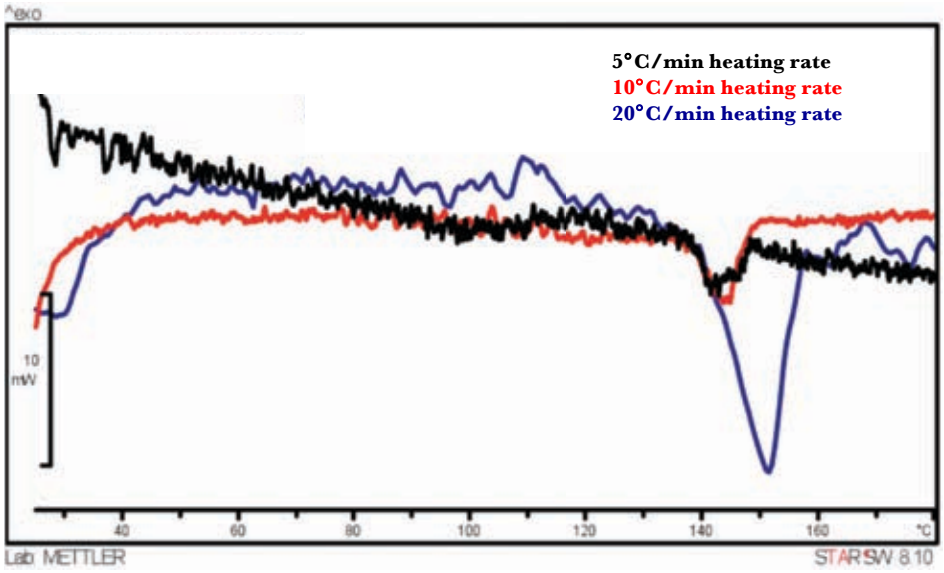


Fig. 5.18. Comparison of heating rates 5, 10 and 20°C/min with a $CO_2$ soak time of 30 minutes.

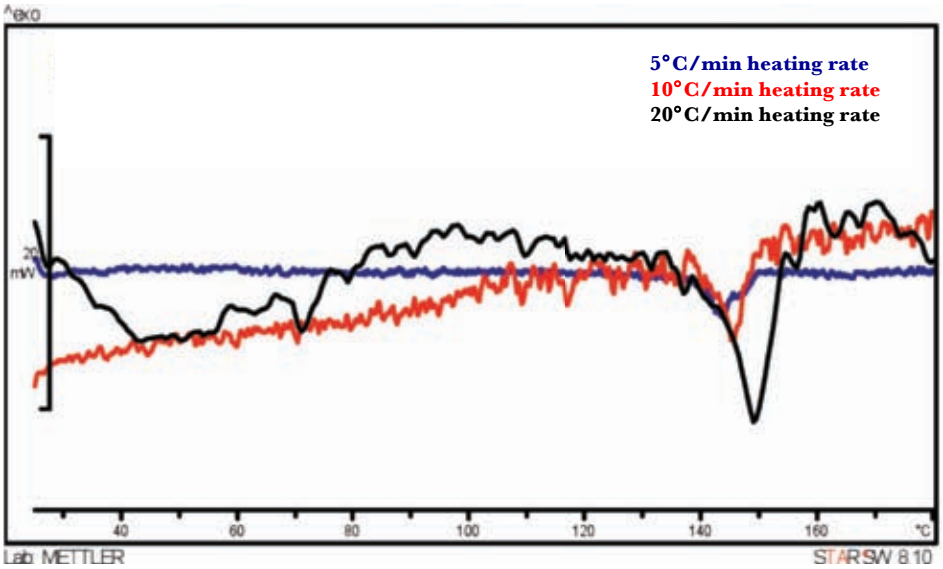


Fig. 5.19. Comparison of heating rates 5, 10 and 20°C/min with a $CO_2$ soak time of 60 minutes.

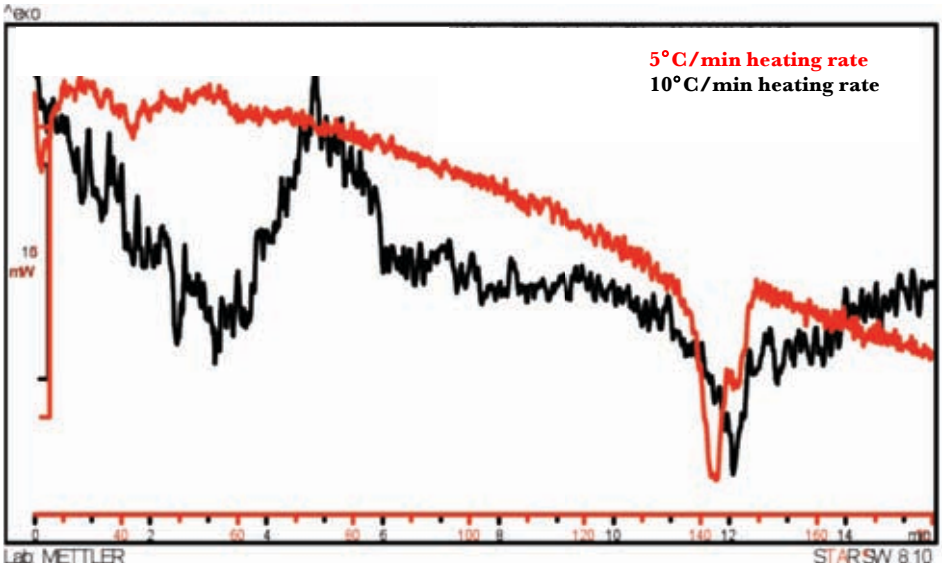


Fig. 5.20. Comparison of heating rates 5 and10°C/min with a $CO_2$ soak time of 120 minutes.

### *5.2.2 Measurement of Melting Point Depression in PLA*

The effect of $CO_2$ pressure on the thermal response of PLA3051D is shown in fig 5.21. It was apparent that as the background pressure of $CO_2$ increased, the melting point was found to decrease, this variation in melting point with pressure is illustrated in fig. 5.22.

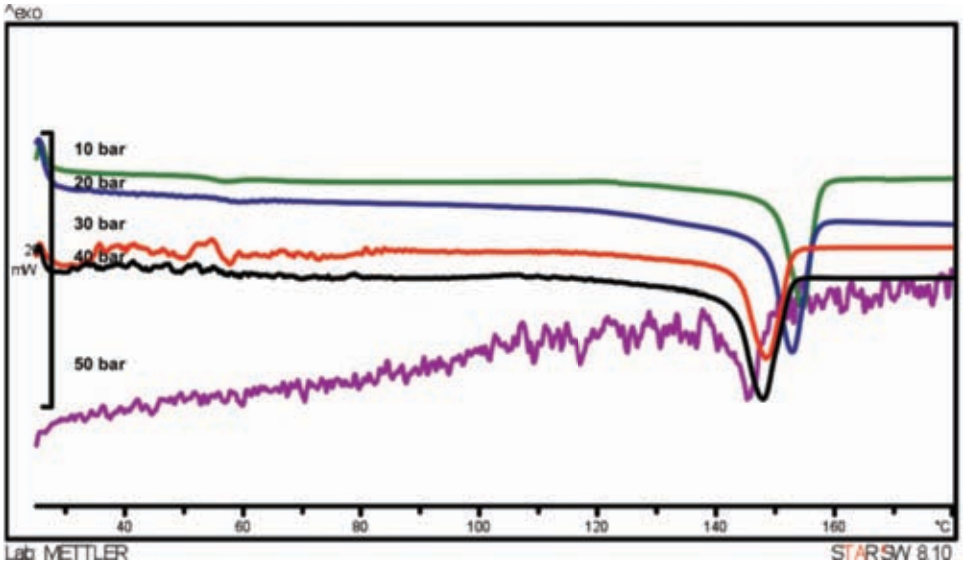


Fig. 5.21. The effect of $CO_2$ pressure on the thermal response of PLA3051D.

The gaseous properties of $CO_2$ enable it's diffusion into the free volume of PLA, between the individual chains. Once inside, $CO_2$ forms Lewis acid-base interactions with the carbonyl groups of PLA. This disrupts the inter/intra molecular interactions within PLA and consequently reduces the $T_m$ [41]. Elevating the pressure subsequently increases the amount of $CO_2$ present. This results in a more significant interaction with PLA and increasingly depresses the melting point.

It should be noted that there is a limit to the extent to which the melting point can be reduced. Interpolation of the data shown in fig. 5.19. would result in the formation of a plateau at which point no further decrease in melting point would be observed. Given the fact that the DSC traces become subject to increasing noise as the background pressure increases, no useful data can be obtained above 60 bar.

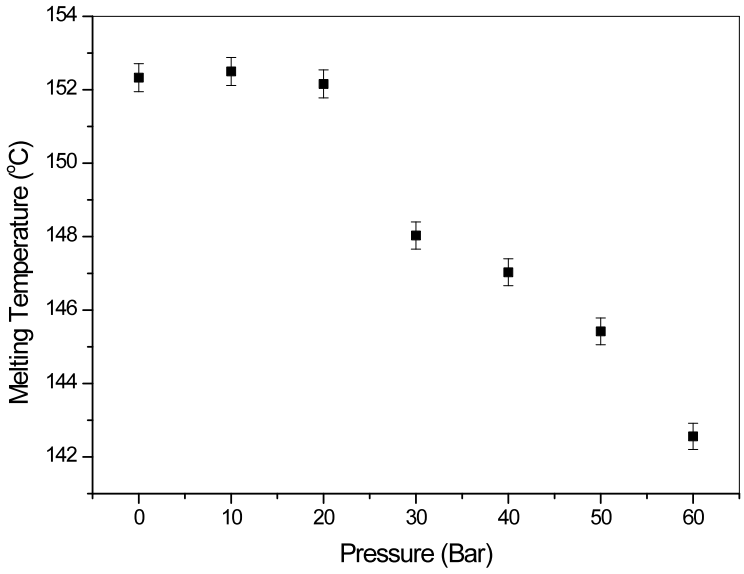


Fig. 5.22. The variation in melting point with pressure in PLA.

## *5.3 PCL CAPA6800*

### *5.3.1 Initial Characterisation of PCL*

The thermal response of PCL indicated that the morphology of the polymer 'as received' is semi-crystalline. Fig. 5.23 shows a broad melting region spanning from 40°C to 65°C. The melting temperature as shown by the peak melting point was 60°C. On cooling from the melt at 10 °C per min, a crystallisation exotherm was clearly visible in the temperature region from 40 to 30°C. Fig 5.24 illustrates the re-heat of the sample shown in fig 5.23. The only difference in the traces is the temperature corresponding to the peak melting point, in the case of the re-heated sample shown in fig. 5.24, the melting point appeared at 54°C. The difference in melting points was simply due to a difference in thermal history between the sample 'as received' and that imposed by the cooling rate adopted in the DSC.

### *5.3.2 Characterisation of The Melting Point Depression Using High-Pressure DSC.*

As in section 5.2, the high-pressure DSC adopted for these experiments presents endothermic events as troughs on the heat-flow versus temperature traces. With this in mind, it is clear to see in fig. 5.25 that the melting point (as defined by the melting peak position) decreased with increasing background $CO_2$ pressure. This variation in melting point with pressure is illustrated in fig 5.26. Again, the traces at elevated background pressures become increasingly noisy and as a result, the lower limit of melting point depression was not reached.

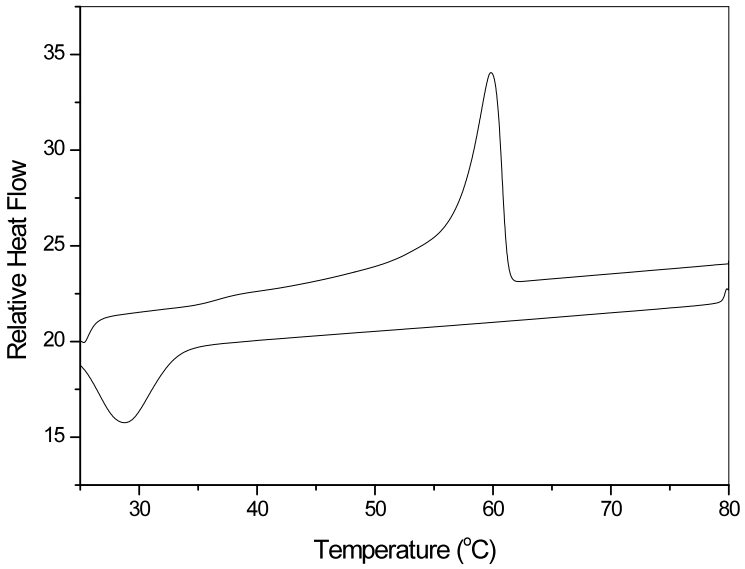


Fig. 5.23. The thermal response of the 'as received' PCL6800.

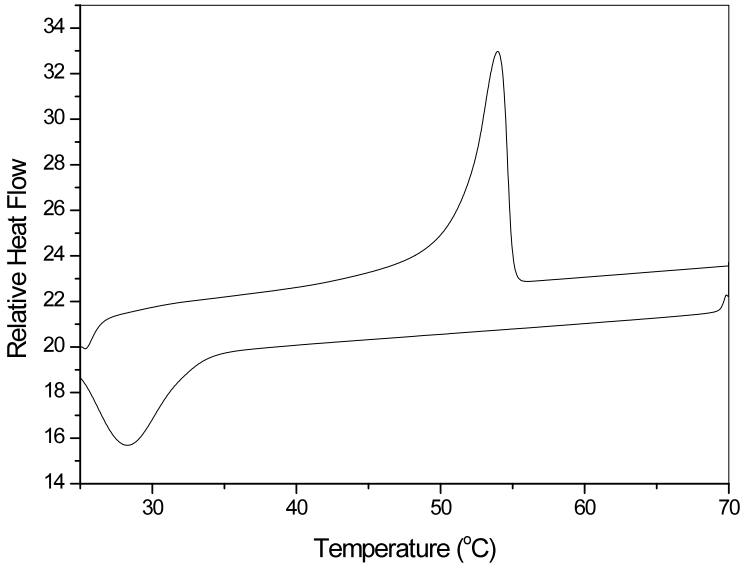


Fig. 5.24. The re-heat thermal response of PCL.

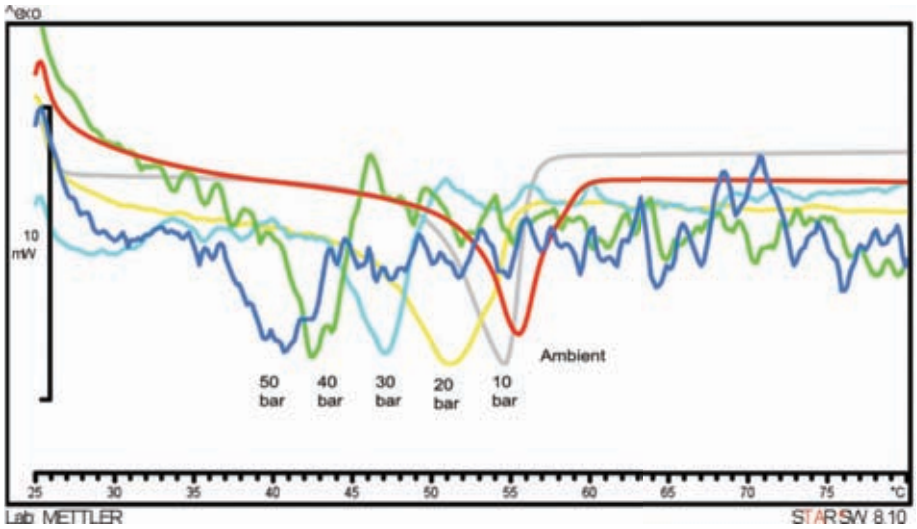


Fig. 5.25. Melting point depression in PCL detected using high pressure DSC.

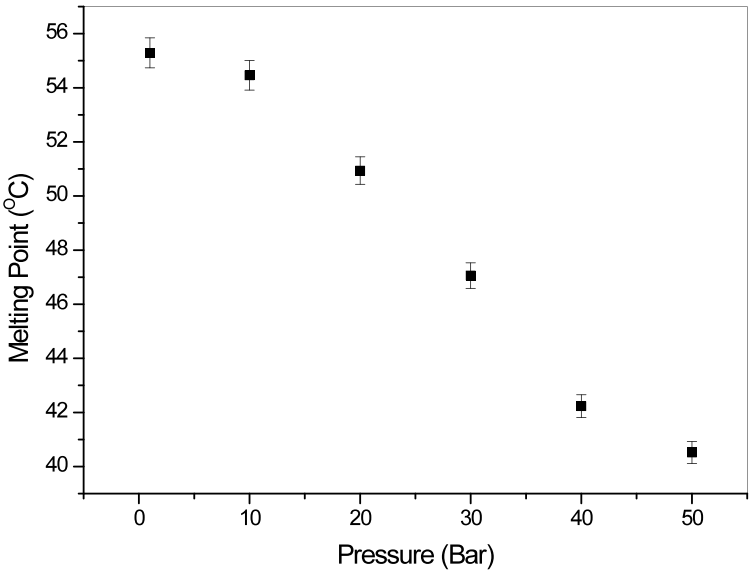


Fig. 5.26. The variation in melting point with pressure in PCL.

## 6.0 Conclusions and Future Work

Biodegradable polymers are becoming increasingly popular as their applications broaden into all aspects of the biomedical field and food packaging industries. The growing interest for the use of PLA in many biomedical applications as well as food packaging is clearly apparent in recent literature. A major reason for the increasing attention towards PLA is due to it being derived from natural resources allowing it to become easily composted therefore reducing the pressure upon landfill. With this in mind PLA is set to play a large role in many future applications as it provides a much lower environmental impact than other polymers currently used. Unfortunately, to process PLA high temperatures are needed, at which degradation of the material begins destroying many of its important properties. The aim of this study therefore was to investigate the potential use of $CO_2$ in processing PLA. $CO_2$ would act as a solvent, disrupting the molecular interactions within the polymer and thereby lowering the melting point and processing conditions.

The crystallisation kinetics and thermal properties of PLA were established using DSC and hot-stage microscopy. The use of hot-stage microscopy provided useful information that enabled the re-processing of PLA into more suitable sample sizes for investigation with all techniques undertaken in this study.

Using a $CO_2$/sample diffusion time of 60 minutes in the high pressure DSC, it was found that melting point of PLA was reduced with increasing $CO_2$ pressures. Due to limitations in the particular equipment used, the noise above 50 bar of $CO_2$ became too great to be able to detect and measure a melting point. Several attempts at subtracting data and running blank experiments were made, but this made no improvement on results obtained above 50 bar. However, the results obtained up to 50 bar clearly indicated a depression of the melting point with increasing $CO_2$ pressures. Speculations can be made towards the results above 50 bar,

however it is thought that at some point the reduction of the melting point of PLA will reach a minimum and then continue to plateau.

Polycaprolactone, an alternative biomaterial was also investigated as a comparison. Similarly, PCL had a significant reduction in melting point when soaked with $CO_2$ at varying pressures.

These results give promising solutions towards the processing of inherently problematic polymers. For future work, a more detailed analysis of the melting point depression could be undertaken using a high pressure rheometer or alternatively fourier transform infrared spectroscopy (FTIR) where results could be obtained for experiments above 50 bar. Further detail into the hot-stage method could also be carried out, with the possibilities of performing a direct comparison between the photo multiplier and photo resistor.

Using the melting point depression data, extrusion trials can be undertaken. Some exploration into the injection of $CO_2$ into the processing of PLA is needed. One suggestion could be to use a number of injection nozzles into the polymer melt and barrel of an extruder or an alternative method could be by an initial diffusion of $CO_2$ in a purposely designed vacuum hopper at the beginning of the process. As a consequence of using certain pressures of $CO_2$, foaming of the material may occur adding another dimension to the processing of PLA and expanding the applications into which PLA can be used.

## 7.0 References


[1] Plastics – The Facts 2010, An analysis of European plastics production, demand and recovery for 2009, 1-31. (Found on http://www.plasticseurope.org/)

[2] http://news.bbc.co.uk/1/hi/sci/tech/7316441.stm

[3] http://www.resbrasil.com.br/default.asp?i=10&a=0&c=496

[4] Lee, S.-T.; and Scholz, D. Polymeric Foams – Technology and Developments in Regulation, Process and Products, CRC Press, Taylor and Francis Group, Boca Raton, 2009.

[5] Aionicesei, E.; Skerget, M.; and Knez, Z. Measurement of $CO_2$ solubility and diffusivity in poly(L-lactide) and poly(D,L-lactide-*co*-glycolide) by magnetic suspension balance. *The Journal of Supercritical Fluids*, 2008, 47, 296-301.

[6] Callister, W.D. Materials Science and Engineering, An Introduction, 6th ed., USA, *John Wiley & Sons*, 2003, 469-473.

[7] Ehrenstein, G., W. Polymeric Materials, Structure – Properties –Applications, USA, *Hanser*, 2001, ch 2, 3-24.

[8] Morton-Jones, D.H. Polymer Processing. United Kingdom, *Chapman & Hall*, 1989, ch 1, 1-29.

[9] Kroschwitz, J.I. Concise Encyclopedia of Polymer Science and Engineering. *John Wiley & Sons Inc*, USA, 1998, 231-234.

[10] Jenkins, M.J.; and Harrison, K. The effect of molecular height on the crystallisation of PCL, *Polymers for advanced technologies*, 2006, 17, 1-5.

[11] Kesel, C.De.; Lefevre,C.; Nagy, J.B.; and David, C. Blends of polycaprolactone with polyvinylalcohol: a DSC, optical microscopy and solid state NMR study. *Polymer*, 1999, 40, 1969-1978.

[12] Farrington, D.W.; Lunt, J.; Davies, S.; and Blackburn, R.S. Poly(lactic acid) fibres. *Biodegradable and sustainable fibres*, 2005, Ch 6, 191-220.

[13] Garlotta, D. A Literature Review of Poly(lactic acid). *Journal of Polymers and the Environment*, 2002, 9 (2), 63-84.

[14] Lipinsky, E.S.; and Sinclair, R.G. Is lactic-acid a commodity chemical. *Chemical engineering progress*, 1986, 82 (8), 26-32.

[15] Vert, M.; Schwacch, G.; and Coudance, J. Present and future of PLA polymers. *Journal of macromolecular science-pure and applied chemistry*, 1995, A32 (4), 787-796.

[16] Siracusa, V.; Rocculi, P.; Romani, S.; & Dalla Rosa, M. Biodegradable polymers for food packaging: a review. *Trends in Food Science & Technology*, 2008, 19, 634-643.

[17] Lim, L.-T.; Auras, R.; and Rubino, M. Processing technologies for poly(lactic acid). *Progress in Polymer Science*, 2008, 33, 820-852.

[18] Liao, R.; Yang, B.; Yu, W.; and Zhou, C. Isothermal Cold Crystallisation Kinetics of Polylactide/Nucleating Agents. *Journal of Applied Polymer Science,* 2007, 104, 310-317.

[19] Miyata, T.; and Masuko, T. Crystallisation Behaviour of Poly(L-lactide). *Polymer*, 1998, 39 (22), 5515-5521.

[20] Mano, J.F.; Wang, Y.; Viana, J.C.; Denchev, Z.; and Oliveira, M.J. Cold Crystallization of PLLA Studied by Simultaneous SAXS and WAXS. *Macromolecular Materials Engineering*, 2004, 289, 910–915.

[21] Schmidt, S.C.; and Hillmyer, M.A. Polylactide stereocomplex crystallites as nucleating agents for isotactic polylactide. *Journal of polymer science part b-polymer physics*. 2001, 39 (3), 300-313.

[22] Baratian, S.; Hall, E.S.; Lin, J.S.; Xu, R.; and Runt, J. Crystalization and solid-state structure of random polylactide copolymers: Poly(L-lactide-co-D-lactide)s. *Macromolecules*, 2001, 34, 4857.

[23] Kolstad, J.J. Crystallization Kinetics of Poly(L-lactide-co-meso-lactide). *Journal of Applied Polymer Science*, 1996, 62, 1079-1091.

[24] Huang, J.; Lisowski, M.S.; Runt, J.; Hall, E.S.; Kean, R.T.; Buehler, N.; and Lin, J.S. Crystallization and Microstructure of Poly(l-lactide-*co*-*meso*-lactide) Copolymers, *Macromolecules*, 1998, 31 (8), 2593-2599.

[25] Cho, J.; Baratian, S.; Kim, J.; Yeh, F.; Hsiao, B.S.; and Runt, J. Crystallization and structure formation of poly(L-lactide-co-meso-lactide) random copolymers: a time-resolved wide- and small-angle X-ray scattering study. *Polymer*, 2003, 44, 711–717.

[26] Kanchanasopa, M.; Manias, E.; and Runt, J. Solid-state microstructure of poly(L-lactide) and L-lactide/meso-lactide random copolymers by atomic force microscopy (AFM). *Biomacromolecules.* 2003, 4 (5), 1203-1213.

[27] Abe, H.; Harigaya, M.; Kikkawa, Y.; Tsuge, T.; and Doi, Y. Crystal growth and solid-state structure of poly(lactide) stereocopolymers. *Biomacromolecules*, 2005, 6 (1), 457-467.

[28] Lunt, J. Large-scale production, properties and commercial applications of polylactic acid polymers. *Polymer degradation and stability*. 1998, 59 (1-3), 145-152.

[29] Plastics Technology. 1998, 13-15.

[30] Elzein, T.; Nasser-Eddine, M.; Delaite, C.; Bistac, S.; Dumas, P. FTIR study of Polycaprolactone chain organisation at interfaces. *Journal of Colloid and Interface Science*, 2004, 273, 381-387.

[31] Labet, M.; and Thielemans, W. Synthesis of polycaprolactone: a review. *Chemical Society Reviews*, 2009, 38, 3484-3504.

[32] Zhu, G.; Xu, Q.; Qin, R.; Yan, H.; and Liang, G. Effect of *y*-radiation on crystallization of Polycaprolactone. *Radiation Physics and Chemistry*, 2005, 74, 42-50.

[33] Coombes, A.G.A.; Rizzi, S.C.; Williamson, M.; Barralet J. E; Downes S.; and Wallace W.A. Precipitation casting of polycaprolactone for applications in tissue engineering and drug delivery. *Biomaterials*, 2004, 25 (2), 315.

[34] Ahmed, J.; Varshney, S.K.; Zhang, J-X.; and Ramaswamy, H. S. Effect of high pressure treatment on thermal properties of polylactides. *Journal of Food Engineering*, 2009, 93, 308-312.

[35] Maharana, T.; Mohanty, B.; and Negi, Y.S. Melt-solid polycondensation of lactic acid and its biodegradability. *Progress in Polymer Science*, 2009, 34, 99-124.

[36] Huang, J.; Lisowski, M.S.; Runt, J.; Hall, E.S.; Kean, R.T.; Buehler, N.; and Lin, J.S. Crystallization and Microstructure of Poly(L-lactide-co-*meso*-lactide) Copolymers. *Macromolecules*, 1998, 31, 2593-2599.

[37] Karst, D.; and Yang, Y. Effect of Arrangement of L-lactide and D-lactide in Poly[(L-lactide)-*co*-(D-lactide)] on its Resistance to Hydrolysis Studied by Molecular Modeling. *Macromolecular Chemistry and Physics*, 2008, 209, 168-174.

[38] Park, K.I.; and Xanthos, M. A study on the degradation of polylactic acid in the presence of phosphonium ionic liquids. *Polymer Degradation and Stability*, 2009, 1-11.

[39] Zhang, Z.; and Handa, P.Y. $CO_2$-Assisted Melting of Semicrystalline Polymers. *Macromolecules*, 1997, 30, 8505-8507.

[40] Leeke, G.A.; Cai, J.; and Jenkins, M. Solubility of Supercritical Carbon Dioxide in Polycaprolactone (CAPA 6800) at 313 and 333 K. *Journal of chemical and engineering data.* 2006, 51, 1877-1879.

[41] Shen, Z.; McHugh, M.A.; Xu, J.; Belardi, J.; Kilic, S.; Mesiano, A.; Bane, S.; Karnika, C.; Beckman, E.; and Enick, R. CO2-solubility of oligomers and polymers that contain the carbonyl group. *Polymer*, 2003, 44, 1491-1498.

[42] Kazarian, S.G. Polymer Processing with Supercritical Fluids. *Polymer Science Series C*, 2000, 42 (1), 78-101.

[43] Shieh, Y.-T.; Su, J.-H.; Manivannan, G.; Lee, P.H.C.; Sawan, S.P.; and Spall, W.D. Interaction of Supercritical Carbon Dioxide with Polymers. I. Crystalline Polymers. *Journal of Applied Polymer Science*, 1996, 59, 695-705.

[44] Reignier, J.; Tatibouet, J.; and Gendron, R. Effect of Dissolved Carbon Dioxide on the Glass Transition and Crystallisation of Poly(lactic acid) as Probed by Ultrasonic Measurements. *Journal of Applied Polymer Science*, 2009, 112, 1345-1355.

[45] Yu, L.; Liu, H.; Dean, K.; and Chen, L. Cold Crystallization and Postmelting Crystallization of PLA Plasticized by Compressed Carbon Dioxide. *Journal of Polymer Science: Part B: Polymer Physics*, 2008, 46, 2630-2636.

[46] Zhai, W.; Ko, Y.; Zhu, W.; Wong, A.; and Park, C.B. A Study of the Crystallization, Melting, and Foaming Behaviours of Polylactic Acid in Compressed $CO_2$. *International Journal of Molecular Sciences*, 2009, 10, 5381-5397.

[47] http://www.newworldencyclopedia.org/entry/Supercritical_fluid

[48] Tsivintzelis, I.; Pavlidou, E.; and Panayiotou, C. Porous scaffolds prepared by phase inversion using supercritical $CO_2$ as antisolvent I. Poly(L-lactic acid). *Journal of Supercritical Fluids*, 2007, 40, 317-322.

[49] Reverchon, E.; and Cardea, S. Production of controlled polymeric foams by supercritical $CO_2$. *Journal of Supercritical Fluids*, 2007, 40, 144-152.

[50] Davies, O.R.; Lewis, A.L.; Whitaker, M.J.; Tai, H.; Shakesheff, K.M.; and Howdle, S.M. Applications of supercritical $CO_2$ in the fabrication of polymer systems for drug delivery and tissue engineering. *Advanced Drug Delivery Reviews*, 2008, 60, 373-387.

[51] Tsivintzelis, I.; Pavlidou, E.; Panayiotou, C. Biodegradable polymer foams prepared with supercritical $CO_2$-ethanol mixtures as blowing agents. *Journal of Supercritical Fluids,* 2007, 42, 265-272.

[52] Berens, A.R.; Huvard, G.S.; Korsmeyer, R.W.; and Kunig, F.W. Application of compressed carbon dioxide in the incorporation of additives in polymers. Journal of Applied Polymer Science, 1992, 46 (2), 231-242.

[53] Watson, M.S.; Whitaker, M,J.; Howdle, S,M.; and Shakesheff, K.M. Incorporation of Proteins into Polymer Materials by a Novel Supercritical Fluid Processing Method. *Advanced Materials*, 2002, 14 (24), 1802-1804.

[54] Fischer, E.W.; Sterzel, H,J.; and Wegner, G. Investigation of structure of solution grown crystals of lactide copolymers by means of chemical-reactions. *Kolloid-Zeitschrift and Zeitschrift fur Polymere*. 1973, 251 (11), 980-990.

[55] He, Y.; Xu, Y.; Wei, J.; Fan, Z.Y.; and Li, S.M. Unique crystallization behavior of poly(L-lactide)/poly(D-lactide) stereocomplex depending on initial melt states. *Polymer,* 2008, 49 (26), 5670-5675.

[56] Sarasua JR, Arraiza AL, Balerdi P, Maiza I. Crystallinity and mechanical properties of optically pure polylactides and their blends. *Polymer engineering and science,* Vol. 45, Issue 5, p745-753 (2005).

[57] Tsuji, H.; and Tezuka, Y. Stereocomplex Formation between Enantiomeric Poly(lactic acid)s, 12. Spherulite Growth of Low-Molecular-Weight Poly(lactic acid)s from the Melt. *Biomacromolecules*, 2004, 5 (4) 1181-1186.

[58] Collins, N. J.; Leeke, G.A.; Bridson, R. H.; Hassan, F.; Grover, L.M. The influence of silica on pore diameter and distribution in PLA scaffolds produced using supercritical $CO_2$, *J. Mat. Sci.*, 2008, 19, 1497-1502.

[59] MacDonald, R.T.; McCarthy, S.P.; Gross, R.A. Enzymatic Degradability of Poly(lactide): Effects of Chain Stereochemistry and Material Crystallinity. *Macromolecules*, 1996, 29, 7356-7361.

[60] Natureworks LLC. http://www.natureworksllc.com (accessed March 2009).

[61] Acierno, S., Di Maio, E., Iannace, S., Grizzuti, N. (2006). Structure development during crystallization of polycaprolactone. *Rheol Acta*, 45, 387-392.

[62] Harrison, K.L.; Jenkins, M.J. The effect of crystallinity and water absorption on the dynamic mechanical relaxation behaviour of polycaprolactone. *Polymer International*, 2004, 53, 1298-1304.

[63] http://perstorpcaprolactones.com/ (accessed October 2010)

[64] Aras, L.; Richardson, M.J.; The glass transition behaviour and thermodynamic properties of amorphous polystyrene. *Polymer*, 1989, 30 (12), 2246-2252.

[65] Van Der Elst, M.; Klein, C.,P.,A.,T.; De Blieck-Hogervorst, J.,M.; Patka, P.; and Haarman, H. Bone tissue response to biodegradable polymers used for intra medullary fracture fixation: A long-term in vivo study in sheep femora. *Biomaterials*, 1999, 20,121.

[66] Ahmed, J.; Zhang, J.-X.; Song, Z.; and Varshnet, S.K. Thermal Properties of Polylactides: Effect of molecular mass and nature of lactide isomer. *Journal of Thermal Analysis and Calorimetry*, 2009, 95 (3), 957-964.

[67] Pratt, C.F.; and Hobbs, S.Y. Comparative study of crystallization rates by DSC and depolarization microscopy, *Polymer*, 1976, 17, 12-16.

[68] Booth, A.; and Hay, J.N. The Use of Differential Scanning Calorimetry to Study Polymer Crystallization Kinetics. *Polymer*, 1969, 10, 95-104.

[69] Cheng, S.Z.D.; and Lotz, B. Nucleation control in polymer crystallization: structural and morphological probes in different length- and time-scales for selection processes. *Philosophical Transactions, The Royal Society London*, 2003, 361, 517-537.

# Appendix 1

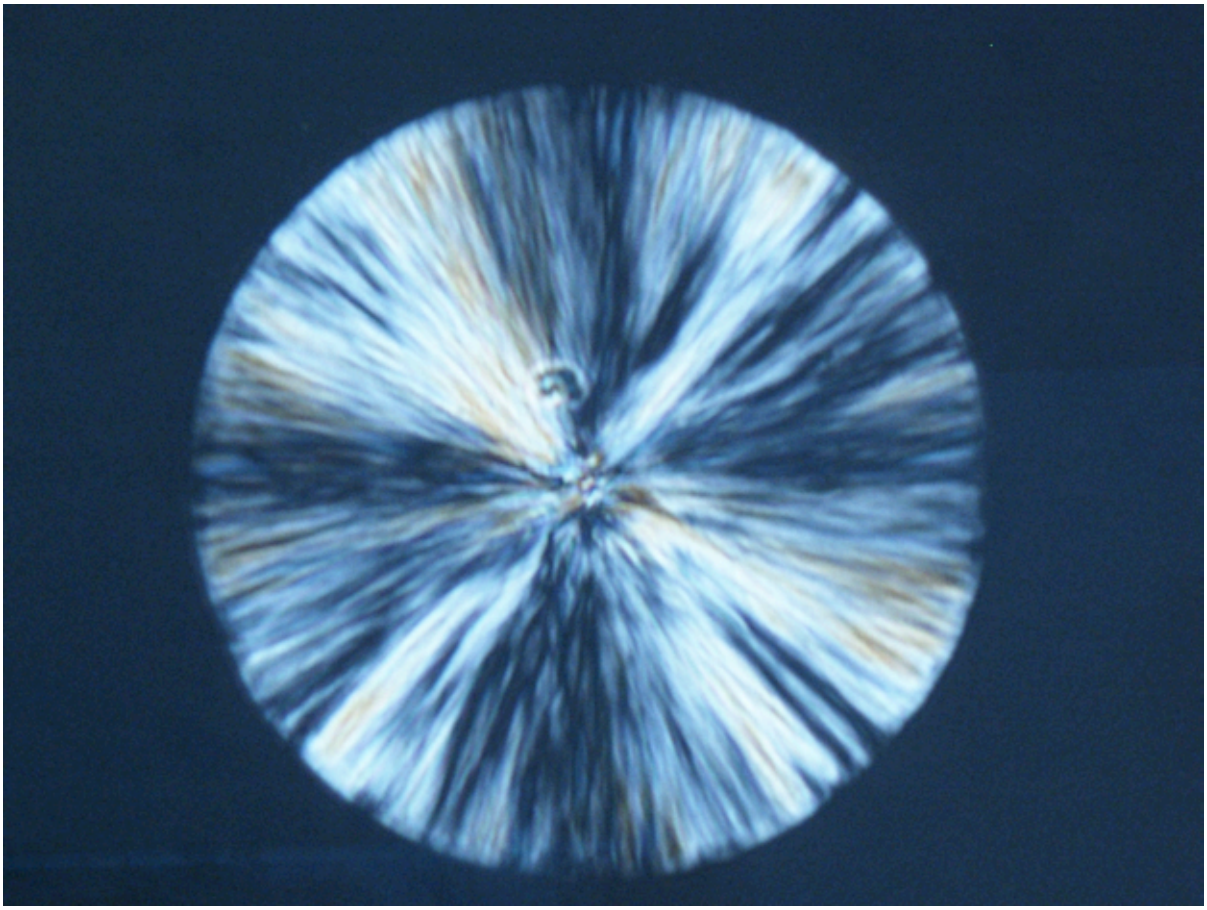

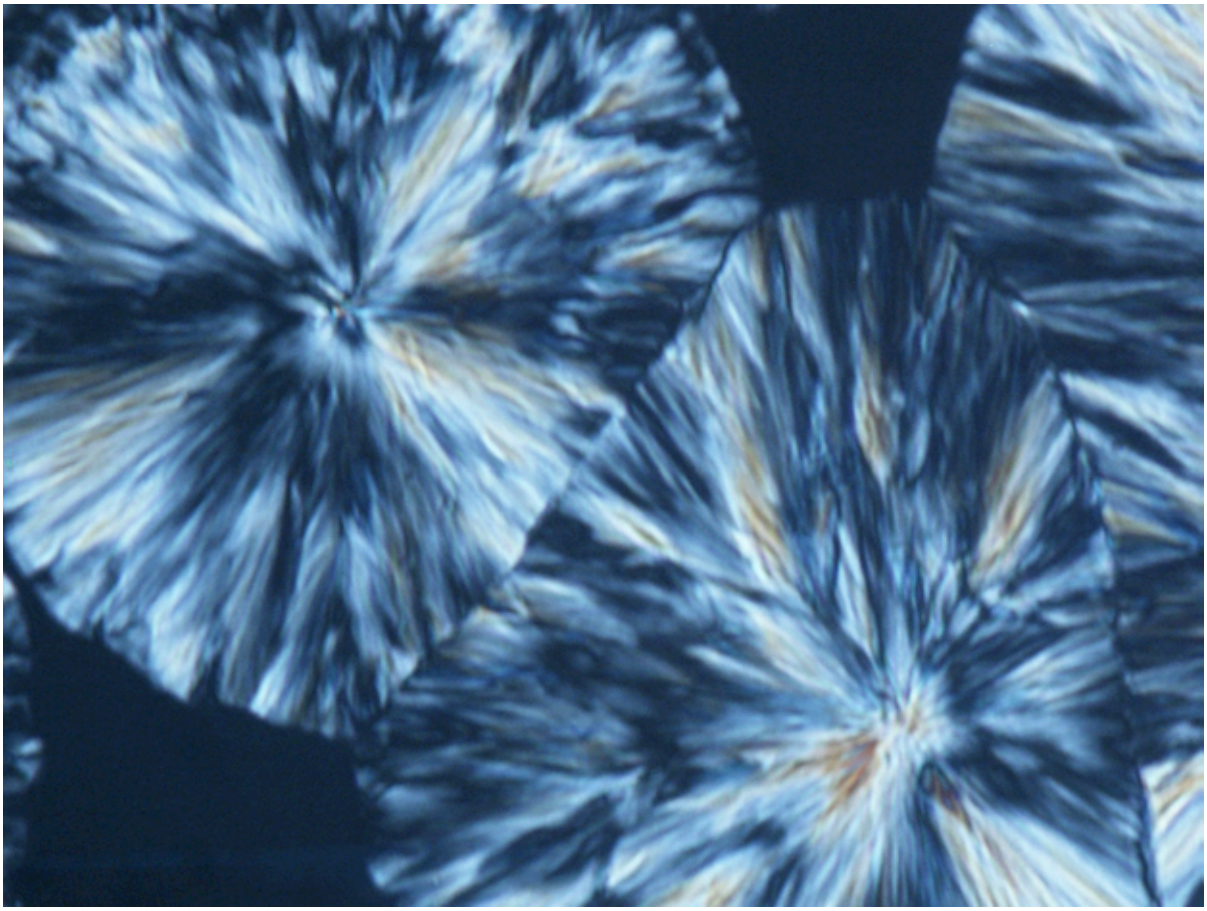

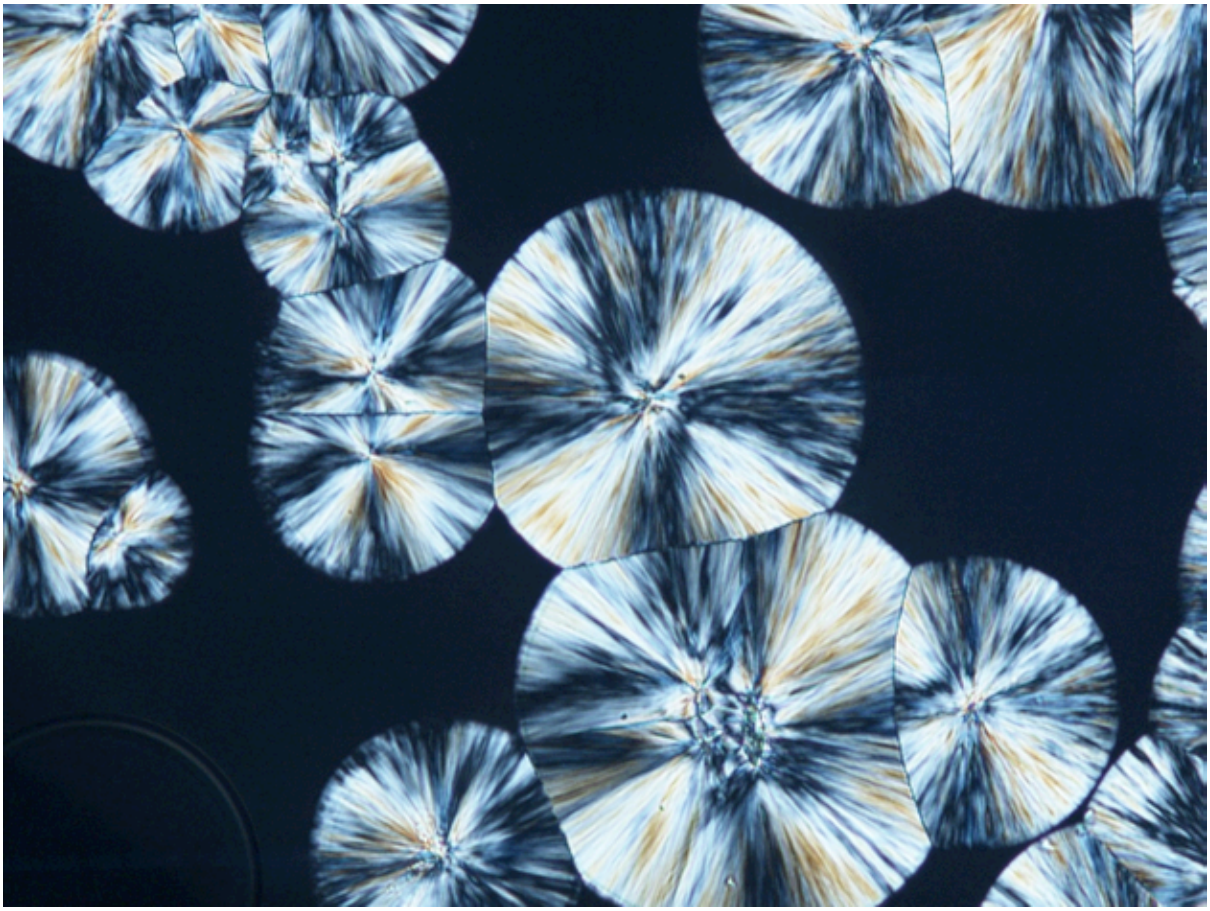

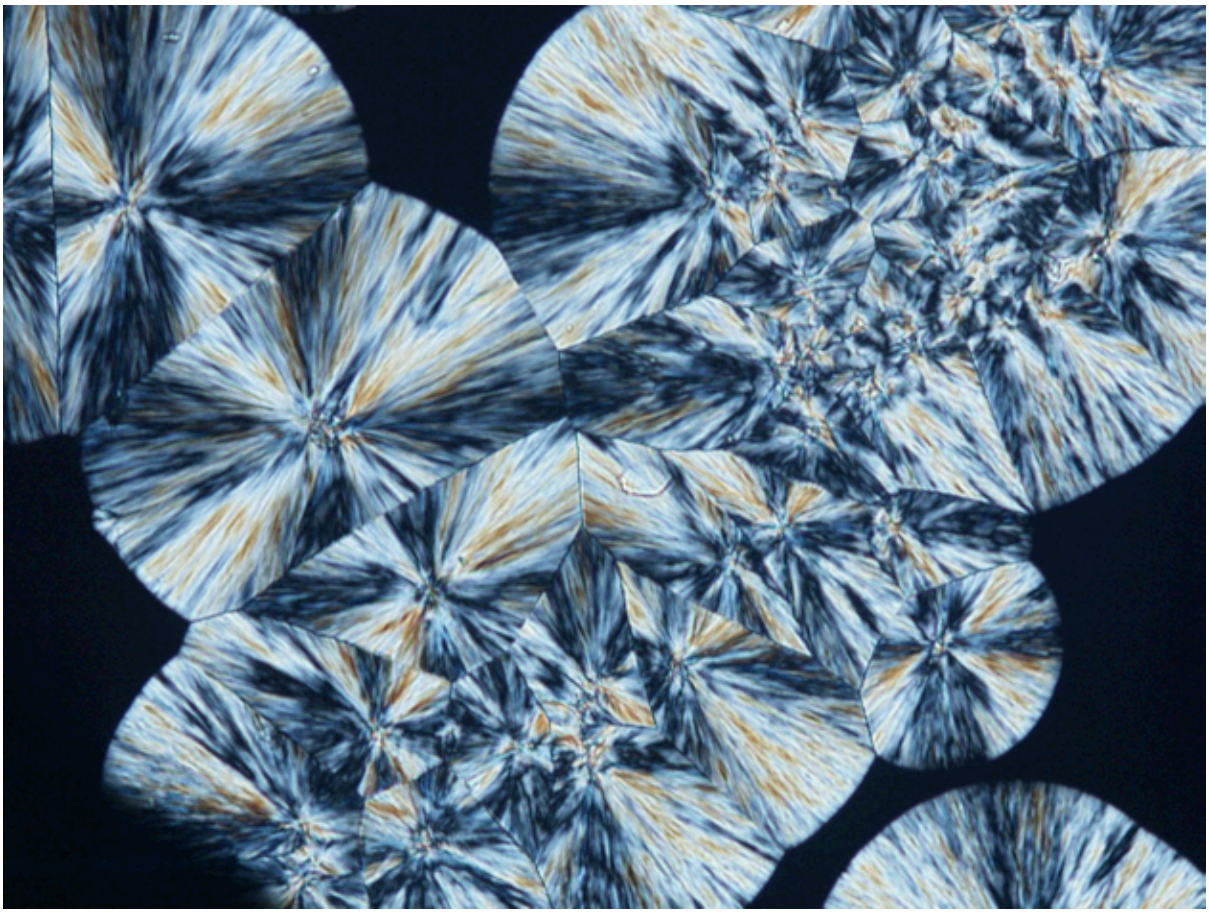

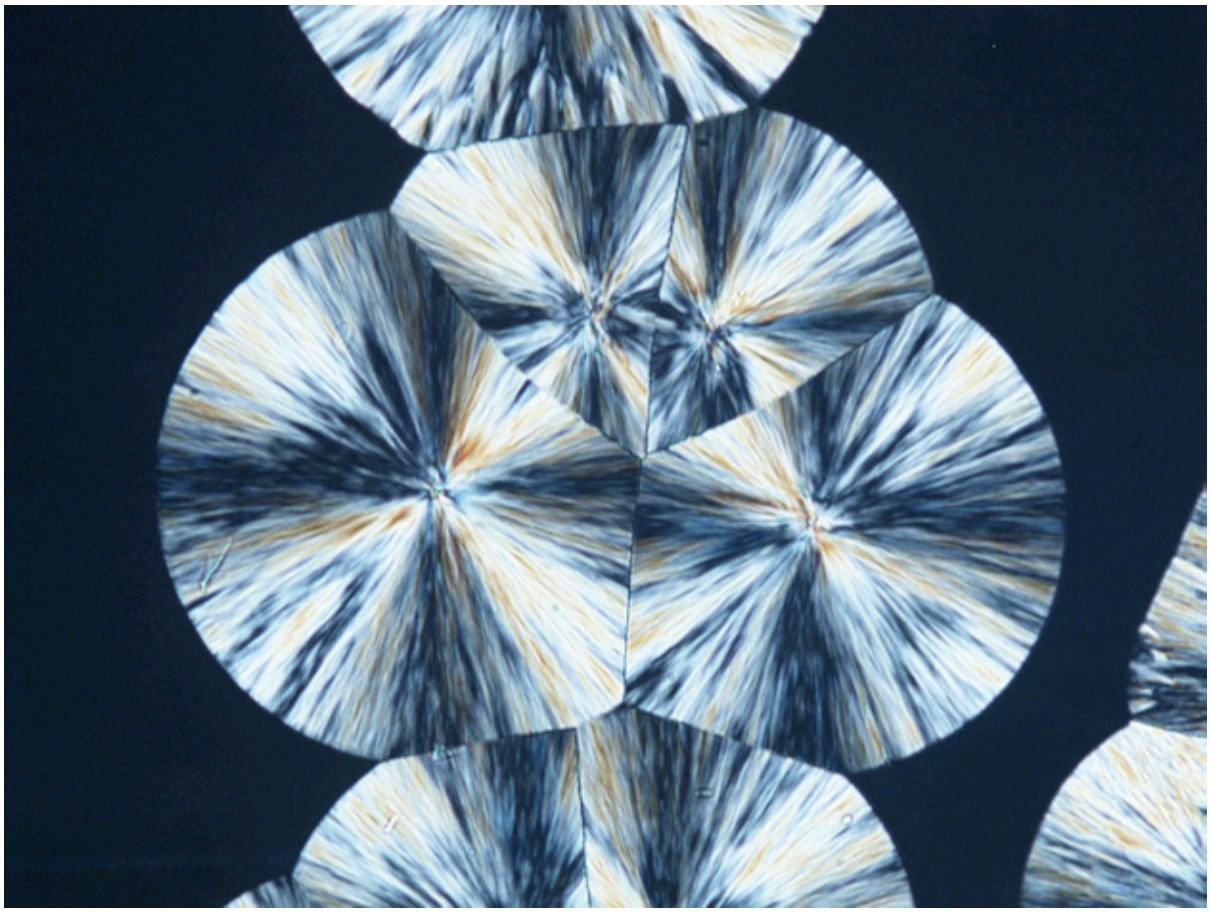

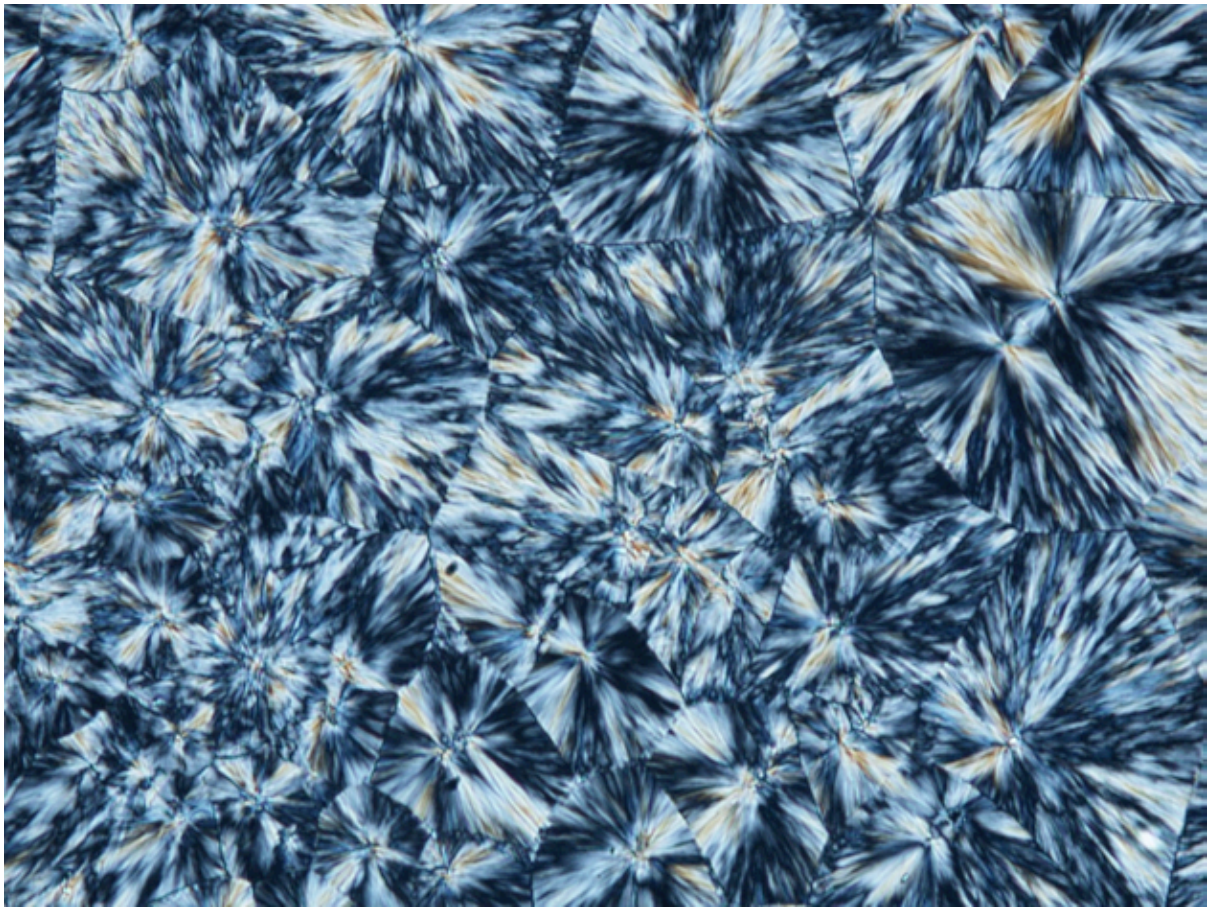

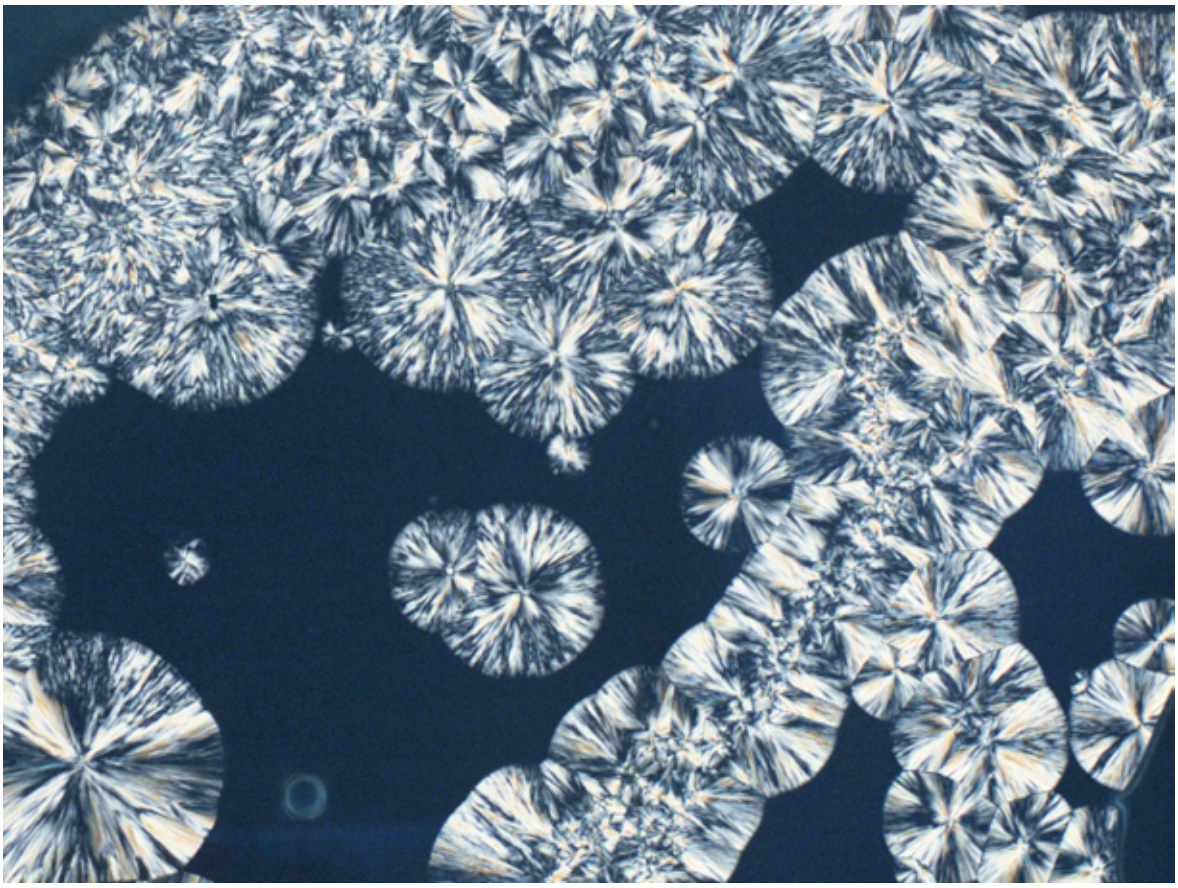

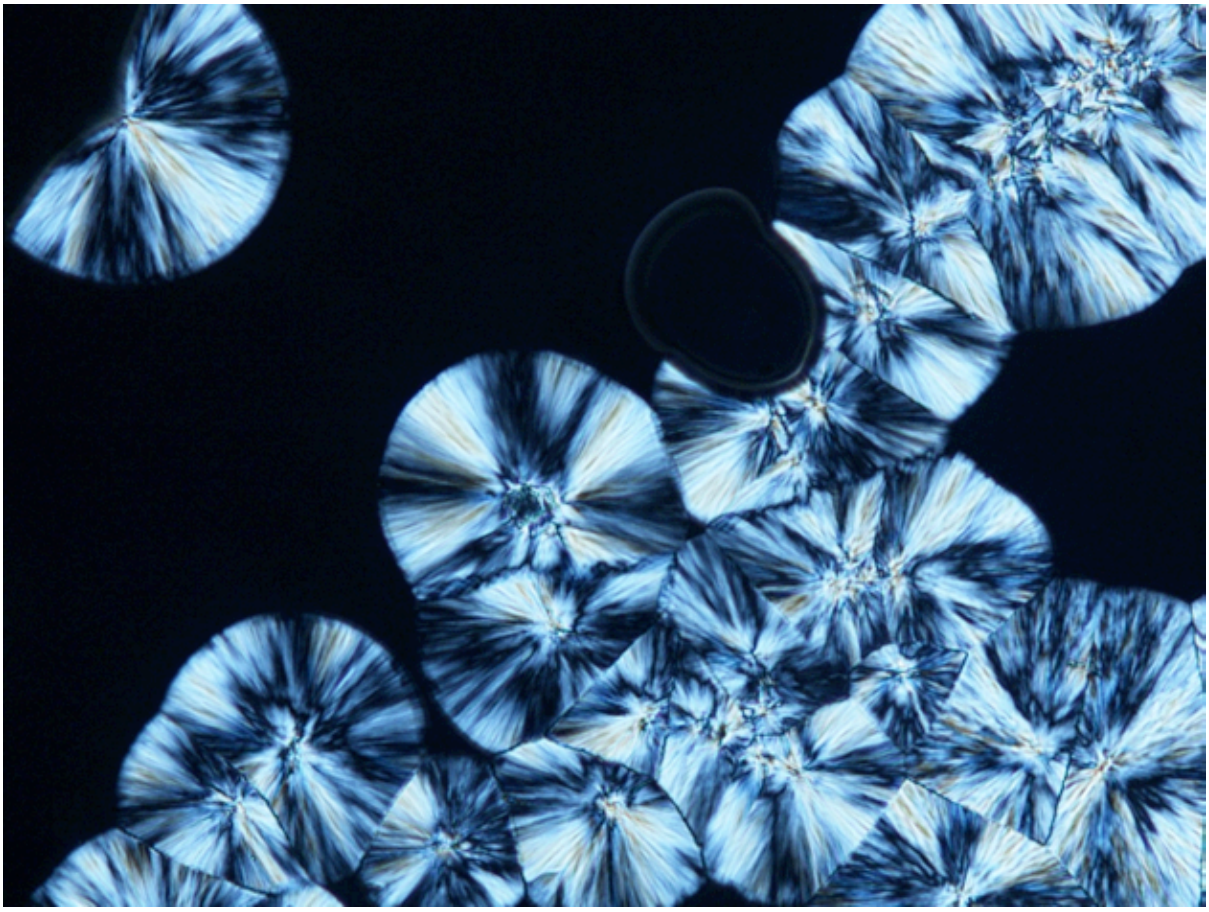

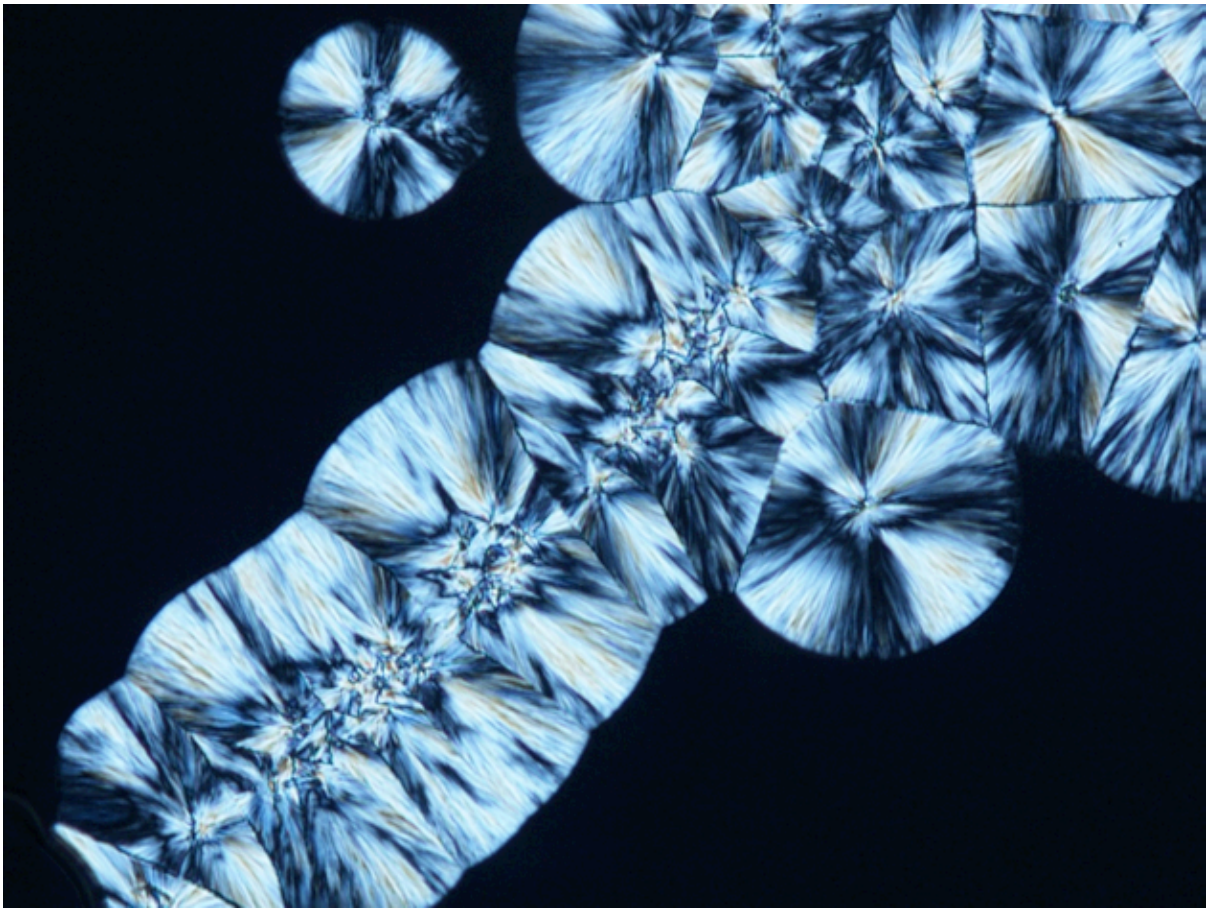

# Appendix 2

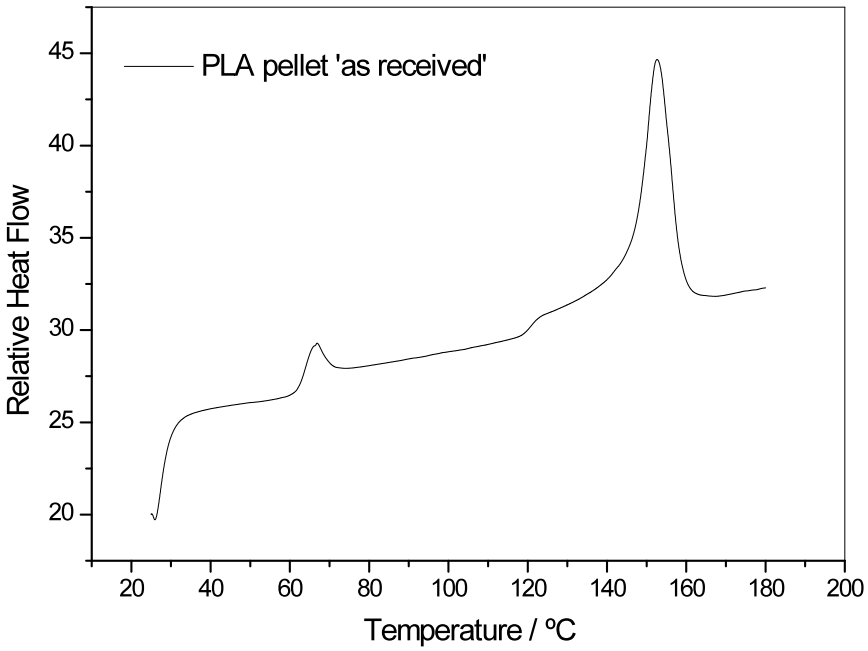
PLA pellet 'as received'
Relative Heat Flow
Temperature / °C
45
40
35
30
25
20
20
40
60
80
100
120
140
160
180
200

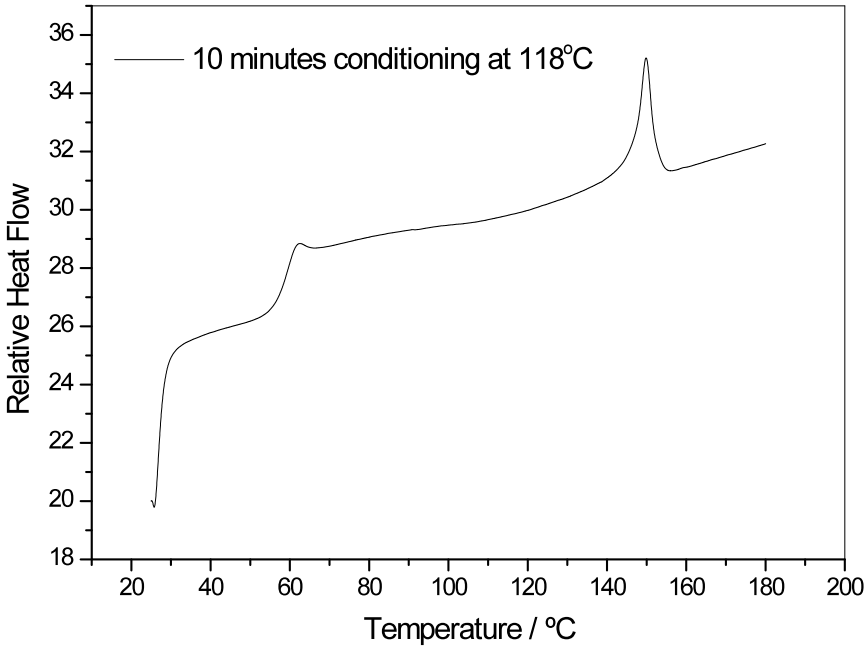
10 minutes conditioning at 118°C
Relative Heat Flow
Temperature / °C
36
34
32
30
28
26
24
22
20
18
20
40
60
80
100
120
140
160
180
200

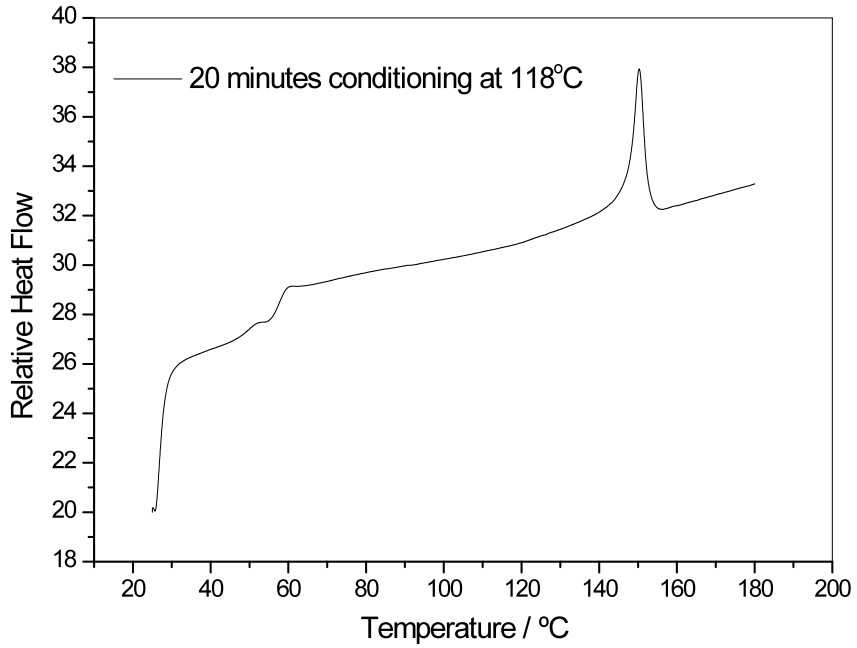
20 minutes conditioning at 118°C
Relative Heat Flow
Temperature / °C
40
38
36
34
32
30
28
26
24
22
20
18
20
40
60
80
100
120
140
160
180
200

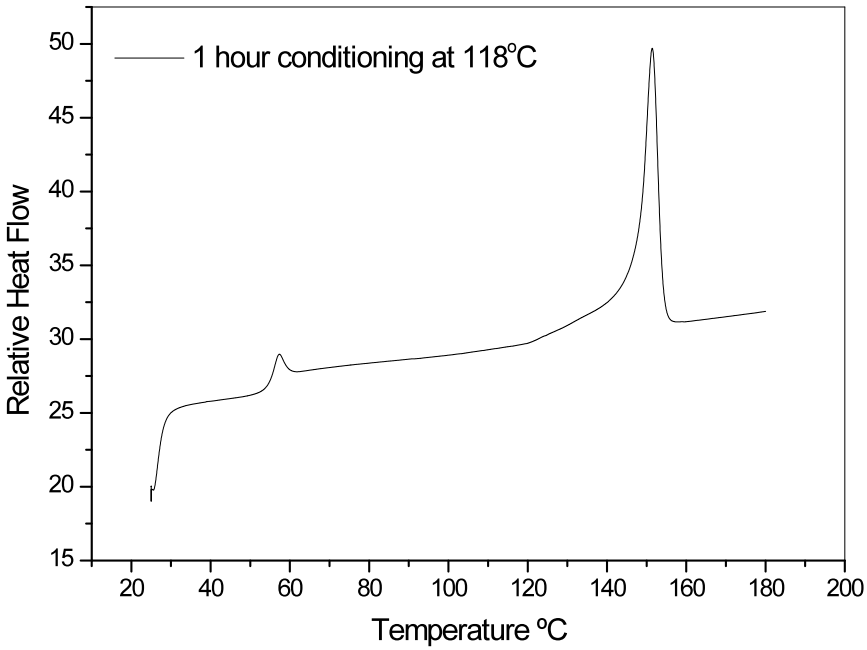
1 hour conditioning at 118°C
Relative Heat Flow
Temperature °C
50
45
40
35
30
25
20
15
20
40
60
80
100
120
140
160
180
200

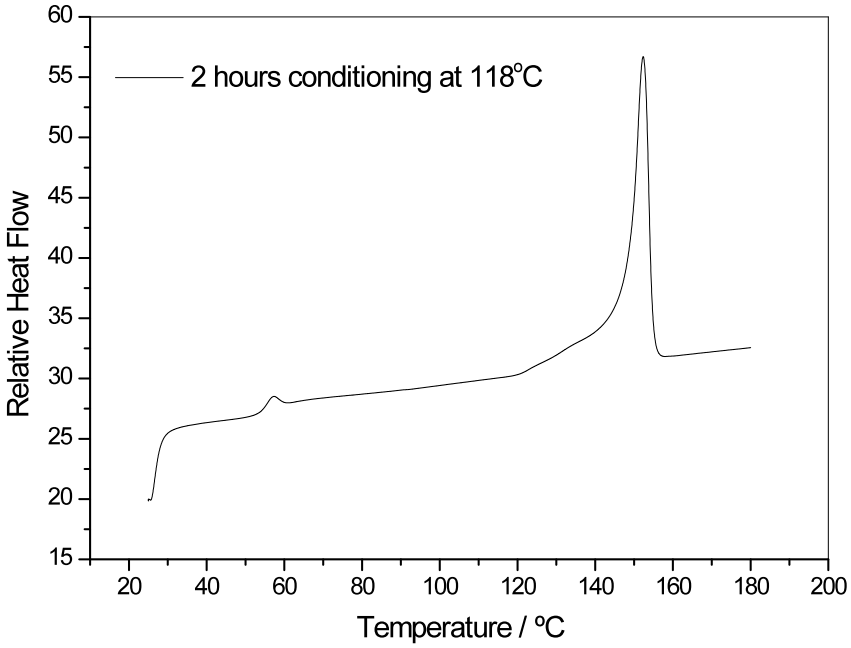
2 hours conditioning at 118°C
Relative Heat Flow
Temperature / °C
60
55
50
45
40
35
30
25
20
15
20
40
60
80
100
120
140
160
180
200

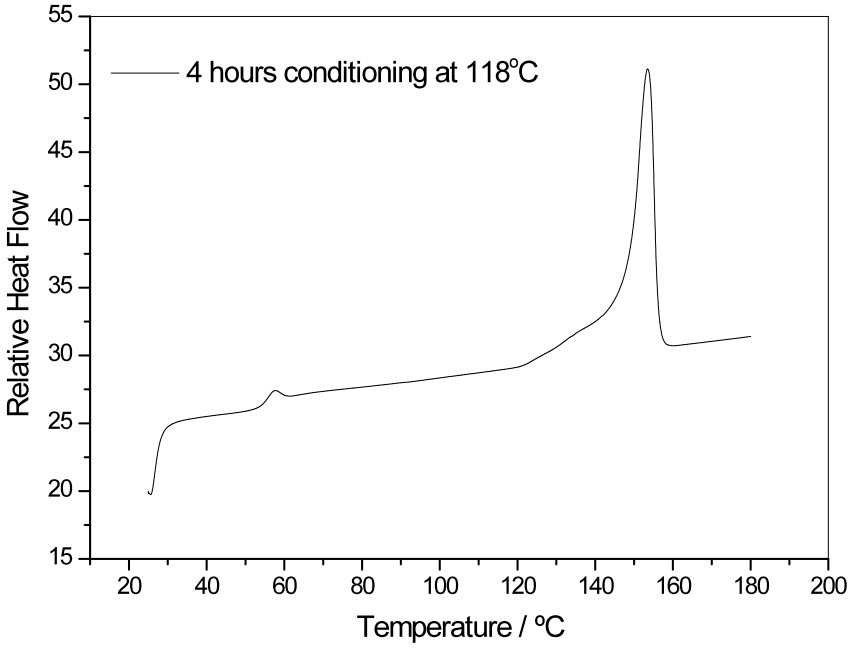
4 hours conditioning at 118°C
Relative Heat Flow
Temperature / °C
55
50
45
40
35
30
25
20
15
20
40
60
80
100
120
140
160
180
200

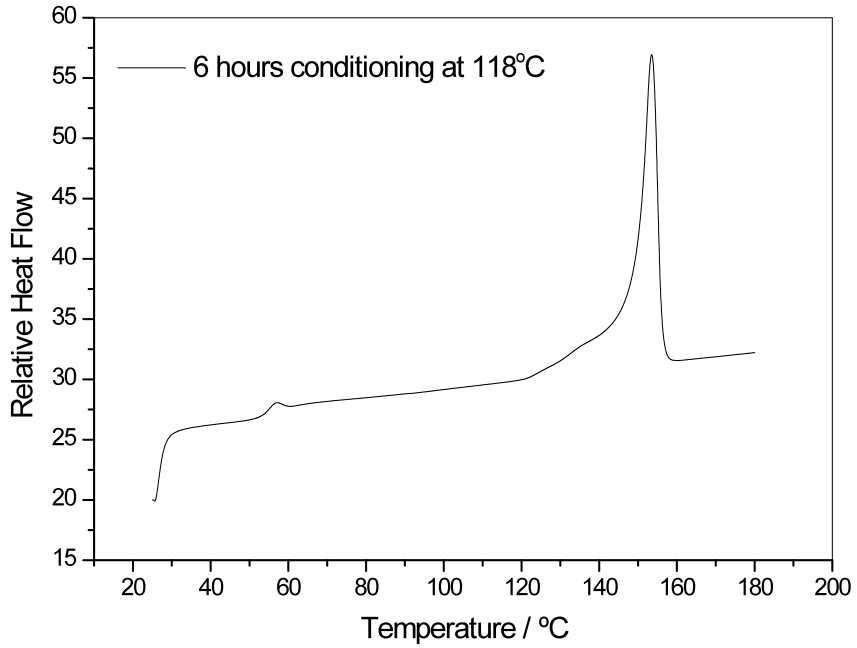
6 hours conditioning at 118°C
Relative Heat Flow
Temperature / °C
60
55
50
45
40
35
30
25
20
15
20
40
60
80
100
120
140
160
180
200

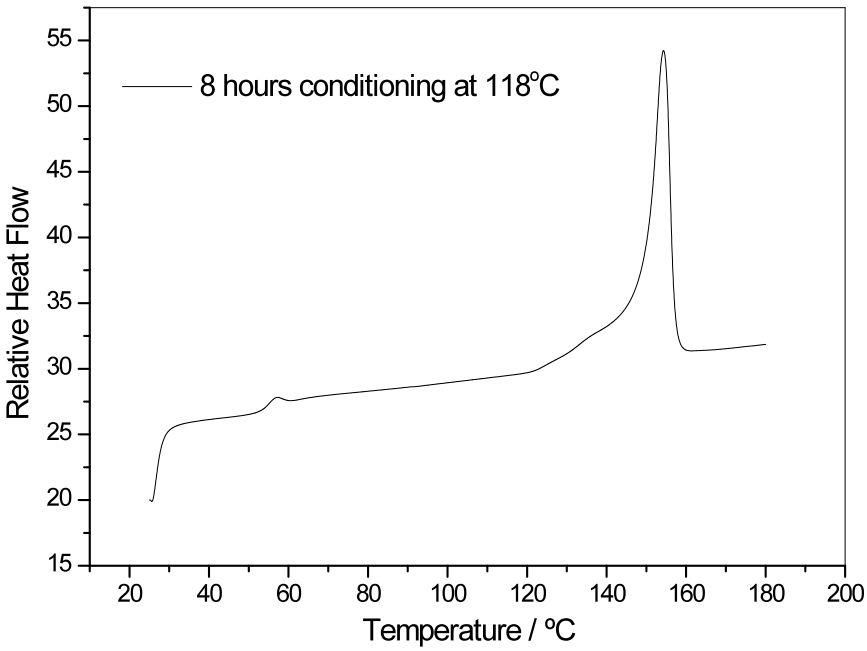
8 hours conditioning at 118°C
Relative Heat Flow
Temperature / °C
55
50
45
40
35
30
25
20
15
20
40
60
80
100
120
140
160
180
200

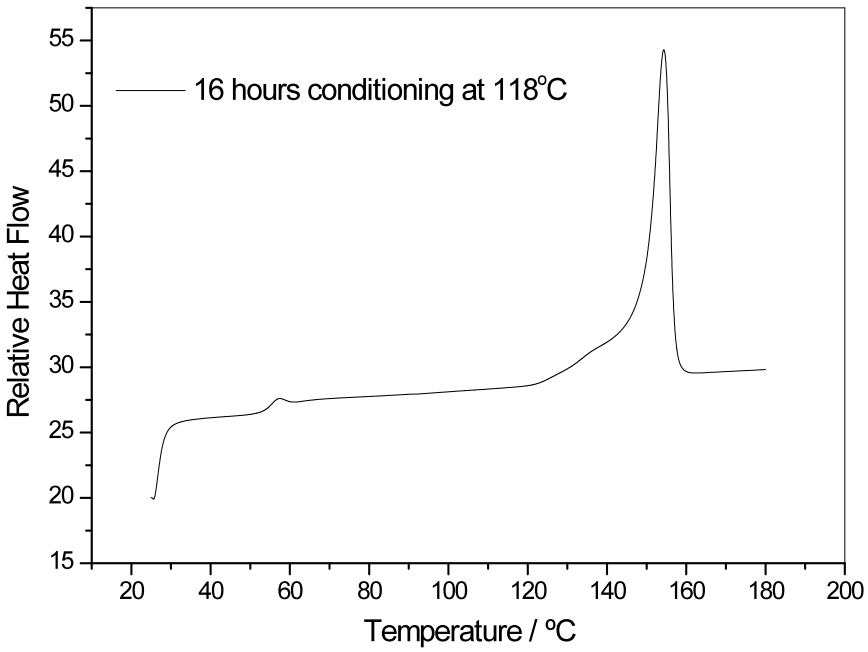
16 hours conditioning at 118°C
Relative Heat Flow
Temperature / °C
55
50
45
40
35
30
25
20
15
20
40
60
80
100
120
140
160
180
200

# Appendix 3

# *A Comparison of the use of FTIR spectroscopy with DSC in the characterisation of melting and crystallisation in polycaprolactone*

MJ Jenkins* and SH Murphy

School of Metallurgy and Materials, University of Birmingham, Edgbaston, Birmingham, B15 2TT, UK

* Corresponding author

MJ Jenkins, (T) +44 121 414 2841 (F) +44 121 414 5232 (e) m.j.jenkins@bham.ac.uk

## Abstract

The infra-red spectrum of polycaprolactone has been recorded as a function of temperature in the range where melting and crystallisation of the polymer can occur. Examination of the carbonyl band of the spectra reveals a clear morphological sensitivity; heating the semi-crystalline polymer through the melting region results in a decrease in the intensity of the crystalline component of the carbonyl band. Accordingly, there was a subsequent increase in intensity of the crystalline carbonyl band on cooling. To enable comparison of these findings with a more conventional method of thermal analysis, similar experiments were conducted using a differential scanning calorimeter. The heated ATR accessory adopted for use in the FTIR spectrometer imposed significant limitations in the range of possible heating and cooling rates, but when these rates were carefully matched between FTIR and DSC, close correlation between the melting point and onset of re-crystallisation was observed. The results confirm that FTIR can be used as an alternative, if more laborious, way of investigating melting and re-crystallisation.

## 1.0 Introduction

Polycaprolactone (PCL) is a semi-crystalline aliphatic polyester. Both biocompatible and biodegradable, PCL is used in a wide range of applications including, tissue engineering scaffolding, bioabsorbable sutures and macromolecular drug release in the human body [1, 2]. PCL typically has a glass transition temperature of -60 °C and exhibits a melting peak in the region of 60 °C. The temperature at which the crystallisation process proceeds most rapidly is in the region of 30 °C [3]. Understanding the crystallisation

process and its effect on crystallinity is important as this characteristic in a polymer can control material properties such as stiffness, strength and the biodegradation rate [4].

Characterisation of the degree of crystallinity is conventionally investigated using techniques such as differential scanning calorimetry (DSC), X-ray analysis and density measurements. The kinetics of the crystallisation process are readily measured by DSC. However, in recent years, the use of infra-red spectroscopy as a method of characterisation of crystallinity has grown in prominence. In the case of PCL, one of the first and often cited studies concerned the study of a PCL/PVC blend system using FTIR spectroscopy [5]. In this work, the authors report on the morphological origin of the prominent carbonyl band in the PCL component. The PCL carbonyl band was shown to be split into two components, a crystalline band at 1724 $cm^{-1}$ and an amorphous band at 1737 $cm^{-1}$. The authors conclude by suggesting that FTIR provides a means of studying the crystallisation process via spectroscopic means and that rapid acquisition of data offers a way of exploring the early stages of crystallisation. However, it is also noted that measurements of crystallinity determined using FTIR should also be correlated with other techniques such as X-ray spectroscopy.

While other papers followed in the area of PCL blends [6,7], the next study to focus solely on the exploration of crystallinity of PCL using FTIR was that reported by Yong et al, 2000 [8]. In this work, the carbonyl band was used to determine a measure of the extent of crystallinity. Good agreement with literature values from other techniques including X-ray and NMR were reported. However, related studies concentrating on the detection of the melting process and non-isothermal crystallisation in PCL using FTIR have received little or no attention in the literature. Therefore, the purpose of this paper is to extend the scope of earlier studies by adopting a time-resolved approach to the detection of melting and crystallisation processes in PCL, and in particular, to correlate the processes of melting and crystallisation as detected by FTIR with the conventional technique of differential scanning calorimetry. It will be shown that in the case of non-isothermal crystallisation, there is good agreement between melting and crystallisation processes measured using FTIR and DSC.

## 2.0 **Experimental**

### *2.1 Materials*

Polycaprolactone (CAPA 6800) was supplied in pellet form by Solvay Interox Ltd (UK). The number and weight average molecular weights of CAPA6800 were 69000 and 120000 respectively (manufacturers data). Plaques of thickness 0.3mm were produced by compression moulding at 150°C using a heated press. The plaques were removed from the press and allowed to cool to room temperature. Circular samples with a diameter of 4mm were cut from the plaque using a hole-punch. The sample mass was typically 6mg.

### *2.2 Differential Scanning Calorimetry (DSC)*

The melting and crystallisation behaviour of PCL was measured using a Perkin Elmer differential scanning calorimeter (DSC 7) interfaced to a personal computer. The thermal response of the instrument was calibrated from the enthalpy of fusion of a known mass of indium (99.999% pure). The temperature of the calorimeter was calibrated using the melting points of benzoic acid, stearic acid and octadecane. Corrections were made for thermal lag by extrapolation to zero heating rate. Plots of actual vs. experimental melting points were linear and were used to calibrate the calorimeter temperature.

Samples were contained in aluminium pans, and an empty pan was used as a reference. Samples were initially heated from 20 to 100 °C at 20 °C/min and then cooled back to 20 °C at 20 °C/min to enable the creation of a known thermal history within the sample. Melting traces were recorded at a low heating rate of 0.5 °C/min in order to match the heating rates imposed by the infra-red spectroscopy experiments. Non-isothermal crystallisation was achieved by cooling from the melt at 0.5 °C/min. Again, very slow cooling rates were selected in order to match the rates imposed by the limitations of the temperature control of the ATR unit on the FTIR spectrometer.

Isothermal crystallisation was achieved by heating the samples to 5°C above the observed melting point, holding for 2 minutes and then cooling to the selected crystallisation temperature of 46 °C for 120 minutes. To minimise crystallisation during the cooling

phase, crystallisation temperatures close to the melting point were selected. The relative crystallinity was calculated according to the following expression,

$$Xt = \frac{\int_0^t (dH/dt)dt}{\int_0^\infty (dH/dt)dt} \qquad [1]$$

in which (dH/dT) is the relative heat flow rate. The variation of Xt with time was used in the production of an Avrami plot.

*2.3 Infra-red spectroscopy*

Changes to the infra-red spectrum of PCL during either heating or cooling were recorded using a Nicolet 860 FTIR**.** Measurements were made using a heated Golden Gate ATR supercritical fluids analyser supplied by Specac (p/n 10585). The temperature was controlled and monitored by a dedicated heater control unit. A thermocouple and digital temperature sensor were used to calibrate the temperature of the ATR cell. A plot of actual vs. control temperature was constructed and used to calibrate the temperature of the cell. Infra-red spectra were recorded at a resolution of $2cm^{-1}$ and 200 scans. This combination was found to be the best compromise between high spectral quality and minimum acquisition time.

Samples of known thermal history were created using DSC (by heating the sample to above the melting point and cooling to room temperature at 20 °C/min) and extracted from the DSC pans prior to placement on the ATR cell. To detect the melting process, the infra-red spectrum of PCL was recorded as a function of temperature by heating the semi-crystalline samples from ambient temperature to 70 °C at 0.5 °C/min. To detect the non-isothermal crystallisation process, the resulting amorphous samples were then cooled from the melt to room temperature at 0.5 °C/min. This relatively slow cooling rate was imposed by the lack of forced cooling on the ATR cell. Isothermal crystallisation was detected by heating a semi-crystalline PCL sample to 70°C and then cooling at 0.5°C/min to 46 °C. The rationale for the selection of this temperature was to ensure the crystallisation process occurred within a reasonable timescale but did not initiate before the isothermal crystallisation temperature was reached.

## 3.0 Results and discussion

The carbonyl region of the FTIR spectrum of PCL is shown in fig. 1. It is clear that the band is composed of two separate, but overlapping peaks. There is a relatively broad band centred at 1737 $cm^{-1}$ and a sharper and more intense band at 1724 $cm^{-1}$, it has be shown previously that the origin of the above peaks can be traced to the amorphous and crystalline phases of the polymer respectively [9, 10]. The amorphous band is relatively broad due to the wider range of possible local environments of the carbonyl group in the amorphous phase. The situation in the crystalline phase is different due to the higher degree of ordering which leads to a reduction in the number of local environments and hence a sharper peak is observed. A further consequence of the high degree of ordering in the crystalline phase is the presence of inter and intramolecular forces. These forces affect the dipole moment of the carbonyl groups bound into the crystalline lamellae and the associated band shifts to a lower wavenumber.

On heating from 30 to 70°C, the intensity of the amorphous and crystalline peaks in the carbonyl band were found to vary. The most prominent change was found in the crystalline band at 1724 $cm^{-1}$ where the intensity of the band decreased from an initial absorbance of 0.77 at 30 °C to 0.59 at 70°C. Due to the overlapping nature of the carbonyl peaks, it was not possible to measure the absorbance of the crystalline band above 55°C as beyond this temperature the crystalline peak became fully obscured by the amorphous band, which, increased in intensity as the temperature increased. Given that the carbonyl band is in effect diagnostic of the morphology of the sample under investigation, the changes in band intensity shown in fig. 1 can be attributed to the melting process.

The variation in the intensity of the crystalline carbonyl band with temperature is shown in fig. 2. The most striking feature of the figure is the close correlation of the sharp decrease in crystalline carbonyl absorbance in the region 50 to 56°C with the melting point of the polymer as detected by DSC. Clearly the heating rate adopted in the DSC

experiment will affect the temperature at which melting is observed, but in the case of the comparison shown in fig. 2, the heating rates were matched at 0.5 °C/min to minimise the effects associated with thermal lag. Various comparisons between the traces shown in fig. 2 are possible. These include; the extrapolated onset of melting, the peak melting temperature and the temperature corresponding to the last trace of crystallinity.

The extrapolated onset of melting from DSC was found to be 51.8 °C. By applying a similar geometrical construction to the variation of crystalline carbonyl peak intensity with temperature, the onset of melting as detected by FTIR was found to be 51.5 °C. The last trace of crystallinity detected by DSC and FTIR was 55.2 °C and 56.1 °C respectively. The peak melting temperature measured by DSC was found to be 53.7 °C, but no corresponding measure from FTIR was possible due to the fact that the crystalline carbonyl peak became obscured by the amorphous band and therefore impossible to resolve with the apparatus required for the experiment. The difference between the above measures is limited to a maximum of 0.9 °C, which can easily be attributed to a combination of the error in the measurement of temperature and subtle differences in the thermal lag characteristics of both techniques. Therefore, providing that the heating rates are matched, it appears that FTIR offers an alternative (if rather more laborious) method to DSC for the detection and measurement of the melting process in PCL.

It is worth noting the decrease in absorbance from 30 to 50 °C, which occurs prior to the main melting process. This decrease in absorbance may suggest the melting of relatively thin lamellae, but a more reasonable interpretation can be found in the effect of thermal expansion of the sample on heating, which effectively reduces the number of molecules within the sampling area of the beam and results in a progressive decrease in absorbance.

The effect of cooling PCL from the melt on the carbonyl band is shown in fig. 3. A strong similarity to fig. 1 can be observed in that the band is clearly temperature dependent, but in the case of fig. 3, on cooling there is a progressive growth in the crystalline component of the carbonyl band and a corresponding (but much less pronounced) decrease in the amorphous component of the band. This variation can be ascribed to the process of

crystallisation on cooling. The variation of the intensity of the crystalline component of the band with temperature is shown in fig. 4. For comparison, the corresponding DSC cooling curve is also shown.

Analysis of the curves shown in fig. 4 reveals a strong correlation between the onset of crystallisation process as detected by DSC and FTIR. In the case of DSC, the temperature at which the crystallisation exotherm becomes apparent is 41.7 °C. In the case of FTIR, the onset of the crystallisation process can be defined as the point at which the first data point corresponding to the crystalline carbonyl band can be resolved, which can be shown be 43 °C. If an uncertainty of ±1°C is assumed in the measurement of temperature in the heated ATR unit, then the techniques of DSC and FTIR can be said to correlate reasonably well in the detection of the onset of crystallisation. However, there is a clear dissimilarity in the breadth of the crystallisation process as detected by these techniques.

The difference in the breadth of the crystallisation process as detected by DSC and FTIR may be explained by a difference in the thermal characteristics of the DSC cell and the heated ATR unit. In the case of the heated ATR unit, the FTIR spectrometer samples only a fraction of the crystallising polymer (in the case of the unit adopted for this study, the sample area is limited to an area of 2 $mm^2$ and the sampling depth is in the region of 2 microns). In the case of DSC, the sample thickness is far in excess of this at 0.3 mm, so the effects of thermal lag are likely to be far more pronounced, causing an increase in the breadth of the transition.

The effect of isothermal crystallisation on the carbonyl band of the PCL FTIR spectrum is illustrated in fig. 5, the crystallisation temperature was 46°C. The response is almost identical to that shown in fig. 3 in that the crystalline component of the band increases with time. There is also a corresponding decrease in the intensity of the amorphous band with time. Furthermore, it is also apparent from fig. 5 that there is evidence of a well-defined isosbestic point, indicating that the conversion of amorphous to crystalline material at this temperature does not involve an intermediate species. While figs. 1 and 3

also show evidence of isosbestic points, they are less pronounced. Since these figures show FTIR data gathered under non-isothermal conditions, it is likely that the absorption coefficients of the crystalline and amorphous phases of semi-crystalline PCL exhibit some degree of temperature dependence and thus a loss of clarity in the definition of this point.

Fig. 6 shows the variation of the normalised peak intensity of the crystalline carbonyl band with time (crystallisation temperature 46 °C). The sigmoidal shape of the transformation of amorphous to crystalline PCL shown in fig. 6 is clearly amenable to analysis using an Avrami approach and the inset figure shows the Avrami plot for the data. The shape of the Avrami plot shown in the inset of fig. 6 suggests that FTIR is able to resolve both the primary and secondary crystallisation processes in PCL and is similar to Avrami plots reported elsewhere [11].

## 4. Conclusions

A clear morphological sensitivity of the carbonyl band in PCL has been observed. The variation of the crystalline component of the band with temperature has been compared with that of relative heat flow obtained from DSC and a good correlation has been found. Furthermore, the crystallisation process detected using FTIR spectroscopy was observed to be sharper than the corresponding exotherm observed using DSC. This observation was interpreted in terms of reduced thermal lag in the ATR cell due to a much smaller effective sample volume. Despite showing some technical advantages, this work has shown that FTIR spectroscopy is a cumbersome method to determine the crystallinity and crystallisation in PCL and that DSC is a far more practical approach to measurements of this kind.

**References**

[1] Zhu G, Xu Q, Qin R, Yan H, Liang G. Effect of [gamma]-radiation on crystallization of polycaprolactone. Radiation Physics and Chemistry 2005;74:42-50

[2] Hutmacher DW. Scaffolds in tissue engineering bone and cartilage. Biomaterials 2000;21:2529-2543

[3] Acierno S, Di Maio E, Iannace S, Grizzuti N. Structure development during crystallization of polycaprolactone. Rheologica Acta 2006;45:387-392

[4] Jenkins MJ and Harrison KL. The effect of crystalline morphology on the degradation of PCL in a solution of PBS and lipase. Polymers for Advanced Technologies 2008;19;1901-1906

[5] Coleman MM, Zarian J. Fourier-transform infrared studies of polymer blends. II. Poly(ε−caprolactone)-poly(vinyl chloride) system. Journal of Polymer Science: Polymer Physics Edition 1979;17:837-850

[6] Wang J, Cheung MK, Mi Y. Miscibility and morphology in crystalline/amorphous blends of poly(caprolactone)/poly(4-vinylphenol) as studied by DSC, FTIR, and 13C solid state NMR. Polymer 2002;43:1357-1364

[7] Jiang H, Wu P, Yang Y. Variable Temperature FTIR Study of Poly(ethylene-co-vinyl alcohol)-graft-poly(Îμ-caprolactone). Biomacromolecules 2003;4:1343-1347

[8] Yong H, Yoshio I. Novel FTIR method for determining the crystallinity of poly(ε-caprolactone). Polymer International 2000;49:623-626

[9] Xu J, Guo B-H, Yang R, et al. In situ FTIR study on melting and crystallization of polyhydroxyalkanoates. Polymer 2002;43:6893-6899

10] Kansiz M, Domínguez-Vidal A, McNaughton D, Lendl B. Fourier-transform infrared (FTIR) spectroscopy for monitoring and determining the degree of crystallisation of polyhydroxyalkanoates (PHAs). Analytical and Bioanalytical Chemistry 2007;388:1207-1213

[11] Jenkins MJ and Harrison KL. The effect of molecular weight on the crystallisation kinetics of PCL. Polymers for Advanced Technologies 2006;17;474-47

**Figure Captions**

Fig. 1 The carbonyl band in PCL showing the effect of heating a semi-crystalline sample from 30 °C through the melting region to 70 °C

Fig. 2 Melting in PCL as detected by DSC and from the variation of the crystalline carbonyl band intensity.

Fig. 3 Variation of the carbonyl band intensity on cooling from 70°C through the hot-crystallisation region.

Fig.4 Crystallisation in PCL as detected by DSC and from the variation of the crystalline carbonyl band intensity.

Fig. 5 Variation in the carbonyl band of PCL during iso-thermal crystallisation at 46°C.

Fig. 6 The development of crystallinity in PCL at 46°C as detected by FTIR (inset plot shows an Avrami analysis of the data).

## Figures

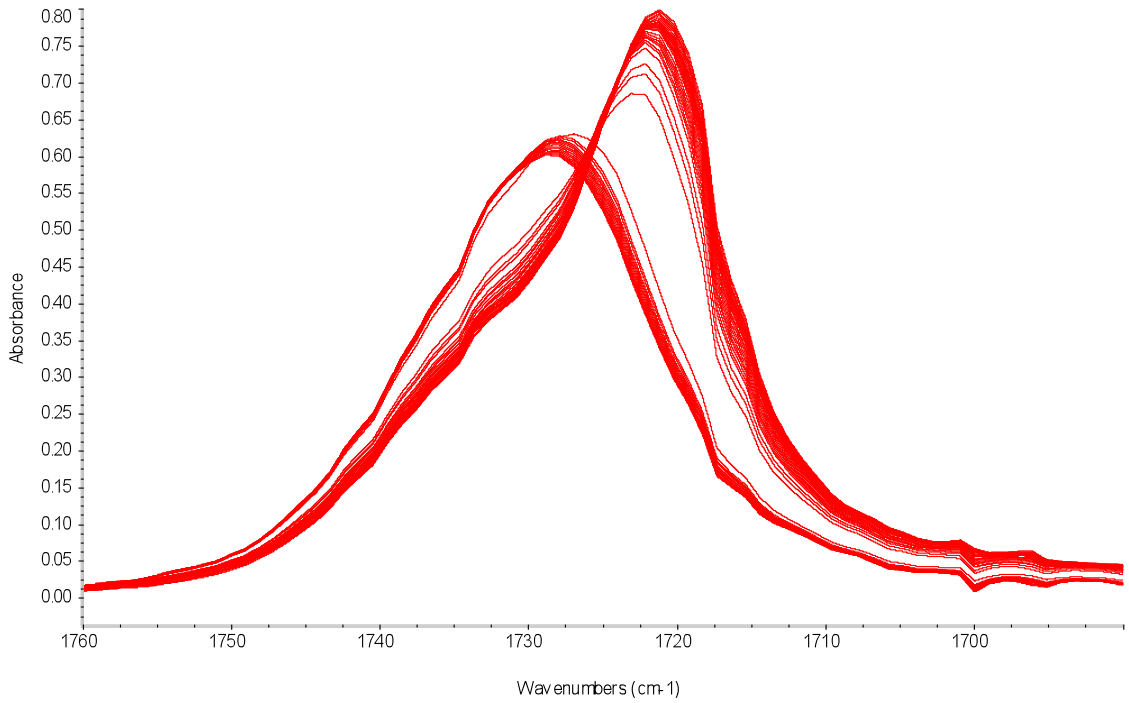


Figure 1

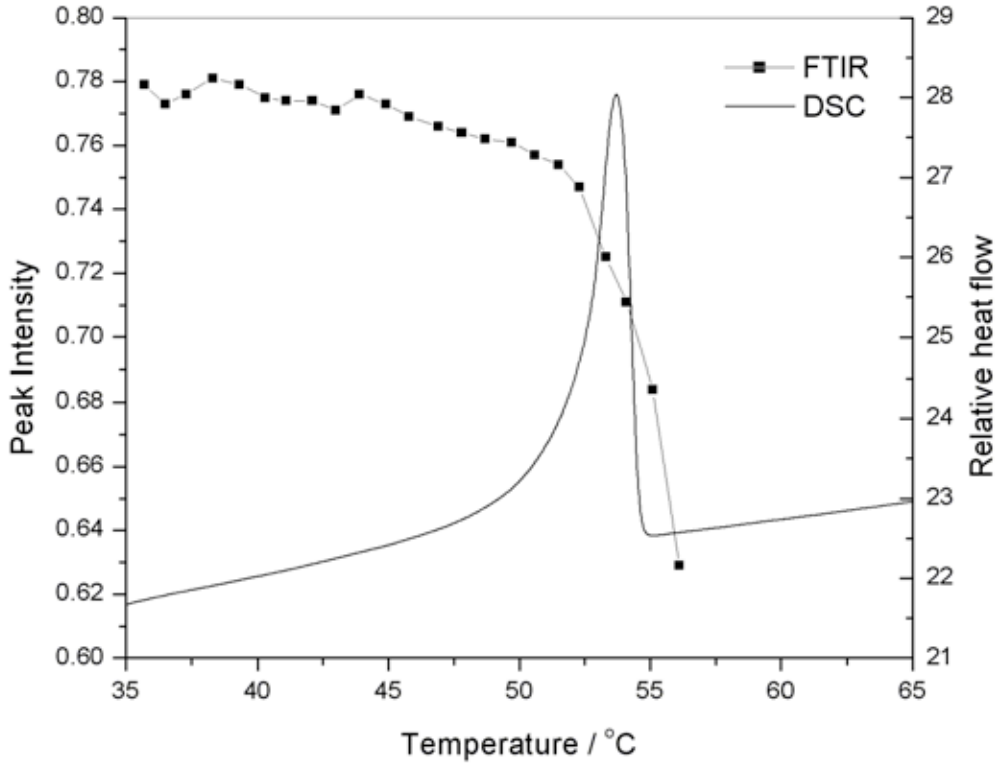
FTIR
DSC
Peak Intensity
Relative heat flow
Temperature / °C
0.80
0.78
0.76
0.74
0.72
0.70
0.68
0.66
0.64
0.62
0.60
29
28
27
26
25
24
23
22
21
35
40
45
50
55
60
65

Figure 2

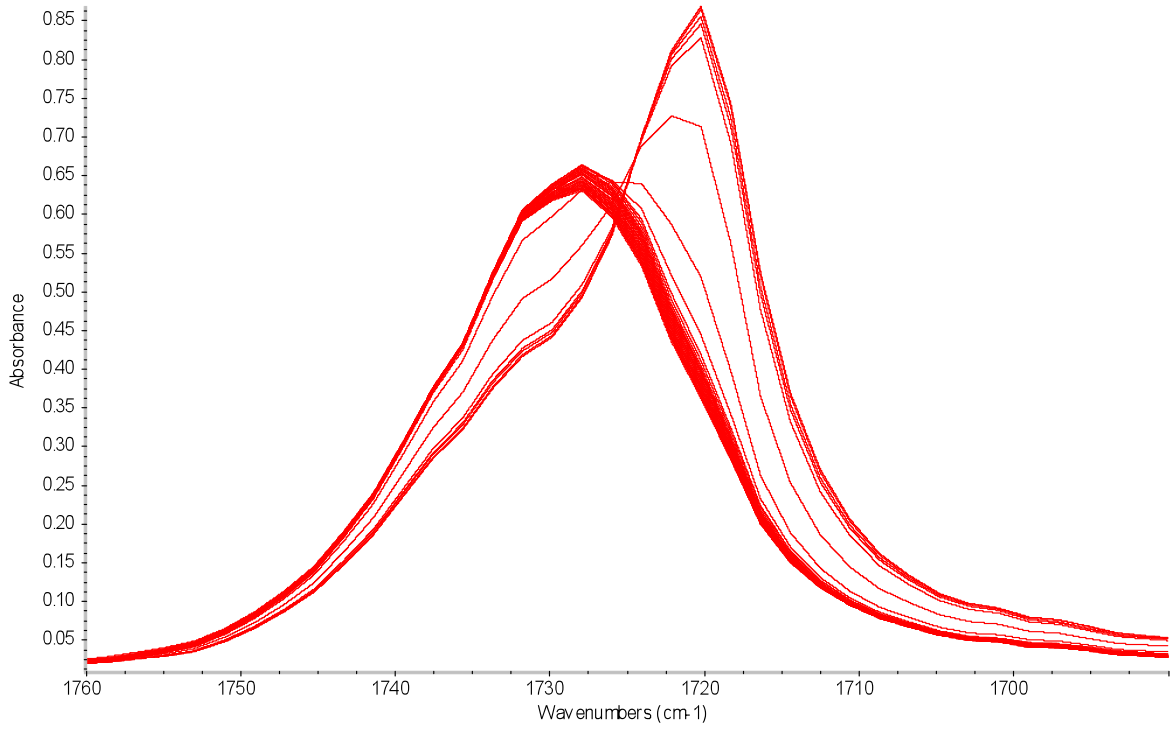
Absorbance
0.85
0.80
0.75
0.70
0.65
0.60
0.55
0.50
0.45
0.40
0.35
0.30
0.25
0.20
0.15
0.10
0.05
1760
1750
1740
1730
1720
1710
1700
Wavenumbers (cm-1)

Figure 3

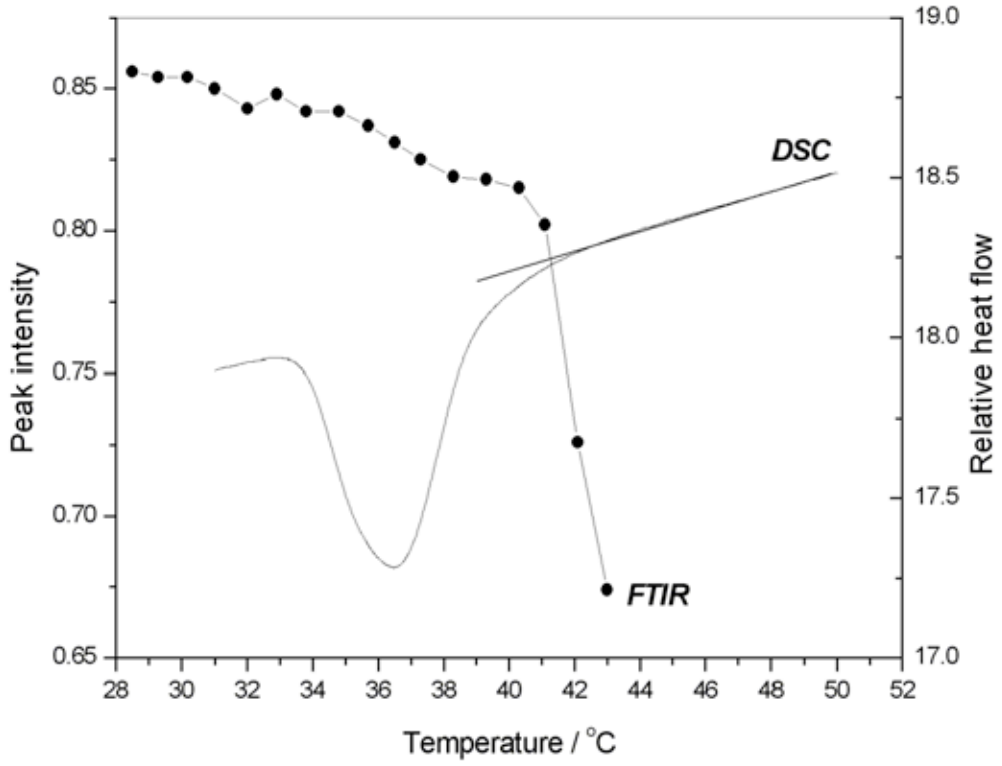
Peak intensity
Relative heat flow
Temperature / °C
DSC
FTIR
0.85
0.80
0.75
0.70
0.65
19.0
18.5
18.0
17.5
17.0
28
30
32
34
36
38
40
42
44
46
48
50
52

Figure 4

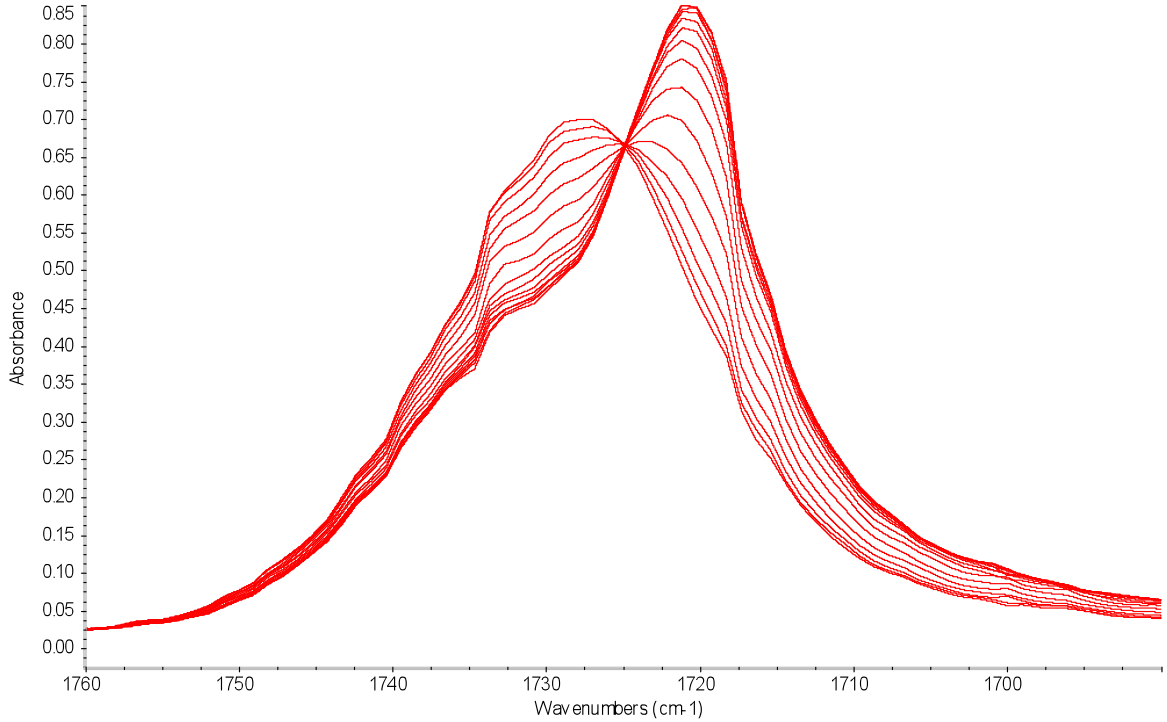
Absorbance
0.85
0.80
0.75
0.70
0.65
0.60
0.55
0.50
0.45
0.40
0.35
0.30
0.25
0.20
0.15
0.10
0.05
0.00
1760
1750
1740
1730
1720
1710
1700
Wavenumbers (cm-1)

Figure 5

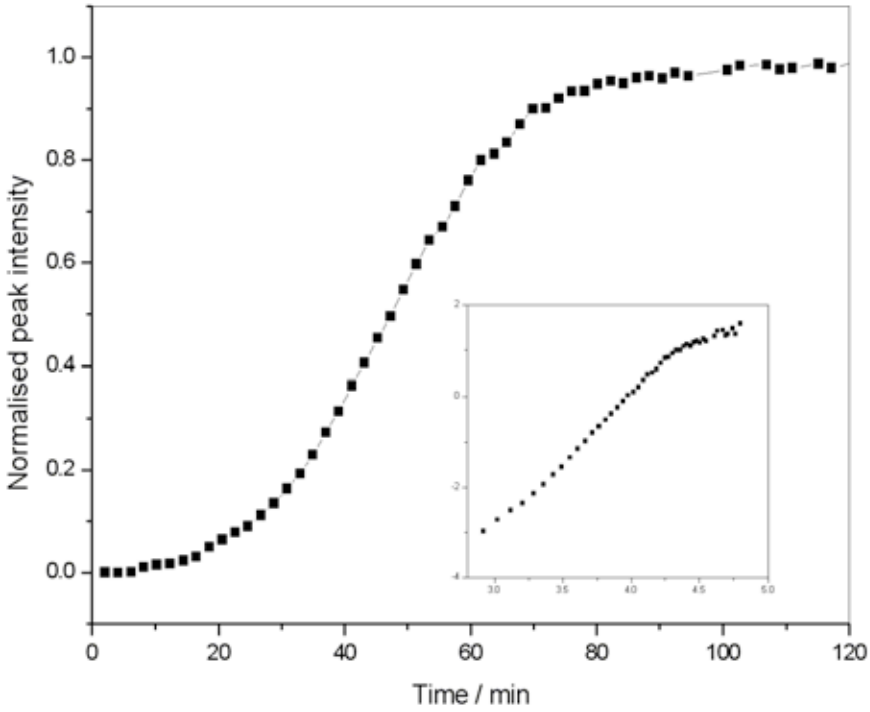
Normalised peak intensity
1.0
0.8
0.6
0.4
0.2
0.0
0
20
40
60
80
100
120
Time / min

Figure 6